The

PHILOSOPHICAL MAGAZINE

FIRST PUBLISHED IN 1798

VOL. 45 SEVENTH SERIES No. 368 September 1954

A Journal of Theoretical Experimental and Applied Physics

PRICE 15s. 0d.
Annual Subscription £8 0s. 0d. payable in advance

PRINTED AND PUBLISHED BY TAYLOR & FRANCIS LTD., RED LION COURT, FLEET ST., LONDON, E.C.4.

C. *The Calculation of Heats of Formation of Binary Alloys*

By J. H. O. Varley*
Department of Metallurgy, The University, Birmingham†

[Received December 16, 1953, revised May 13, 1954]

Abstract

A theoretical treatment for calculating the heats of formation of binary alloys for any composition is put forward. The model is based upon the assumption that the free electrons in a binary alloy exist in two sets of energy levels associated with the potential fields of the ions of the two elements in the alloy. This assumption is a natural consequence of neglecting the changes in the Wigner–Seitz boundary conditions, imposed upon the electrons in the pure elements, when the atoms are randomly mixed in an alloy. Fair agreement between calculated and experimental heats of formation is obtained for many systems, in which the two elements composing a given system are not too far removed from one another in the periodic classification of the elements.

Some consequences of the theory are discussed, in particular the magnetic behaviour of alloys can be qualitatively explained, the relative valency effect is also a natural prediction of the theory and the observed dependence of Fermi band width on composition in some binary alloys is accounted for.

§ 1. Introduction

The range of heats of formation of the binary alloys of metals is small compared with that of chemical compounds. Thus the most stable intermediate phases in metal binary alloy systems, e.g. AlNi, SnTe, have a negative heat of formation of the order of 8 kilocalories per gram atom, cf. MnO, TiO, which have heats of formation of the order of 70 kcal per g atom. Again in those binary systems which show extremely limited solid solubility and only partial miscibility in the liquid state, the heat of formation is positive and of the order of 4 kcal per g atom for an equiatomic alloy, e.g. Pb–Cu has a positive heat of formation of about 2 kcal per g atom for the equiatomic composition in the liquid state at 1200°c (Kubaschewski and Evans 1951). This small range of heats of formation is due to the chemical similarity of the typical metals.

* Now at Atomic Energy Research Establishment, Harwell.
† Communicated by the Author.

When an alloy is formed between two such metals, the redistribution of electrons and the resultant energy changes associated with it will be small, resulting in small negative heats of formation. If there is no redistribution of the valence electrons no bonding will be produced between the unlike atoms. In addition, the sizes of the atoms vary considerably amongst metals, ranging from a radius of about 3·0 Å for caesium to 1·24 Å for beryllium. The radius r is related to the atomic volume Ω thus :—

$$\Omega=\tfrac{4}{3}\pi r^3 \quad . \quad . \quad . \quad . \quad . \quad . \quad . \quad . \quad . \quad (1)$$

This results in strain energy being produced in the lattice when atoms of different sizes are forced together into a disordered solid solution. There is also a misfit energy produced in the liquid state. This strain energy produces a positive heat of formation upon alloying.

In addition to these two principal factors others, such as the change in the interaction between the underlying filled shells of electrons in the ion, the change in stability of the electrons in these closed shells and Brillouin Zone effects, may affect the heat of formation of the alloy.

The interplay of these factors gives rise to this narrow range of heats of formation in metal systems and no empirical order is apparent in the observed values.

Theoretical calculations of heats of formation of dilute solid solutions have been made by Arafa (1949) for copper–silver and silver–gold systems, by Huang (1948) for the silver–gold system and by Friedel (1952) for several systems involving elements of different valencies. There is no theory for calculating heats of formation of concentrated solid solutions.

The model employed here to calculate heats of formation of concentrated solid solutions is something of a hybrid between the quantum mechanical approach of Sommerfeld and the wave-mechanical cellular method of Wigner and Seitz for determining the binding energies of pure metals. The method cannot be interpreted from a collective electron viewpoint and is basically a classical type of treatment subject to the condition that the electrons obey the Fermi–Dirac statistics. However, results which are only obtainable from a collective electron treatment, such as the exchange and correlation energies between electrons of the same and different spins, have been incorporated in the theory. The screening of the potential wells of the solute atoms by a non-uniform charge distribution about them has, however, been neglected. This may be only a small effect in concentrated disordered solutions, but in dilute solutions neglect of this factor will be important.

In the case of ordered solid solutions the model breaks down badly, resulting in calculated heats of transformation for the order–disorder change of an entirely wrong order of magnitude ; this is due to neglecting the effect of screening in ordered solid solutions.

In § 2 the theoretical treatment is set out. Justification for the model is given in § 3 while § 4 deals with deductions which can be made from the theory.

§ 2. Theoretical Treatment

2.1. *General Considerations*

The formation of a phase γ in a binary alloy system from two pure components A and B, with structures α and β respectively, may be considered as taking place in the following stages :—

(i) Transformation of pure A from the α to the γ structure. Transformation of pure B from the β to the γ structure.

(ii) Assembly of A and B atoms into the γ phase. Stage (i) involves heat being supplied to the system giving in general positive contributions to the resultant heat of formation. Stage (ii) will involve a positive contribution to the heat of formation resulting from strain energy produced when the different sized atoms are mixed together in the structure. This strain energy will in general be less for an ordered arrangement than for a disordered array. Stage (ii) will also involve a negative contribution to the heat of formation arising from the change in energy of the valence electrons of the A and B atoms. Effects due to Brillouin zone overlaps and interactions between the underlying closed shells of the ions will also arise in stage (ii), so influencing the resultant heat of mixing.

It is the purpose of this paper to give a quantitative method for determining the effects on the heat of formation of strain energy and change in energy of the valence electrons arising in stage (ii) of the alloying process. The other factors will be discussed qualitatively.

An approximate treatment for determining the binding energy of a regular assembly of like atoms is the cellular method of Wigner and Seitz (1933, 1934). In a concentrated disordered solution of A and B atoms the simple Wigner–Seitz boundary condition no longer applies, for A atoms and B atoms have some A and some B neighbours. The eigenfunctions U_{0A} and U_{0B} corresponding to the respective ground state energies, E_{0A} and E_{0B}, will, in general, have different amplitudes at the cell boundaries and will consequently not match. Each U_0 will thus be modified to make the ground state eigenfunction single-valued and continuous throughout the alloy lattice. But if the change in the boundary condition of the eigenfunction in an atomic cell, which is necessary to match it to neighbouring atomic cell eigenfunctions in an alloy, is neglected, it is possible to consider the average energy, E_A, of an electron associated with an A atom in the alloy as equal to the average energy of an electron in an A cell in pure metal A ; similarly E_B will be the same in a B cell in the alloy and in the state of pure B. Thus it is assumed that the energies of the electrons in the alloy are split into two bands, that is to say, two sets of energy levels which are superposed to give a single energy band of non-uniform density. The electrons associated with A atoms will have energies in the set of energy levels based on a minimum energy E_{0A} ; those associated with B atoms will exist in an energy spectrum based on E_{0B} (fig. 1). If electrons move

from the high states of the A-band to the unoccupied energy levels at the top of the B-band, the energy of the whole system will decrease, that is, the alloy will have a negative heat of formation.

The quantitative development of this idea gives reasonable agreement between experimentally observed and calculated heats of formation. The calculated heats of formation are, however, in many cases, smaller (i.e. more negative) than the observed values; this is attributed to the neglect of changes in the boundary condition. The strongest support for the model lies in the observations of changes in the widths of the Fermi bands derived from x-ray spectroscopic data. For instance, the x-ray spectroscopic work of Bearden and Friedman (1940) on copper–zinc alloys indicates that the band of zinc, that is of those electrons in zinc cells, decreases on the high energy side with increasing dilution of zinc, while the copper band increases on the high energy side with increasing dilution of zinc. This suggests that only the high energy electrons participate directly in the alloying process, as assumed in this model. Quantitative agreement between the calculated and observed changes in Fermi band widths is good.

Fig. 1

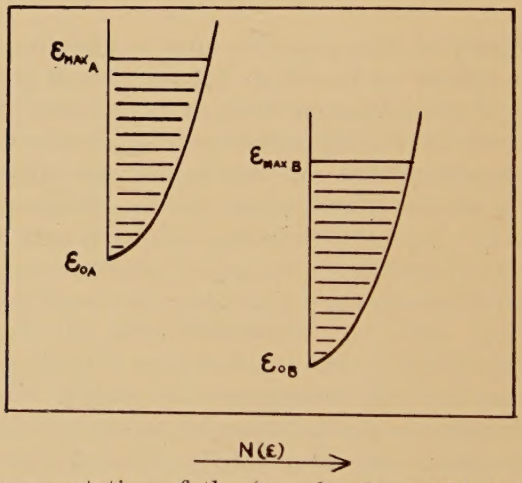

Diagrammatic representation of the 'two-band model' for a binary alloy. $N(\epsilon)d\epsilon$ gives the number of energy states lying in the energy range $d\epsilon$ about ϵ. The energy of the system will be lowered if the high energy electrons in energy levels at the top of the A band transfer to the unoccupied levels at the top of the B band.

In a disordered alloy containing $N(1-c)$ A atoms and Nc B atoms $(1 \geqslant c \geqslant 0)$ the free or valence electrons are thus to be regarded as being distributed amongst the A cells and the B cells so that those in A cells have an average energy given by

$$E_A = E_{0A} + \frac{3}{5} k \frac{Z_A^{2/3}}{r_A^2} \; ; \qquad k = \frac{h^2}{8m} \left(\frac{9}{4\pi^2} \right)^{2/3} \quad . \quad . \quad . \quad . \quad (2)$$

(m is assumed equal to the normal electronic mass throughout), while those in the B cells have a corresponding average energy E_B, *provided* that there is no transfer of charge from A cells (say) to B cells. Z_A and Z_B are the numbers of free electrons per atomic cell of pure A and pure B respectively; r_A and r_B are the corresponding equilibrium cell radii in the pure states. The total energy, NE, of the $N(1-c)Z_A$ electrons in the A cells and the NcZ_B electrons in the B cells would then be :—

$$NE=N(1-c)Z_AE_A+NcZ_BE_B. \quad . \quad . \quad . \quad . \quad . \quad . \quad (3)$$

This is the same as the energy of a phase mixture of pure A and pure B in proportion $(1-c):c$ and as such gives no contribution to the heat of formation of the disordered alloy. Suppose now that charge is transferred from the A cells to the B cells, so that on average an amount of charge n leaves each A cell and is *evenly* distributed over the Nc B cells. The number of electrons per A cell will *decrease* from Z_A to (Z_A-n) while the average number of electrons per B cell will *increase* from Z_B to $(Z_B+n(1-c)/C)$. The average energy of an electron in an A cell will consequently change from E_A to E_A' and similarly E_B will change to E_B'. The energy NE', of the disordered alloy will now be

$$NE'=N(1-c)(Z_A-n)E_A'+Nc(Z_B+n(1-c)/c)E_B'. \quad . \quad . \quad (4)$$

Moreover, charge will only flow from the A cells (say) to the B cells if the resultant energy of the system is lowered as a consequence. Hence $E'-E\leqslant 0$ always, and it is this transfer of charge which gives a negative contribution to the heat of formation of the alloy. This tendency to transfer charge expresses the magnitude of the electrochemical factor in the alloy system. The greater the electrochemical factor the greater the tendency to alloy formation, i.e. the more negative is the heat of formation

When charge flows from A cells to B cells, several other factors contribute to the resultant energy change. First, the energy of the remaining (Z_A-1) valence electrons in an A cell is decreased since there is now no repulsion between these (Z_A-1) electrons and the electron which has partially moved into a B cell (the fractional nature of the charge shift may be interpreted as meaning that the probability of an electron being in an A cell is $(1-n/Z_A)$ and the probability that an electron is in a B cell is $(1+n(1-c)/cZ_B)$). Similarly the average energy of the electrons in the B cells increases through repulsive forces between the charge Z_B already present in each cell and the charge $n(1-c)/c$ introduced. Secondly, as has already been observed by Jaswon (private communication), the donor cells (A) will become smaller when they lose charge and the cells which accept charge, (B), will expand. The minimum energies E_0 of electrons in the A and B cells will thus change as will also the additional kinetic or Fermi energy per electron, E_F, since this term involves both Z and r explicitly.

The change in the relative sizes of the cells produces a further effect. When cells of differing initial sizes are forced together into a disordered array, a strain energy is set up in the system. Flow of charge resulting

in a change of relative cell sizes will alter this strain energy. Thus if the donor atom is the larger, strain energy will be relieved by charge transfer, and conversely.

An attempt has been made to take all the factors discussed above into account in a quantitative manner. Before discussing the quantitative development of these ideas, however, a short qualitative discussion of such effects as interactions between the closed shells of the underlying ions and Brillouin zone effects will be given.

Brillouin Zone Effects

The model used here to calculate heats of formation is not capable of taking Brillouin zone effects into account, since the detailed arrangement of atoms around any given atom is neglected. However, analysis of experimental data, such as the heat of formation–composition relation for

Fig. 2

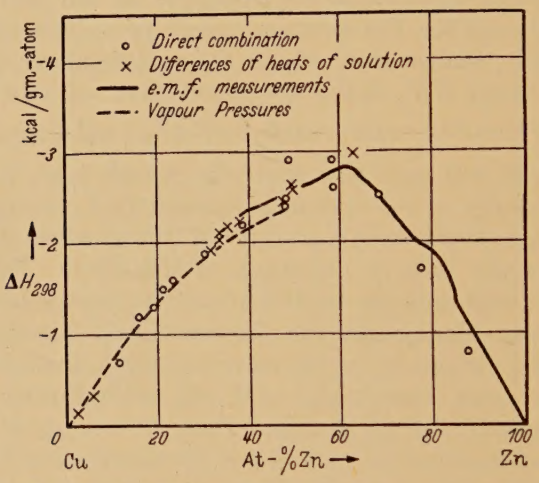

(From Kubaschewski and Evans, *Metallurgical Thermochemistry*, by permission of the publishers.)

copper-zinc alloys shown in fig. 2 (after Kubaschewski and Evans), suggests that the extrapolation of the heat of formation curve from the copper-rich primary solid solution composition range to the compositions of the electron compounds would produce no violent deviation from the experimental curve. Thus in the copper–zinc systems the maximum deviation would be about 500 calories per g atom.

It is suggested, therefore, that the negative contribution to the heat of formation in disordered solutions is primarily due to charge transfer, i.e. the electrochemical factor. Brillouin zone effects are perturbations superposed upon this main effect, and they determine which of many possible crystal structures, all of nearly the same energy, is adopted at a given alloy composition.

The Effect of Closed Shell Interactions

Exchange repulsions between filled closed shells are only of importance in the so-called full metals, i.e. those in which the radius of the metal

ions is large compared with the closest distance of approach of atoms in the solid. The repulsive forces between neighbouring ions are of very short range. Their contribution to the binding energy in the pure metal is small, being of the order of 300 calories per g atom for copper (Mott 1937).

The derivative of this energy term is, however, large, so that this *force* controls the closeness of approach of the atoms in the solid. Consideration of the work of Fuchs on copper (1935) suggests that removal of these forces will result in a contraction of the cell size. This may have an important effect on the average energy of a valence electron in the cell and also upon the average elastic constants and the strain energy produced on alloying, so affecting the resultant heat of formation. The neglect of the change in the heat of formation, brought about by the removal of the closed shell interactions, *per se*, will not be important.

Friedel (1952) has suggested that the instability of the 3d and 5d shells of copper and gold respectively, which gives rise to their colour, will give appreciable contributions to the binding energies of the pure metals, i.e. their heats of sublimation. In this way he accounts for the discrepancy of 30 kcal per g atom between the observed binding energy of copper and that calculated by Fuchs (1935). The magnitude of the Van der Waals energy in copper, as calculated by Friedel, may however be too large, for if it is as large as he calculates it to be, the following problem arises.

Suppose an atom of zinc is substituted for an atom of copper in a pure copper lattice, then the Van der Waals contribution to the binding energy will change considerably, for an easily polarizable copper atom has been replaced by a zinc atom with a much more stable d-shell and, consequently, a less readily polarizable ion. This means that there will be a very large positive contribution, per atom of copper replaced, to the heat of formation of the resultant dilute alloy of zinc in copper. It is not obvious that there will be an opposing negative contribution to the heat of formation of the same order of magnitude, although this may, of course, be the case.

It is possible, then, that the contribution of the Van der Waals energy changes to the heats of formation of the alloys of copper and gold is small. Neglect of this factor in the case of gold alloys does seem to be important, however, for the calculated heats of formation in these alloys are much too negative compared with the experimental values.

For binary systems in which the ions of the elements are not easily polarized, the Van der Waals energies will make very small contributions to the binding energies.

2.2. *The Energies of the Valence Electrons and the Misfit Energy in a Binary Alloy*

Consider an alloy composed of $N(1-c)$ A atoms and Nc B atoms. To evaluate the average energy of the electrons in the two types of atomic cell it is necessary to determine the ground state energies, E_0, the average interaction energies E_i between electron pairs in one cell,

the variation of cell size, r, with charge transfer, n, and the effect of this variation on E_0, E_i and E_F, where E_F is the mean additional kinetic energy of an electron.

(i) *The deduction of E_0 and its variation with charge transfer and the resultant change in atomic volume*

E_0 is the energy of the lowest energy electron in the pure metal, relative to the energy of an electron at rest in free space as zero.

(*a*) *Univalent metals*

When a univalent metal is sublimated into the state of free atoms, the boundary condition imposed upon the valence electron in an atomic cell is altered, so changing the average potential and kinetic energy of the electron. It is assumed that each atomic cell contains only one electron.

If energy contributions from all other effects are neglected it follows that

$$E_0 = -[\Lambda + I_1 + E_F], \quad . \quad . \quad . \quad . \quad . \quad . \quad . \quad . \quad (5)$$

where E_F is the mean additional kinetic energy of an electron in the solid state at 0°K, I_1 is the first ionization potential and Λ is the heat of sublimation per atom of the solid relative to the state of free atoms. $-(E_0+E_F)$ is the mean additional energy which an electron must receive to raise its energy to zero. This must equal $(\Lambda+I_1)$, if all other factors are neglected.

(*b*) *Polyvalent metals*

When a polyvalent metal is sublimated into the state of free atoms, two factors contribute to the energy of sublimation. First, the boundary condition imposed upon the valence electrons in any one atom is altered and this changes the potential and kinetic energies of the electrons. Secondly, the interaction energy between electrons is altered, as the following argument shows.

In the metallic state it is assumed that the electrons are free and that Z electrons exist in each atomic cell, where Z is the valency. Following the treatment of Wigner and Seitz (1933, 1934) therefore, there is a Coulomb interaction energy of $1{\cdot}2\, e^2/r$ per electron pair in an atomic cell of radius r, giving a positive contribution to the net interaction energy per electron pair. This is offset by the sum of two negative contributions, one of $-0{\cdot}916\, e^2/r$ per electron pair from exchange interactions between electrons having the same spin, and the other of $-be^2/r$ per electron pair from the correlation interactions between electrons having opposite spins. Wigner and Seitz assume a random mixing of spins so that the average interaction energy, (q_0/r), per electron pair in any one atomic cell is

$$\frac{q_0}{r} = \frac{e^2}{r}(0{\cdot}284 - b); \qquad b = b(r). \quad . \quad . \quad . \quad . \quad . \quad (6)$$

The total mean interaction energy, Q_m, per atomic cell containing Z valence electrons is then given by the product of the number of electron pairs and the interaction energy per pair, viz :—

$$Q_m = \frac{Z(Z-1)}{2} \cdot \left(\frac{q_0}{r}\right) . \quad . \quad . \quad . \quad . \quad . \quad . \quad . \quad . \quad (7)$$

In the corresponding free atom of a divalent metal, the total interaction energy, Q_f, between the electrons is given by the difference between the energy which would be necessary to remove the two electrons completely from the ion if no interaction were present, viz. $2I_2$, where I_2 is the second ionization potential, and the energy which is necessary to remove them with interaction present, viz. (I_1+I_2); I_1 is, as before the first ionization potential. Thus

$$Q_f = 2I_2 - (I_1+I_2) = I_2 - I_1 . \quad . \quad . \quad . \quad . \quad . \quad . \quad . \quad (8)$$

For a trivalent metal a similar argument applies. However, in this case, the energy which would be necessary to remove all three electrons from the ion if no interactions were present will be $3I_3 - I_T$. I_T is the energy required for the s–p transition in the ionization spectrum, M^{2+}. This term must be included to allow for the fact that one of the three electrons is in a P-state, the other two being in S-states. Thus for trivalent metals Q_f is given by

$$Q_f = 3I_3 - I_T - (I_1+I_2+I_3) \quad . \quad . \quad . \quad . \quad . \quad . \quad . \quad (9)$$

and for four-valent elements

$$Q_f = 4I_4 - 2I_T - (I_1+I_2+I_3+I_4) . \quad . \quad . \quad . \quad . \quad (10)$$

The difference $(Q_f - Q_m)$ in mean interaction energies of electron pairs in free atoms and in the metallic state must be taken into account in order to deduce the ground state energy for an electron in a polyvalent metal. In doing this the following assumptions are made :—

(1) The spins of the valence electrons in any one atomic cell in the metallic state are the same as for the valence electrons in the free atoms.

(2) The interaction energy between the valence electrons in a given atomic cell in the metal is assumed to be the same as in the free atom.

(3) The whole of the difference between the total mean interaction energy of the valence electrons Q_m in the metal and the corresponding interaction energy Q_f in the free atom arises from exchange interactions between a given valence electron in one atomic cell and electrons with like spin in neighbouring atomic cells.

(4) While assumption (iii) differs from that of Wigner and Seitz, which assumes a random mixing of spins, the mean interaction per electron pair as calculated by them has been retained.

This assumption, that the difference between electron–electron interactions in the metal and in the free atom arises from exchange interactions between electrons of like spin not in the same atomic cells, is supported

to some extent by the calculations of Wigner and Seitz. These show that there is a greater tendency for electrons of like spin to keep apart than is the case for electrons of opposite spin. Thus it might reasonably be assumed (Raimes 1951) that in a divalent metal the two electrons in a given atomic cell have opposite spins. Exchange and correlation energies between electrons in neighbouring cells have been neglected in the case of univalent metals.

The principle of the method for determining E_0 in the case of a polyvalent metal is as follows. Consider a divalent free atom with ionization potentials I_1 and I_2. The average energy of each electron is $-(I_1+I_2)/2$, while the interaction energy per electron is $(I_2-I_1)/2$. To remove one electron from the atom its energy must be increased by $(I_1+I_2)/2$, but in the act of removing the electron its energy is also decreased by the amount of the positive interaction energy per electron, $(I_2-I_1)/2$, for the repulsion between the electrons decreases to zero. The net work done, I, on removing the electron is thus given by

$$I=(I_1+I_2)/2-(I_2-I_1)/2=I_1 \quad . \quad . \quad . \quad . \quad . \quad (11)$$

i.e. the first ionization potential. From similar considerations, E_0 can be deduced for a polyvalent metal. If the average energy of an electron in the solid state is E, the change in energy of an electron on passing from the condensed state to that of free atoms is

$$-\frac{1}{Z}\sum_{i=1}^{i=Z} I_i-E, \quad . \quad . \quad . \quad . \quad . \quad . \quad . \quad . \quad . \quad (12)$$

where the first term is the average energy of an electron in the free atom. In addition the mean interaction energy per electron between the electrons changes by $(Q_f-Q_m)/Z$. The work done, i.e. the heat of vaporization per electron at absolute zero Λ/Z, where Λ is the heat of vaporization per atom, is thus given by

$$\frac{\Lambda}{Z}=-\frac{1}{Z}\sum_{i=1}^{i=Z} I_i-E+\frac{1}{Z}(Q_f-Q_m)$$

whence

$$E=-\frac{1}{Z}\left[\Lambda+\sum_{i=1}^{i=Z} I_i-Q_f+Q_m\right]. \quad . \quad . \quad . \quad . \quad (13)$$

Since $E=E_0+E_F$, it follows that

$$E_0=-\frac{1}{Z}\left[\Lambda+\sum_{i=1}^{i=Z} I_i+ZE_F-Q_f+Q_m\right]. \quad . \quad . \quad . \quad (14)$$

E_0 includes the interaction with other valence electrons in the cell.

(ii) *The variation of E_0 and the atomic cell radius with charge transfer*

In a pure metal the equilibrium radius, r_0, of the atomic cell is approximately determined by the relation

$$\left(\frac{\partial E_0}{\partial r}\right)_{r_0}=-\left(\frac{\partial[E_F(Z)]}{\partial r}\right)_{r_0}, \quad . \quad . \quad . \quad . \quad . \quad (15)$$

where the atomic volume $\Omega=\frac{4}{3}\pi r_0^3$. Equation (15) neglects the effect of closed shell interactions upon the equilibrium radius, r_0.

Suppose that, on average, there is a change n ($n \gtrless 0$) in the amount of charge in the cell. If each cell is considered as independent of its neighbours, the new equilibrium cell radius, r, will be determined by the relation

$$\left(\frac{\partial E_0}{\partial r}\right)_r = -\frac{\partial[E_F(Z+n)]}{\partial r}. \quad . \quad . \quad . \quad . \quad . \quad . \quad (16)$$

If it is assumed that $\partial E_0/\partial r$ is constant in the region $r=r_0$, and if the direct dependence of E_0 upon n is neglected, since this effect will be small, then

$$\left(\frac{\partial E_0}{\partial r}\right)_{r_0} = \left(\frac{\partial E_0}{\partial r}\right)_r \quad . \quad . \quad . \quad . \quad . \quad . \quad . \quad (17)$$

and hence

$$\left(\frac{\partial[E_F(Z+n)]}{\partial r}\right)_r = \left(\frac{\partial[E_F(Z)]}{\partial r}\right)_{r_0}. \quad . \quad . \quad . \quad . \quad (18)$$

Since

$$[E_F(Z)]=\frac{3k}{5}\frac{Z^{2/3}}{r_0^2}\ ; \quad [E_F(Z+n)]=\frac{3k}{5}\frac{(Z+n)^{2/3}}{r^2},$$

it follows that

$$r=r_0(1+n/Z)^{2/9}. \quad . \quad . \quad . \quad . \quad . \quad . \quad . \quad (19)$$

This gives an approximate relation between the size of the cell and the charge transfer, n.

The effect of the change in the total interaction energy between electrons, as the average amount of charge in the cell changes, is neglected in this approximation since its effect will be small.

E_0 can now be expressed as a function of r and hence n, as follows :—

$$E_0(r)=E_0(r_0)+(r-r_0)(\partial E_0/\partial r)_{r_0}, \quad . \quad . \quad . \quad . \quad . \quad (20)$$

whence, using eqns. (15) and (19)

$$E_0(r) \equiv E_0(Z+n)=E_0(r_0)-\frac{6kZ^{2/3}}{5r_0^2}\left\{1-\left(1+\frac{n}{Z}\right)^{2/9}\right\}. \quad . \quad . \quad (21)$$

The above method was suggested by Nabarro (private communication).

(iii) *The change in electron interaction energy due to charge transfer*

In the B cells which receive charge the change in interaction energy is proportional to the fraction of charge entering the cell, the amount of charge already present, and the average strength of interaction per electron pair. Thus if charge n' enters a cell already containing Z_B electrons, $Z_B n'$ interactions of average energy (q_{0B}/r_B) are produced. The total interaction energy change is thus

$$\frac{q_{0B}Z_B n'}{r_B}=\frac{Z_B n' e^2(0{\cdot}284-b(r_{0B}))}{r_{0B}(1+n'/Z)^{2/9}}. \quad . \quad . \quad . \quad . \quad (22)$$

In the A cells which give up charge n, the total interaction energy change $(q_{0A}(Z_A-1)n)/r_A$, is given by

$$\frac{q_{0A}(Z_A-1)n}{r_A}=\frac{(Z_A-1)ne^2(0{\cdot}284-b(r_{0A}))}{r_{0A}(1-n/Z_A)^{2/9}}. \quad . \quad . \quad . \quad (23)$$

(iv) *The strain energy*

To calculate the strain energy, E_s, produced when n_B A atoms of radius r_A are replaced by n_B B atoms of radius r_B, the solid is regarded as a continuous medium. The strain energy per A atom replaced in an alloy already containing $(N-n_B')$ A atoms and n_B' B atoms is then approximately given by

$$\frac{dE_s}{dn_B'}=\frac{6G[V_A(n_B')][\delta^2(n_B')]}{1+4G/3K} \quad . \quad . \quad . \quad . \quad . \quad (24)$$

by an extension of the formula for strain energy given by Nabarro (1940). δ, the misfit, is defined by

$$1+\delta(n_B')=\frac{r_A(n_B')}{r_B}\ ;\quad (r_A \gtrless r_B). \quad . \quad . \quad . \quad . \quad . \quad (25)$$

Also

$$V_A(n_B')=\frac{4\pi}{3}[r_A(n_B')]^3. \quad . \quad . \quad . \quad . \quad . \quad . \quad (26)$$

G is the shear modulus for the matrix and K the bulk modulus for the atom introduced. As an approximation, the radius, $r_A(n_B')$, of the hole left when an A atom is removed, which is a function of the number of A atoms already replaced, is taken to be

$$r_A(n_B')=r_A\frac{N-n_B'}{N}+r_B\frac{n_B'}{N}. \quad . \quad . \quad . \quad . \quad . \quad (27)$$

Substitution of (27) in (25) gives

$$\delta(n_B')=\left(1-\frac{n_B'}{N}\right)\delta\ ;\quad \delta=\frac{r_A}{r_B}-1. \quad . \quad . \quad . \quad . \quad (28)$$

The total strain energy E_s is then given by

$$E_s=\int_0^{n_B}\frac{6G}{1+4G/3K}V_A(n_B')\delta^2(n_B')\,dn_B'.$$

Putting $n_B/N=c$ and integrating

$$E_s=\frac{8\pi GN\delta^2{r_A}^3}{1+4G/3K}\left\{c-c^2+\frac{c^3}{3}-3\delta\left(\frac{c^2}{2}-\frac{2c^3}{3}+\frac{c^4}{4}\right)+\text{higher powers of }\delta\right\}.$$

. . . (29)

If Poisson's ratio is taken as $\frac{1}{3}$, if the elastic constants of A and B are assumed equal, if δ is small, and if, further, the bracket is approximated by $c(1-c)$, a rough estimate of the strain energy will be

$$E_s=NP(r_A-r_B)^2c(1-c)\ ;\quad P=2\pi Kr_A. \quad . \quad . \quad . \quad (30)$$

Kr_A has been taken as the average of the values for the two pure components.

This rather crude expression for the strain energy fails for dilute solutions. The symmetrical form has been chosen for simplicity and will give an order of magnitude for the strain energy in the region $c=\frac{1}{2}$. In particular, asymmetry of the strain energy E_s is neglected; this effect will be most important in dilute solutions of A in B and B in A. Since it has been neglected, a detailed study of the variations of solid solubility with temperature, in those systems where strain energy is predominant, cannot be discussed: a more careful estimate of strain energy in dilute solutions will be necessary for such an analysis.

2.3. *The Energy of Formation of a Binary Alloy*

The average energy per atom, E, at absolute zero, neglecting the zero point vibrational energy, of an alloy containing Nc B atoms and $N(1-c)$ A atoms is

$$E=[E_{0A}](Z_A-n)(1-c)+[E_{0B}]\left(Z_B+\frac{n(1-c)}{c}\right)c-\frac{q_{0A}}{r_A}n(1-c)(Z_A-1)$$
$$+Z_B\frac{q_{0B}}{r_B}\frac{n(1-c)}{c}c+\frac{3}{5}\frac{k}{{r_A}^2}(Z_A-n)^{5/3}(1-c)$$
$$+\frac{3}{5}\frac{k}{{r_B}^2}\left(Z_B+\frac{n(1-c)}{c}\right)^{5/3}c+Pc(1-c)(r_A-r_B)^2 \quad . \quad . \quad . \quad (31)$$

where an amount of charge n has, on average, left each A cell and distributed itself uniformly over Nc B cells. The sizes of the A and B cells have thereby changed so that

$$r_A=r_{0A}\left(1-\frac{n}{Z_A}\right)^{2/9}; \quad r_B=r_{0B}\left(1+\frac{n(1-c)}{Z_Bc}\right)^{2/9}, \quad . \quad . \quad (32)$$

where r_{0A}, r_{0B} are the atomic radii in pure A and B.

The ground state energies, $[E_0]$, are also a function of the $r_{A,B}$ and hence of n; thus from (30)

$$\left.\begin{aligned}[E_{0A}]&=E_{0A}-\frac{6kZ_A^{2/3}}{5{r_{0A}}^2}\left\{1-\left(1-\frac{n}{Z_A}\right)^{2/9}\right\},\\ [E_{0B}]&=E_{0B}-\frac{6kZ_B^{2/3}}{5{r_{0B}}^2}\left\{1-\left(1+\frac{n(1-c)}{Z_Bc}\right)^{2/9}\right\}.\end{aligned}\right\} \quad . \quad . \quad . \quad (33)$$

The terms containing $(q_{0A})/r_A$, $(q_{0B})/r_B$ give the changes in the interaction energy, E_i, and hence in E_{0A} and E_{0B}, as charge transfers from A to B (eqns. (22) and (23)). Substituting eqns. (32) and (33) into the

expression (31) for E and expanding to the second power in n, we obtain

$$E=Z_{\mathrm{A}}E_{0\mathrm{A}}(1-c)+Z_{\mathrm{B}}E_{0\mathrm{B}}c+\frac{3}{5}\frac{kZ_{\mathrm{A}}{}^{5/3}}{r_{0\mathrm{A}}{}^{2}}(1-c)+\frac{3}{5}\frac{kZ_{\mathrm{B}}{}^{5/3}}{r_{0\mathrm{B}}{}^{2}}c$$
$$+Pc(1-c)(r_{0\mathrm{A}}-r_{0\mathrm{B}})^{2}+n(1-c)X+\frac{n^{2}(1-c)}{c}Y, \quad . \quad . \quad (34)$$

where

$$X=\left\{E_{0\mathrm{B}}-E_{0\mathrm{A}}+\frac{kZ_{\mathrm{B}}{}^{2/3}}{r_{0\mathrm{B}}{}^{2}}-\frac{kZ_{\mathrm{A}}{}^{2/3}}{r_{0\mathrm{A}}{}^{2}}+\frac{q_{0\mathrm{B}}Z_{\mathrm{B}}}{r_{0\mathrm{B}}}-\frac{q_{0\mathrm{A}}(Z_{\mathrm{A}}-1)}{r_{0\mathrm{A}}}\right.$$
$$\left.+\frac{4P}{9}(r_{0\mathrm{B}}-r_{0\mathrm{A}})\left(\frac{r_{0\mathrm{B}}(1-c)}{Z_{\mathrm{B}}}+\frac{r_{0\mathrm{A}}c}{Z_{\mathrm{A}}}\right)\right\},$$

and

$$Y=\left\{\frac{11kZ_{\mathrm{A}}{}^{-1/3}}{45r_{0\mathrm{A}}{}^{2}}c+\frac{11kZ_{\mathrm{B}}{}^{-1/3}}{45r_{0\mathrm{B}}{}^{2}}(1-c)-\frac{2q_{0\mathrm{B}}(1-c)}{9r_{0\mathrm{B}}}-\frac{2q_{0\mathrm{A}}(Z_{\mathrm{A}}-1)c}{9r_{0\mathrm{A}}Z_{\mathrm{A}}}\right.$$
$$+\frac{2P}{81}\left[\frac{7c^{2}}{Z_{\mathrm{A}}{}^{2}}+\frac{7(1-c)^{2}}{Z_{\mathrm{B}}{}^{2}}+\frac{4c(1-c)}{Z_{\mathrm{A}}Z_{\mathrm{B}}}\right]r_{0\mathrm{A}}r_{0\mathrm{B}}$$
$$\left.-\frac{10P}{81}\left[\frac{r_{0\mathrm{A}}{}^{2}c^{2}}{Z_{\mathrm{A}}{}^{2}}+\frac{r_{0\mathrm{B}}{}^{2}(1-c)^{2}}{Z_{\mathrm{B}}{}^{2}}\right]\right\}. \quad (35)$$

The first four terms in the expression for E represent the energy of a phase mixture of pure A and pure B; hence the energy of formation per atom of the alloy is

$$\Delta E=Pc(1-c)(r_{0\mathrm{A}}-r_{0\mathrm{B}})^{2}+n(1-c)X+\frac{n^{2}(1-c)}{c}Y, \quad . \quad . \quad (36)$$

where n satisfies the equation $\partial\Delta E/\partial n=0$. This gives

$$n=-Xc/2Y \quad . \quad . \quad . \quad . \quad . \quad . \quad . \quad . \quad . \quad (37)$$

and

$$\Delta E=c(1-c)[P(r_{0\mathrm{A}}-r_{0\mathrm{B}})^{2}-X^{2}/4Y]. \quad . \quad . \quad . \quad . \quad (38)$$

The term $c(1-c)P(r_{0\mathrm{A}}-r_{0\mathrm{B}})^{2}$, which is always positive or zero, is the zero order strain energy term arising from the random mixing of atoms of different initial sizes. The term, $-c(1-c)X^{2}/4Y$, which is always negative or zero, is the electrochemical factor.

It will be observed that the energy parameters X and Y govern the magnitude of the first and second order energy changes, brought about by unit charge transfer in an alloy of given concentration. These parameters thus incorporate the effect of charge transfer upon the change in the degree of misfit of the atoms with its consequent modification of the zero order strain energy, as well as its effect upon the kinetic and potential energies of the electrons. The term which is called the electrochemical factor here is thus of a somewhat complex nature, in that it does not deal with the change in the kinetic and potential energies of the electrons due to charge transfer alone.

2.4. *Electrostatic Interaction between Neighbouring Shells of Atoms and a given Atom*

It might be thought that, since charge transfer has produced a disordered array of positively and negatively charged cells, a contribution to the energy will be produced from this effect. The following argument shows that this effect is small for disordered solid solutions. In ordered solutions an energy term of considerable magnitude may arise, and this will be discussed later.

Consider a solid solution containing Nc B atoms, each cell containing excess negative charge $n(1-c)/c$, and $N(1-c)$ A atoms, each cell containing excess positive charge n. Let the lattice coordination number be p. Approximating the A and B atomic cells by spheres of radii r_A and r_B respectively, the total electrostatic interaction energy, NE_e, between nearest neighbours in a disordered solid solution is given by

$$NE_e \sim e^2n^2\left\{\frac{N_{AA}}{r_{AA}}+\frac{(1-c)^2N_{BB}}{c^2r_{BB}}-\frac{(1-c)N_{AB}}{cr_{AB}}\right\}, \quad . \quad . \quad (39)$$

where N_{AA}, N_{BB} and N_{AB} are the numbers of AA, BB and AB nearest neighbour pairs in the alloy, and r_{AA}, r_{BB}, r_{AB} the corresponding bond lengths. Now

$$N_{AA}=\frac{Np(1-c)^2}{2}\ ; \quad N_{BB}=\frac{Npc^2}{2}\ ; \quad N_{AB}=Npc(1-c). \quad . \quad (40)$$

Substitution of (40) in (39) gives

$$E_e \sim \frac{e^2n^2p(1-c)^2}{2}\left\{\frac{1}{r_{AA}}+\frac{1}{r_{BB}}-\frac{2}{r_{AB}}\right\}. \quad . \quad . \quad . \quad . \quad (41)$$

Taking $r_{AA}\sim 2r_A$, $r_{BB}\sim 2r_B$, $r_{AB}\sim r_A+r_B$,

$$E_e \sim \frac{e^2n^2p(1-c)^2(r_A-r_B)^2}{8r^3} \quad . \quad . \quad . \quad . \quad . \quad . \quad (42)$$

where r_A and r_B are assumed to be not very different in magnitude.

Putting $(r_A-r_B)\sim 0{\cdot}5$ Å, which is an extreme misfit in alloys, $r\sim 1{\cdot}5$ Å, $c=\frac{1}{2}$, $p=12$, $n=0{\cdot}25$, $e^2/r\sim 10$ ev per atom, we obtain

$$E_e \sim +600 \text{ cal/g atom.}$$

The true interaction energy will be less than this, for the distances between atoms of like charge will be slightly greater than those assumed and conversely. It therefore seems reasonable to assume that this electrostatic energy will make only a very small contribution to the heat of formation, in the case of a disordered solution; the effect has therefore been neglected.

All the necessary data for deriving the energy parameters P, X and Y in the expression for the heat of formation, eqn. (38), are set out for the

various metallic elements in table 1. Ionization energies are taken from a paper by Lisitzin (1938–40) and other references given in that paper. Heats of vaporization are taken from Kubaschewski and Evans (1951).

§ 3. Justification of the Theory

3.1. *Comparison between Experimental and Calculated Heats of Formation*

Direct comparison of the theory with experiment is possible by comparing calculated values of ΔE with observed heats of formation. This comparison is only made plausible by making use of the empirically observed rule of Kopp and Neumann. They observed that the specific heats of solids, such as alloys containing more than one element, are a linear combination of the specific heats of the elements composing the solid. Thus in an alloy containing Nc B atoms and $N(1-c)$ A atoms, if K_A and K_B are the specific heats per atom of pure A and of pure B respectively, then the average specific heat, K, per atom in the alloy is given by

$$K=(1-c)K_A+cK_B. \quad . \quad . \quad . \quad . \quad . \quad . \quad . \quad . \quad (43)$$

This relation is found to hold, in many cases, for coordination compounds and alloys to within 5 or 10%. Deviations from this law will be important at low temperatures where the higher energy vibrations are not fully excited.

The contribution, NE_ν, to the internal energy at temperature, T, made by the zero point energy vibrations and the thermal excitation of these vibrations is

$$NE_\nu=\frac{3Nh\nu_0}{2}+N\int_0^T K\,dT, \quad . \quad . \quad . \quad . \quad . \quad (44)$$

where h is Planck's constant and ν_0 is the average vibrational frequency of the atoms at absolute zero. For the Debye model of specific heats in which the number of oscillations, $3N$ in all, having frequencies in the range $\nu \to \nu+d\nu$ is proportional to $\nu^2\,d\nu$, ν_0 is given by

$$\nu_0=\tfrac{3}{4}\nu_D,$$

where ν_D is the Debye frequency. The total vibrational contribution to the additional binding energy, ΔE_ν, in an A–B alloy containing a fraction c of solute atoms is thus

$$\Delta E_\nu=\frac{3h}{2}(\nu_0-\nu_{0A}(1-c)-\nu_{0B}c)+\int_0^T (K-K_A(1-c)-K_BC)\,dT. \quad (45)$$

If the Kopp–Neumann rule holds exactly, the last term vanishes for all values of T. The first term will also vanish, for implicit in the Kopp–Neumann rule is the identity

$$\nu_D \equiv \nu_{DA}(1-c)+\nu_{DB}c,$$

where ν_D is the Debye characteristic frequency in the alloy.

Table 1

Element	Ionization energies						q_0/r_0	$\left(\frac{5}{3}E_F = \frac{kz^{2/3}}{r_0^2}\right)$	$-E_0$	$(-E_{max} = -E_0 - \frac{5}{3}E_F)$
	A	I_1	I_2	I_3	I_4	I_T (s–p transition)				
Cu	3·54	7·68	—	—	—	—	1·2	7·10	15·48	8·38
Ag	3·00	7·54	—	—	—	—	0·9	5·52	13·85	8·33
Au	3·93	9·18	—	—	—	—	0·9	5·56	16·47	10·91
Mg	1·55	7·61	14·96	—	—	—	0·6	7·23	13·03	5·80
Cd	1·16	8·96	16·84	—	—	—	0·6	7·49	14·33	6·84
Zn	1·37	9·36	17·89	—	—	—	1·0	9·57	16·29	6·72
Hg	0·7	10·39	18·65	—	—	—	0·6	7·23	15·38	8·15
Al	3·30	5·96	18·74	28·31	—	6·64	0·9	11·76	18·30	6·54
Ga	2·5	5·97	20·43	30·6	—	8·15	0·7	10·49	17·94	7·45
In	2·56	5·76	18·79	27·9	—	7·32	0·5	8·71	16·08	7·37
Tl	1·88	6·07	20·32	29·7	—	8·83	0·5	8·26	16·72	8·46
Ge	5·2	8·09	15·86	34·07	45·5	10·21	0·6	11·70	20·59	8·89
Sn	3·5	7·30	14·5	30·5	39·4	8·98	0·5	10·24	18·71	8·47
Pb	2·04	7·38	14·96	31·9	42·11	10·70	0·5	9·51	18·38	8·87

Deviations from the Kopp–Neumann rule will thus be reflected in the heat of formation at all temperatures, including absolute zero.

The magnitude of this effect on the heat of formation is likely to be small. The major part of the deviation will occur below the Debye temperature. The thermal contribution to the internal energy at the Debye temperature is

$$E_v < 3k\theta_D ; \qquad (k, \text{ Boltzmann's constant}).$$

Taking $\theta_D \sim 250^\circ$K as an average value for typical metals

$$E_v \lesssim 1500 \text{ cal per g atom.}$$

A deviation of 10% from the Kopp–Neumann law will then involve a thermal contribution ΔE_v to the heat of formation of less than 150 cal per g atom. The contribution to ΔE from thermal vibrations will thus generally be small, and considerably less than 150 cal per g atom. For these reasons the Kopp–Neumann rule has been assumed true and heats of formation at elevated temperatures have been used for comparison.

However, there is a more serious objection to the use of heats of formation of binary alloys at high temperatures if considerable strain energy exists in the alloy, for the elastic constants of pure metals decrease appreciably with increasing temperature. Thus the value of Young's modulus for a metal at temperatures near the melting point is of the order of 60% of its value at room temperature (Köster 1948). Heats of formation of solid solutions measured at high temperatures will thus be lower than corresponding values at low temperature.

Although the strain energy in liquid alloys is smaller than in the corresponding solid solutions, heats of solution of liquid alloys might be used for comparison with the calculated heats of formation. The calculated values can be expected to be greater (more positive) than the measured values for liquid alloys, since there is less residual misfit energy in the liquid state. In addition, such a comparison neglects any difference between the energies of the electrons in the pure solid and liquid states. The manifestation of these differences is the latent heat of fusion. Since the latter are at most 6% of the latent heat of evaporation, A, for the typical metals, the errors incurred in the calculated values by neglecting latent heats of fusion should not be serious.

Comparisons between calculated and experimentally measured heats of solutions for equi-atomic binary alloys are given in table 2. Experimental values have been taken from Kubaschewski and Evans (1951).

Figures 3, 4, 5 and 6 show the calculated heats of formation over the whole range of compositions for four systems.

The experimentally determined heat of formation (solid) or heat of solution (liquid) curves are plotted for comparison.

The calculated values refer to a 'structureless alloy', in the sense that a quantitative account of stage (i) of the alloying process discussed in § 2.1 has been neglected.

Table 2

System		Strain energy (ev) $P(r_{0A}-r_{0B})^2$	Electro-chemical factor $X^2/4Y$ (ev)	Charge transfer n at $c=\frac{1}{2}$	Calculated heat of formation at $c=\frac{1}{2}$, cal/g atom ($T\sim273°$ A)	Observed heat of formation $c=\frac{1}{2}$
Acceptor	Donor					
Cu	Zn	0·08	0·50	0·28	− 2420	−2500 (298° A)
Cu	Cd	0·53	0·52	0·30	+ 60	+ 50*
Cu	Hg	0·56	0·03	0·08	+ 3050	—
Cu	Ga	0·35	0·53	0·31	− 1040	—
Cu	In	0·93	0·60	0·34	+ 1900	—
Cu	Tl	1·23	0·14	0·16	+ 6280	—
Cu	Ge	0·67	0·16	0·18	+ 2940	—
Cu	Sn	1·14	0·32	0·25	− 60† + 4720	−1150*
Cu	Pb	1·45	0·20	0·20	0† + 7200	+1890*
Ag	Zn	0·02	0·43	0·28	− 2360	−1700 (298° A)
Ag	Cd	0·09	0·44	0·29	− 2020	−1300 (298° A)
Ag	Hg	0·12	0·01	0·05	+ 630	—
Ag	Ga	0·03	0·48	0·31	− 2590	—
Ag	In	0·28	0·54	0·34	− 1500	—
Ag	Tl	0·43	0·09	0·05	+ 1960	—
Ag	Ge	0·13	0·11	0·06	+ 115	—
Ag	Sn	0·37	0·25	0·13	+ 690	+1370*
Ag	Pb	0·55	0·15	0·08	+ 2300	+ 420*
Cu	Ag	0·22	0	0	+ 1250	+ 800*
Au	Cu	0·29	0·02	0·04	+ 1560 − 4030†	− 900 (773° A)
Au	Ag	0	0·30	0·18	− 1700 − 1250‡	− 945 (773° A) −1010‡
Zn	Mg	0·15	0	0	+ 865	−4270*
Cd	Mg	0	0·08	0·16	− 460	—
Hg	Mg	0	0·88	0·5	− 5040	—
Cd	Zn	0·13	0	0	+ 750	+ 530*
Hg	Zn	0·14	0·26	0·26	− 690	+ 170*
Hg	Cd	0	0·33	0·30	− 1890	−1100 (298° A) (c 0·6)
Ga	Al	0·03	0·08	0·16	− 290	—
In	Al	0·25	0·25	0·29	0	—
Tl	Al	0·37	1·18	0·62	− 4670	—
Ga	In	0·08	0	0	+ 460	—
Tl	Ga	0·15	0·19	0·26	− 230	—
Tl	In	0·01	0·11	0·21	− 580	—
Ge	Sn	0·06	0	0	+ 350	—
Ge	Pb	0·15	0·11	0·22	+ 230	—
Pb	Sn	0·02	0	0	+ 115	+ 300*
Zn	Al	—	—	—£	+ 50	+ 560*
Au	Zn	—	—	—	−14500	−5500 (298° A)
Au	Cd	—	—	—	−16400	−3900 (298° A)
Au	Sn	—	—	—	−14400	−4000 (298° A)

* Liquid alloy. † Strain free Alloy. ‡ $c=\frac{1}{4}$ (Brewer *et al.* 1952).

As has already been observed, the theory attempts to account for the effects of strain energy and of charge transfer only. Quantitative estimates of the magnitudes of neglected factors such as Brillouin zone effects, ion–ion interactions and deviations from the Kopp–Neumann law

have already been given and would appear to influence the heats of formation of alloys but little. It is suggested, therefore, that the two

Fig. 3

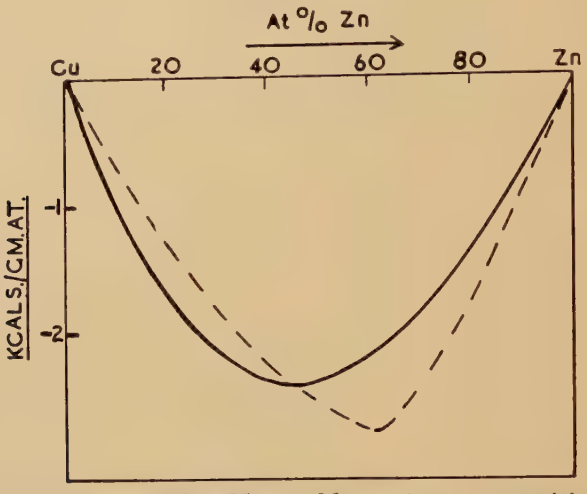

The full curve shows the calculated heat of formation—composition relationship for Cu–Zn alloys. The dotted curve shows the experimental relationship at 298°A (taken from fig. 2).

Fig. 4

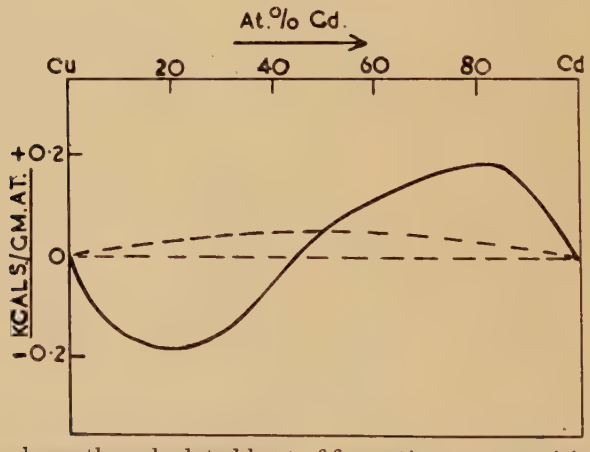

The full curve shows the calculated heat of formation—composition relationship for Cu–Cd alloys. The dotted curve shows the experimental relationship at 700°c.* The experimental value for the solid intermediate phase Cu_5Cd_8 (298°A) is about −0·6 kcal per g atom. The calculated value for this composition, assuming no strain energy, is about 1 kcal per g atom.

* Liquid alloys.

factors quantitatively discussed in the theory, namely strain energy and the electrochemical factor, are the overriding effects which determine

the degree to which two metals tend to alloy, as measured by the heats of formation, and that the other factors mentioned above are secondary

Fig. 5

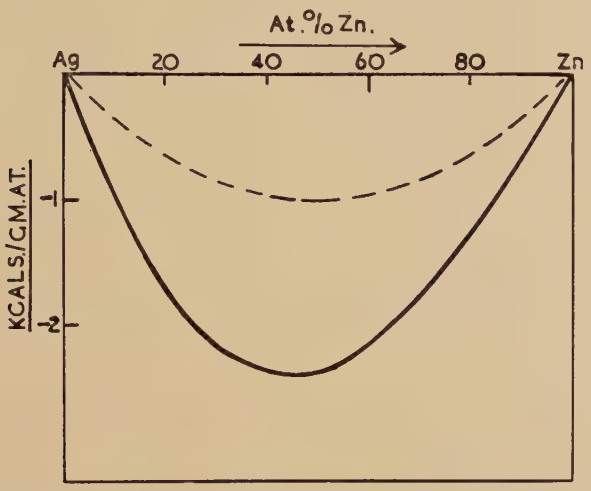

The full curve shows the calculated heat of formation—composition relationship for Ag–Zn alloys. The dotted curve shows the experimental relationship.* The experimental values for the solid intermediate phases AgZn, Ag_5Zn_8, $AgZn_3$, at 298°A are —1·7, —1·9 and —1·3 kcal per g atom respectively. The experimental value for the composition 38% Ag 62% Zn is —2·3 kcal per g atom.

* Liquid alloys.

Fig. 6

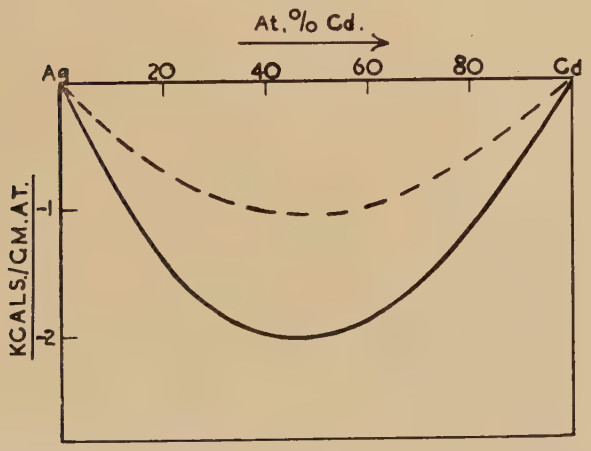

The full curve shows the calculated heat of formation—composition relationship for Ag–Cd alloys. The dotted curve shows the experimental relationship at 727°c.* The experimental values for the solid intermediate phases AgCd, Ag_5Cd_8, $AgCd_3$ at 298°A are —1·3, —1·4 and —1·2 kcals per g atom respectively.

* Liquid alloys.

considerations, which will determine the detailed structures of the solid alloys and will refine the calculated values of the heats of formation.

The calculated values of the heats of formation of gold alloys are very much too negative for all those alloying elements given in table 2, except copper and silver. This is possibly due to changes in the Van der Waals interaction energies upon alloying. All the solute elements considered, save copper, have stable ions. Furthermore, all these elements, with the exception of copper and silver, are open metals, i.e. their ions occupy a relatively small fraction of the atomic volume. Alloyed with the open metals, the ion of the gold atom may be more stable than it is in the gold lattice. This increase in the stability of the gold ion upon alloying will give positive contributions to the heats of formation, offsetting the large negative contributions due to charge transfer. Although the copper ion has a relatively unstable 3d shell, this does not appear to reflect in the heats of formation of the alloys of copper.

3.2. *Comparison of the Calculated Widths of the Valence or Free Electron Energy Spectrum with the Observed Widths as derived from X-Ray Spectroscopy*

The width of the energy spectrum, W, or Fermi band, is given by the expression

$$W=\frac{5}{3}E_{\mathrm{F}}=\frac{kZ^{2/3}}{r^2}, \quad \left[k=\frac{h^2}{8m}\left(\frac{9}{4\pi^2}\right)^{2/3}\right], \qquad . \; . \; . \quad (46)$$

where E_{F} is the mean kinetic energy of an electron.

The model employed here assumes two sets of energy levels, one associated with the solvent and one with the solute.

Substituting $(Z_{\mathrm{A}}-n)$ for Z and $r_{0\mathrm{A}}(1-n/Z_{\mathrm{A}})^{2/9}$ for r gives

$$W_{\mathrm{A}}=W_{0\mathrm{A}}\left(1-\frac{n}{Z_{\mathrm{A}}}\right)^{2/9}; \quad W_{0\mathrm{A}}=\frac{kZ_{\mathrm{A}}{}^{2/3}}{r_{0\mathrm{A}}{}^2}. \qquad . \; . \; . \quad (47)$$

Similarly

$$W_{\mathrm{B}}=W_{0\mathrm{B}}\left(1+\frac{n(1-c)}{Z_{\mathrm{B}}c}\right)^{2/9}; \quad W_{0\mathrm{B}}=\frac{kZ_{\mathrm{B}}{}^{2/3}}{r_{0\mathrm{B}}{}^2}, \qquad . \; . \; . \quad (48)$$

where $W_{0\mathrm{A}}$ and $W_{0\mathrm{B}}$ are the Fermi band widths in pure A and pure B respectively.

The calculated widths are shown plotted against composition in fig. 7 (a, b) for copper and zinc in brass alloys. Experimentally determined widths, observed by Bearden and Freidman (1940) are plotted for comparison.

§ 4. Some Consequences of the Theory

4.1. *The Relative Valency Effect*

It has been observed by Hume-Rothery that if a solute metal has a valency greater than that of the solvent, the solid solubility range is larger than the range obtained when the solute has a valency less than that of the solvent. Thus copper dissolves in zinc less readily than zinc dissolves

in copper at any given temperature. This effect is known as the relative valency effect. An explanation of this effect follows naturally from the theory given above.

Fig. 7

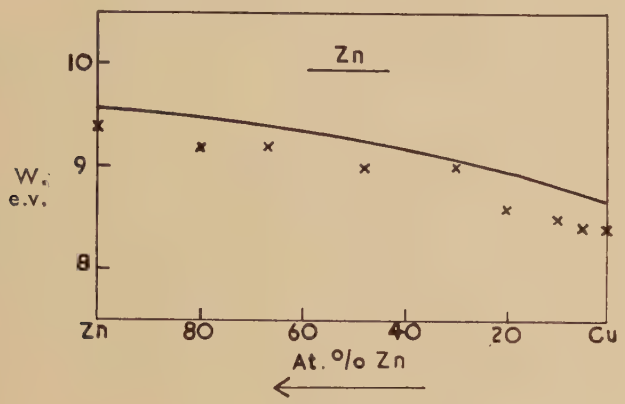

(*a*)

The full curve shows the calculated band width of Zn as a function of composition in Cu–Zn alloys. The crosses indicate experimental values found by Bearden and Friedman.

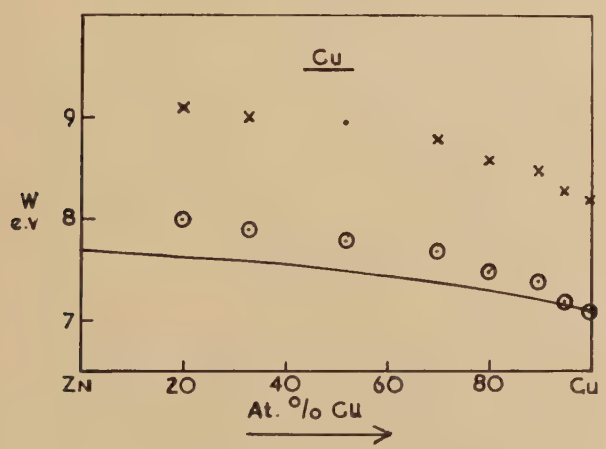

(*b*)

The full curve shows the calculated band-width of Cu as a function of composition in Cu–Zn alloys. The crosses indicate experimental values found by Bearden and Friedman. The latter include contributions from transitions of the 3d electrons. The circles are the corrected experimental values, assuming that the 4s electron band-width in Cu is the same as for free electrons, and that the 3d contribution is independent of composition.

The greater the tendency to alloy in dilute solutions, the more negative will be the slope of the heat of formation composition curve in the region of the pure solvent.

Consider an alloy system in which the strain energy is small and may be neglected. The heat of formation, ΔE, is given, from eqn. (38) by

$$\Delta E = -c(1-c)X^2/4Y \quad . \quad . \quad . \quad . \quad . \quad . \quad (49)$$

where X and Y are defined by eqns. (35). Since it is assumed that $r_{0B}=r_{0A}$, X is independent of concentration. It follows that

$$\frac{\Delta E_{c\to 1}}{\Delta E_{c\to 0}} = \frac{\left|\frac{\partial \Delta E}{\partial c}\right|_{c=1}}{\left|\frac{\partial \Delta E}{\partial c}\right|_{c=0}} = \left(\frac{Z_A}{Z_B}\right)^{1/3}, \quad . \quad . \quad . \quad . \quad . \quad . \quad (50)$$

since the other terms in Y are small and of opposite sign. Now A is the solvent in the region $c\to 0$. Equation (50) may thus be expressed as follows :—

$$\frac{\text{Ease of solubility of A in B}}{\text{Ease of solubility of B in A}} = \left(\frac{Z_A}{Z_B}\right)^{1/3}.$$

If $Z_A > Z_B$, element A should thus dissolve more readily in B than conversely. This is the relative valency effect. The calculated heat of formation–composition relations, shown in figs. 3, 4, 5 and 6, illustrate this effect quite clearly, even in those cases, such as the Cu–Cd system, where there is a large difference in atomic sizes.

4.2. *Deviations from Vegard's Law*

The atomic radius of an element is defined by eqn. (1). If r_{0A} and r_{0B} are the respective sizes, so defined, of A and B atoms in the pure states, then according to Vegard's law, the mean atomic radius, r_0, in an alloy is the weighted mean of r_{0A} and r_{0B}

$$r_0 = (1-c)r_{0A} + cr_{0B}, \quad . \quad . \quad . \quad . \quad . \quad . \quad . \quad (51)$$

where c is the fraction of B, and $(1-c)$ the fraction of A in the alloy.

If, through charge transfer, the radii of the A and B atoms change to r_A and r_B respectively, and if it is assumed that a relation similar to (51) expresses the mean atomic radius, r, in the alloy, then

$$r = (1-c)r_A + cr_B. \quad . \quad . \quad . \quad . \quad . \quad . \quad . \quad (52)$$

If the effect of strain energy in the alloy upon the mean atomic radius, r, is neglected the difference between r and r_0 will give the deviation, Δ, from Vegard's law

$$\Delta \equiv r - r_0.$$

These deviations from Vegard's law have been discussed by Raynor (1949). For instance, Hume-Rothery, Lewin and Reynolds (1936) have shown that equal atomic percentages of cadmium, indium, tin and antimony in silver expand the silver lattice in the ratio 2 : 3 : 4 : 6. Similar relations are

observed in copper-rich alloys. Δ can be related to the charge transfer as follows. Since

$$r_A = r_{0A}\left(1-\frac{n}{Z_A}\right)^{2/3} \; ; \quad r_B = r_{0B}\left(1+\frac{n(1-c)}{cZ_B}\right)^{2/3}$$

and writing $n=n_0c$

$$\Delta = c(1-c)\left\{\frac{2n_0}{9}\left(\frac{r_{0B}}{Z_B}-\frac{r_{0A}}{Z_A}\right)-\frac{7n_0^2}{81}\left(\frac{r_{0A}c}{Z_A^2}+\frac{r_{0B}(1-c)}{Z_B^2}\right)\right\}. \quad . \quad (53)$$

A is the charge donor atom and B the acceptor.

If $r_{0B}/Z_B = r_{0A}/Z_A$, the deviation Δ should be negative. This is observed in the case of silver–gold alloys.

Table 3

System		Deviation, Δ, from Vegard's law	
Solvent	Solute	Calculated	Observed
Cu	Zn	0·08	0·02
Cu	Ga	0·16	0·08
Cu	Ge	0·08	0·18
Cu	Cd	0·07	0·21
Cu	In	0·16	0·47
Cu	Sn	0·13	0·78
Ag	Cd	0·09	0·02
Ag	In	0·19	0·09
Ag	Sn	0·13	0·20
Ag	Zn	0·10	0·05
Ag	Ga	0·20	0·13
Ag	Ge	0·09	0·25
Ag	Au	−0·019	−0·006
Cu	Au	0·004	0·03
Cu	Ag	0	0·02

If $r_{0B}/Z_B > r_{0A}/Z_A$, the deviation will be positive, and this will generally be the case when $Z_A > Z_B$. Values of the change of Δ per unit change in atomic percent of solute are compared with experimental values derived from a paper by Raynor (1949) in table 3. Qualitative agreement is fair but quantitative agreement is poor.

4.3. *Order–Disorder Transformations*

The theory is unable to account satisfactorily for the order–disorder energy changes in systems where an electrochemical factor is present. For instance, consider the ordering of the β phase in the Cu–Zn system. The composition of this phase is approximately equi-atomic and its structure is body-centred-cubic. According to the theory given above,

the zinc cells have a positive charge of $\sim+e/4$ and the copper cells a negative charge, $\sim-e/4$, at this composition. The electrostatic contribution per atom, E_e, to the binding energy of this ordered structure is thus

$$E_e\sim-\frac{e^2M}{32r} \quad . \quad . \quad . \quad . \quad . \quad . \quad . \quad . \quad (54)$$

where M is the Madelung constant and r is the distance between nearest neighbours. Since $M\sim1{\cdot}6$ and $e^2/r\sim5$ ev per atom for β brass,

$$E_e\sim-6 \text{ kcal/g atom.}$$

The ordered structure is in fact about 0·4 kcal per g atom more stable than the disordered structure. The theory thus predicts ordering energies of a completely wrong order of magnitude. The situation is really worse than has already been indicated, for a further decrease in energy, and hence a larger ordering energy, will be brought about by more charge leaving the zinc cells and occupying the copper cells. The further gain in electrostatic energy more than outweighs the increase in energy of the electrons displaced from the equilibrium distribution in the absence of this electrostatic contribution.

The breakdown of the model must be attributed to the neglect of changes in the boundary conditions imposed upon the electrons in the lattice. When these are properly taken into account, the energy changes on alloying may arise not only from a direct transfer of charge from (say) zinc cells to copper cells but also from a redistribution of charge within these cells. The electrostatic contribution to the ordering energy would then be much smaller and this more refined theory would be more in accordance with the experimental observations.

Since ordering energies are small, being of the order of 500 cal per g atom, the theory presented in this paper could still be used in a semi-empirical manner by neglecting the electrostatic contributions to the ordering energy. The relief, by ordering, of the strain energy would then be the only factor considered.

4.4. *Magnetic Properties of Alloys*

Coles (1952) has pointed out that magnetic measurements carried out on the binary system Ni–Cu cannot be interpreted in terms of the collective electron theory used to interpret the magnetic behaviour of pure elements. He discusses the alternative approach of regarding the 3d electrons in the nickel atoms as forming a band of their own. This agrees qualitatively with the alloy model put forward in this paper. The rate of filling up of the d-shells of the solute atoms by electron transfer from solvent (donor) atomic cells to the solute (acceptor) atomic cells will depend upon the magnitude of this tendency to transfer charge.

If the donor atoms are strongly electropositive relative to the acceptor atoms with their partly-filled d-shells, then electron transfer per unit amount of donor atoms will be large. The d-shells of the acceptor atoms

will thus be filled for a relatively small concentration of donor atoms present in the alloy. If, on the other hand, the atoms with partly-filled d-shells are the relatively electropositive atoms in a binary alloy, these atoms will tend to transfer charge from their cells into the cells of the acceptor atoms, which we suppose, have their d-shells full; the alloys of this system will thus always contain some atoms with partly-filled d-shells, and the magnetic susceptibility, which depends upon the number of holes in the d-shell, may change in an approximately linear manner with concentration of solute.

The alloys of the copper–nickel system are predicted to be ferromagnetic in the composition range 100% Ni to 40 atomic per cent of nickel, and diamagnetic in the range 40% Ni to 0% Ni, according to the collective electron theory of magnetism. The ferromagnetism is a result of the holes in the 3d band, which are predicted to be just completely filled for the alloy composition 60% Cu : 40% Ni. Thereafter, the alloys which are more dilute in nickel, should be diamagnetic due to the strong over-riding diamagnetic susceptibility of the now full 3d shells. This in fact is not observed, for alloys containing less than 40% Ni are strongly paramagnetic, and become diamagnetic at compositions containing ~20% Ni or less. This can be explained by the two-band model in the following manner.

If it is assumed that the transition element with the partly-filled d-shell does not change in size as electrons are transferred to or from it, and if, moreover, it is assumed that all the electrons received by the transition atoms from the donor atoms occupy the holes in the d-shells (this will be a fair approximation since the density of states is high for the d-shell compared with the density of states for the s-band), an extension of the treatment given in § 2 gives

$$\Delta E = Pc(1-c)(r_{0A}-r_{0B})^2-(1-c)X^2/4Y \quad . \quad . \quad . \quad (55)$$

for the heats of formation, ΔE, of alloy compositions in the range where there are still holes in the d-shells of the acceptor atoms. X and Y are given by

$$\left.\begin{aligned} X &= E_{\max_B}+E_{iB}-E_{\max_A}-(Z_A-1)\frac{q_{0A}}{r_{0A}}+\frac{4Pc}{9Z_A}r_{0A}(r_{0B}-r_{0A}), \\ Y &= \frac{11}{45}\frac{kZ_A^{-1/3}}{r_{0A}^{\,2}}-\frac{2q_{0A}(Z_A-1)}{9r_{0A}Z_A}+\frac{Pc\overline{r_0^{\,2}}}{20Z_A}. \end{aligned}\right\} \quad . \quad . \quad . \quad (56)$$

In the above expressions

$$E_{\max_A} = E_{0A}+\tfrac{5}{3}E_{FA}.$$

$E_{\max_B}$ is the corresponding energy of the top of the d-band in the transition element.

E_{iB} is the interaction energy between electrons already in the d-shell and one entering it, $\overline{r_0^{\,2}}$ is the mean square of the atomic radii (the last

term in Y is an approximation since this term is usually small). The optimum charge transfer, n, is given by

$$n=-X/2Y. \quad . \quad . \quad . \quad . \quad . \quad . \quad . \quad . \quad (57)$$

Now the observed band-widths for zinc in nickel–zinc alloys as a function of composition have been determined by Bearden and Beeman (1940); these are :—

100 at. % Zn	9·4 ev,
30 at. % Zn	7·2 ev,
17 at. % Zn	7·2 ev.

Using eqns. (47) and (48) of § 3 in conjunction with eqn. (57) above, an approximate value of $(E_{\max}+E_i)_{\mathrm{Ni}}$ can be determined with this information. The value obtained is $\sim$9 ev. Using, now, the values for copper given in table 1 along with this value, the value of n found for nickel-rich copper–nickel alloys (i.e. those with d-shells yet unfilled) is

$$n\sim 0{\cdot}14 \text{ electrons donated per Cu atom.}$$

If there are $N(1-c)$ copper atoms present, they will thus transfer $N(1-c)0{\cdot}14$ electrons to nickel cells, and these electrons are assumed to be uniformly distributed through the Nc nickel cells. The increased charge in the nickel cells is thus

$$0{\cdot}14(1-c)/c \text{ electrons per Ni atom.}$$

When this equals 0·6, the d-shells in the nickel atoms will all be filled. This is satisfied for an alloy containing approximately 20 atomic per cent Ni. Thus, according to these calculations, the alloys of copper and nickel may be expected to be ferromagnetic or strongly paramagnetic in the composition range 100 atomic per cent Ni to 20 atomic per cent Ni, whereafter they are predicted to be diamagnetic, in the range 20 to 0 atomic per cent Ni, in agreement with experiment.

This theory thus gives a satisfactory quantitative account of the variation of magnetic susceptibility with composition in the case of Cu–Ni alloys, and will also account qualitatively for the magnetic behaviour of other binary alloy systems.

§ 5. Conclusions

The term scheme, given in table 1, for calculating the heats of formation of binary alloys, in conjunction with eqns. (35) and (38) is inadequate to account fully for the alloying characteristics of any one element with respect to any other. The most satisfactory agreement is obtained with this model for those metallic elements lying in the middle periods of the periodic classification of the elements. Of those elements for which

calculations have been attempted using this model, the predicted alloying characteristics of the elements magnesium and aluminium, which are A sub-group metals, do not agree with experimental observations. In general, aluminium is too electropositive and magnesium is not electropositive enough, relative to the other components of the possible binary systems. It is thought that the lack of agreement with experiment, in the case of the calculated heats of solution of binary alloys with gold, is explained by changes in van der Waals interactions as has already been discussed.

The general conclusion which must be reached, therefore, is that the simple model presented here can only give a reasonable guide to the heat of formation and the type of binary system which can be expected between those elements of the B sub-groups which have here been examined, namely, Cu, Ag, Au, Zn, Cd, Mg, Ga, In, Tl, Ge, Sn, Pb. The term scheme of table 2 might be improved if a more accurate treatment of the interactions between electrons could be made. The model cannot be extended, with any certainty, to predict the possible occurrence of intermediate phases in a system. For instance, an electrochemical factor, outweighed by a large strain effect, is predicted for the Zn–Pb system. This implies very limited solid solubility, as is observed. It might be possible that an intermediate phase would form in such a system, in which there was little strain energy, with a negative heat of formation due to the electrochemical factor. This in fact is not observed. It should be pointed out that the magnitudes of the electrochemical factors predicted for the binary alloys of elements with three and four valence electrons are most sensitive to the magnitude of electron-pair interactions. A correct knowledge of these interactions used in conjunction with the theory presented here might well predict no electrochemical factor in such systems as Zn–Sn and Zn–Pb, in keeping with experimental observations.

A theoretical treatment giving better agreement with observed heats of formation and alloying characteristics of elements, as observed in binary alloys, will have to take into account the changes produced, by alloying, in the boundary conditions imposed on the electrons and will also have to consider the fact that an electron does not behave as a completely free electron in a metal, as reflected in its effective mass.

Finally, it should be observed that the theory is dealing with relatively small energy differences between large quantities. An accurate knowledge of all the energy terms involved is thus necessary in order to obtain a complete comparison with experimental observations.

Acknowledgments

The author wishes to acknowledge the encouragement afforded him by the late Professor D. Hanson throughout this work. He also wishes to thank Professors F. R. N. Nabarro and G. V. Raynor for most helpful discussions and suggestions.

References

Arafa, M. K. I., 1949, *Proc. Phys. Soc.* B, **62,** 238.

Bearden, J. A., and Beeman, W. W., 1940, *Phys. Rev.*, **58,** 396.

Bearden, J. A., and Friedman, H., 1940, *Phys. Rev.*, **58,** 387.

Brewer, M. B., Ticknon, L. B., Scatchard, G., and Wagner, C., 1952, *U.S. At. En. Comm. Pub.*

Coles, B. R., 1952, *Proc. Phys. Soc.* B, **65,** 221.

Friedel, J., 1952, *Phil. Mag.*, **43,** 153.

Fuchs, K., 1935, *Proc. Roy. Soc.* A, **151,** 585.

Huang, K., 1948, *Proc. Phys. Soc.*, **60,** 161.

Hume-Rothery, W., Lewin, G. F., and Reynolds, P. W., 1936, *Proc. Roy. Soc.* A, **157,** 167.

Köster, W., 1948, *Metallkunde*, **39,** 1.

Kubaschewski, O., and Evans, E. Ll., 1951, *Metallurgical Thermochemistry* (London: Butterworth-Springer Ltd.).

Lisitzin, E., 1938–40, *Soc. Scient. Fennica Com. Phys. Math.*, **10,** No. 4.

Mott, N. F., 1937, *Proc. Phys. Soc.*, **49,** 258.

Nabarro, F. R. N., 1940, *Proc. Roy. Soc.* A, **175,** 519.

Raimes, S., 1950, *Phil. Mag.*, **41,** 568.

Raynor, G. V., 1949, *Trans. Far. Soc.*, **45,** 698.

Wigner, E., and Seitz, F., 1933, *Phys. Rev.*, **43,** 804; 1934, *Ibid.*, **46,** 509, 1002.

CI. *Atmospherics with Long Trains of Pulses*

By F. Hepburn* and E. T. Pierce
Cavendish Laboratory, Cambridge†

[Received March 30, 1954]

Summary

The waveforms of atmospherics having long-continued trains of pulses, and the systematic modifications associated with time of recording, storm distance and the presence of a low-frequency component, are described. Their interpretation is discussed and the results of analysis —assuming the simple ionospheric reflection mechanism—are presented. Estimates of reflection height and storm distance show the applicability of the theory to the temporal parameters of the waveforms, and the origins of two groups of atmospherics having calculated ranges of 4500 and 7000 km are considered. The variation of pulse amplitude with reflection order is shown to lead to the postulation of horizontal radiating elements in the channel during the later stages of the return stroke, although difficulties arise in reconciling this concept with considerations of the magnitude and orientation of the horizontal elements.

§ 1. Introduction

In a previous paper (Caton and Pierce 1952), which will be referred to as (C.P.), the main varieties of atmospherics observed in the British Isles, were described. Among the most striking waveforms are those consisting of an extended series of pulses or oscillations ; these, with rare exceptions, are recorded only at night, and were termed the long oscillatory train types in (C.P.). The purpose of the present paper is to give a more detailed account of these atmospherics.

There is often no intrinsic difference between the Regular Peaked (C.P.) variety of atmospheric and the initial stages of a long-continued train ; both types of waveform belong to a general family of atmospherics for which the number of pulses may vary from four or five to thirty or more. In this paper the phrase ' long-train ' will be applied only to waveforms with a dozen or more pulses none of which is less than about 5 mv/m in peak-to-peak amplitude.

§ 2. Experimental Details

The site at Cambridge, with its low noise level, and the ' Wilson-sphere ' vertical aerial system (C.P.), permits a convenient and reliable assessment of the absolute magnitude of the variations in the vertical

* Now at the Physics Department, University of Nottingham.
† Communicated by T. W. Wormell.

electric field. The output, proportional to the field of the atmospheric, from the aerial circuit, is applied to the grid of an electrometer valve which forms the first stage of a conventional resistance–capacity coupled amplifier with balanced outputs feeding the vertically deflecting plates of a cathode-ray tube. The frequency response of the whole system falls, from the maximum, by 1 db at 100 c/s and 9 kc/s, and by 3 db at 25 c/s and 15 kc/s. The gain is adjustable with a maximum value of 24 000 ; this gives full-scale deflection for a field of 220 mv/m. Mains pick-up from adjacent power lines is reduced by injecting a voltage of suitable amplitude and phase ; a tuned filter circuit is provided, whereby, if necessary, signals at 16·0 kc/s (GBR) or 19·4 kc/s (GBZ) can be greatly decreased.

A continuously-running balanced linear time-base with sweep time of 10 milliseconds, provides the horizontal movement for the trace. Normally the brilliance is low, but it is increased, by the arrival of an atmospheric exceeding a pre-set amplitude, to a level suitable for photographic recording ; this level is maintained for one time-base cycle by the action of a multivibrator circuit. Triggering may occur at any point along the horizontal sweep. The use of such an arrangement has the disadvantage that a portion of the waveform is lost before trigger threshold amplitude is attained.

Photographic records are obtained using an $f/3{\cdot}5$ camera in which the continuously-exposed film moves vertically at a speed of 3 in./min. Only the bright triggered traces corresponding to each waveform exceeding the threshold amplitude are recorded.

Most of the long-train atmospherics discussed in this paper were recorded during the winter months of 1949/50 and 1950/51. Cooperation with the ' Sferics ' organization of the Meteorological Office resulted in the origin of many individual waveforms, photographed during the latter period, being approximately located.

§ 3. Forms of the Long Train Atmospherics

In (C.P.) two kinds of long train night-time atmospheric were distinguished, a type where the successive pulses were predominantly sharply peaked in character and another form in which the oscillations were smooth approximating to a quasi-sinusoidal ripple.

The peaked form usually contains a few large oscillations at the beginning of the waveform and is often rather confused in this region. After about the fourth order pulse there is generally a marked fall in amplitude ; subsequently the pulsations gradually diminish in size although minor fluctuations are often apparent. A low-frequency component or ' slow tail '* (Watson-Watt, Herd and Lutkin 1937), of quasi-frequency about 400 c/s, is often associated with this type of waveform, some of the earlier pulses appearing superimposed upon the

* It is convenient to retain the term ' slow tail ' although this feature occurs in the earlier part of the long train of pulses.

l.f. component. The shapes of the individual peaks and intervening traces show marked variations from one atmospheric to another, and also change gradually throughout a single waveform. Systematic modifications in the form of the repeated motif are associated with the time of recording, the storm distance and the presence or absence of a pronounced slow tail. Subdivision of the long train atmospherics into four predominant types showing this dependence has been found possible. The first two of these (§§ 3.1 and 3.2) both come from storms within 2000 km and the differences observed are apparently source effects. The third (§ 3.3) originates in more distant storms under full night conditions, and also in storms within 2000 km during twilight periods near sunset and dawn. The last type (§ 3.4) comes from very distant sources (beyond about 4000 km).

3.1. *Symmetrical Peaked Long-Train Forms* (fig. 1) (Plate 26, fig. 1 (A–D))

This type is observed from storms within 2000 km under full night-time conditions, defined, in this paper, as the period between two hours after ionosphere sunset and just before ionosphere sunrise for all points of the propagation path. There is no prominent slow tail. In the simplest cases the predominant repeated feature is a double pulse (i.e. one half-cycle of each sign) lasting about 200 μsec, the negative portion usually occurring first (fig. 1 (A)). In the intervening periods minor ripples, of one-fifth or less of the pulse amplitude, and with frequencies three, four or five times that of the pulse repetition interval, may be present. These are subsequently termed ' harmonics '. More complex waveforms are observed when the outer parts of the double pulse have much reduced slope, frequently overlapping the preceding and following peaks to give a sawtooth appearance with superposed ripples (fig. 1 (B)). In some cases, the quasi-symmetrical pulses retain their shape throughout the wave form as in fig. 1 (A) ; more usually, the later pulses become predominantly negative as in fig. 1 (B). Generally, the successive pulses decrease in size, eventually becoming barely discernible in the rippled background.

3.2. *Unsymmetrical Peaked Long-Train Forms* (fig. 2) (Plate 27, fig. 2 (A–D))

This variety, also observed from storms within 2000 km under full night-time conditions, is distinguished from the previous type by the presence, usually, of a pronounced slow tail, and the fact that the two half-cycles of the double pulse are of markedly different amplitudes over a large part (frequently the whole) of the waveform. The degenerate peak may be indistinguishable in the background ripple (figs. 2 (A), 2 (B)).

Any comparability of amplitude of the two half-cycles is usually restricted to the earlier discrete pulses. Occasionally, however, the pulse shape changes from a single half cycle to a symmetrical full cycle and then back again, within a range of some ten pulses (fig. 2 (C)) ; the

earlier unsymmetrical pulses may have either sign with respect to the later ones.

In all these waveforms, the major half-cycle of the late-order pulses is invariably of opposite sign to that of the slow tail, and is most often negative. With increasing pulse order, the minor half cycle tends to negligible proportions and the predominant crest becomes less sharp, while the amplitude of the intervening ripple decreases more slowly than that of the main peaks.

3.3. *Rounded Long-Train Forms* (fig. 3) (Plate 28, fig. 3 (A and B))

For storms beyond about 2000 km at night, and also for closer storms during the twilight periods, the waveforms are of a more rounded nature than those previously described. The ripple content is much less pronounced and confined to the second and third harmonics of the repetition frequency. Again, the sign of the major later order peaks is opposite to that of any associated slow tail.

In some waveforms, the rounded character is most evident for the late-order pulses and the peaks are predominantly of one sign (usually negative). Other atmospherics have a comparatively smooth appearance throughout the complete waveform, and in these cases, the sign of the sharper half cycle of the main pulse often reverses between the earlier and later orders, the amplitude in the intermediate portion being small (fig. 3 (B)).

3.4. *Smooth Long-Train Forms* (fig. 4) (Plate 29, fig. 4 (A and B))

These waveforms are quasi-sinusoidal throughout the trace. The oscillation amplitude is small and in general decreases very slowly with increasing order after the first few crests. The greatest amplitude normally corresponds to about the fourth reflection order, and a minor subsidiary maximum frequently occurs near the twentieth order. On occasions, the slow tail is the only feature in the waveform of sufficient amplitude to trigger the recording system ; in such cases, the earliest peaks of the long train are not photographed.

§ 4. Interpretation of Long-Train Waveforms

The current in the channel of a lightning discharge during a return-stroke is considered to be unidirectional, and although this current may pulsate in magnitude and the radiation field may therefore be complicated, it is generally accepted that the major oscillatory features observed in the waveforms of most atmospherics result from propagation influences. Many workers have analysed waveforms in terms of a simple primary pulse, generated by the discharge, followed by a series of pulses produced by successive specular reflections of the original disturbance between the earth and an ionospheric layer of constant height h, and have attempted to derive values for the distance D of the flash and for h. In (C.P.) a critical discussion was given of the practical application of this approach and of the limitations and uncertainties of such analyses ;

it was concluded that the simple reflection picture successfully interprets the long-train waveforms.

Alternatively, the propagation, in a waveguide formed by the earth's surface and a concentric ionospheric layer, of the disturbance radiated from the discharge can be considered (Hales 1948, Budden 1951). If the reflecting ionospheric boundary is a good conductor, many wave-guide modes are propagated with slight attenuation and the wave-guide approach becomes complicated. In such circumstances, a pulse would be reflected with little distortion; the simple picture of specular reflections might be expected to apply and to yield reliable values of h and D, provided the duration of the primary pulse is less than the smallest interval between reflected pulses.

The existence of long-train atmospherics indicates an equivalent ionospheric layer of fairly high conductivity, and, in consequence, the applicability of the simple reflection picture. That this is so has been confirmed by Caton (1952) from observations using vertical and frame aerials. In addition, the presence of an extended series of pulses suggests that long-train waveforms are peculiarly suited to an accurate determination of h and D. Many long-train atmospherics have been examined on the reflection mechanism and the next section presents the results obtained.

§ 5. Analysis of Long-Train Waveforms

5.1. *Height and Distance Determination*

In the examination of the long-train waveforms the following procedure was found convenient. The major negative peaks were assumed to correspond to the successive sky waves unless the positive peaks were obviously sharper, the first prominent negative peak (the reference peak) being considered as due to the first order (i.e. once reflected) pulse. The intervals between successive peaks were measured and plotted against separation order, separation 'n' being the interval between peaks 'n' and '$n+1$'. The plotted points were then compared with calculated families of graphs, allowing for a curved earth, and drawn on transparent paper for values of h between 70 and 100 km in 5 km steps, and D ranging from 300 to 12 000 km in steps of 300 to 1500 km, and the best fit assessed. Relative movement of the observed and calculated curves along the common 'order' axis provided a sensitive indication of any apparent need to modify the assumption that the first peak was due to the first sky wave.

The quality of the fit with the reflection theory curves has been arbitrarily classed into four categories, corresponding broadly with the A–D classification of (C.P.).

Good fit: If one of the calculated curves fits far better than any other, and none of the observed intervals deviates by more than 15 μsec from the theoretical values indicated by this curve.

Fair fit: If the fit is moderate along any one curve and poor along

all others, or if the fit is moderate along two curves and suggests good agreement with an interpolated one. In a moderate fit few of the measured intervals depart from the calculated curve by more than 15 μsec and none by over 30 μsec.

Poor fit : If one or two curves obviously represent the best approach to a fit but the agreement is poor along these curves, with many intervals deviating by over 15 μsec, and some by over 30 μsec.

No fit : If there is an equally poor fit along several curves or there are major irregularities, i.e. intervals decreasing with increasing order.

Examples of the analysis of two waveforms giving good fits are shown in fig. 5.

Fig. 5

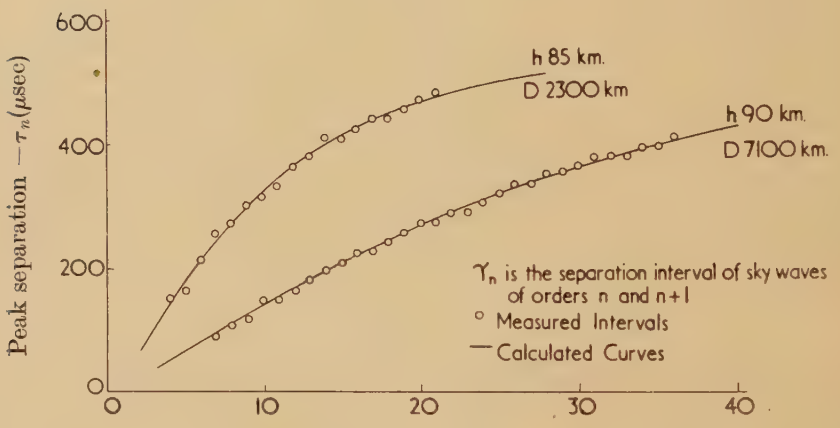

Two examples of the analysis of individual long-train waveforms on the simple reflection mechanism.

The choice of the negative peaks as corresponding to the sky waves follows Chapman (1950), and usually gives the better fit with theory. In addition, the negative peaks are generally more pronounced and less complex than the positive maxima thus simplifying the process of measurement. For the smooth forms the method is fundamentally insensitive to choice of sign.

Seventy-two night-time long trains have been analysed in detail on the basis of the simple reflection theory. 42 were peaked or rounded waveforms, the other 30 being smooth. 48 (67%) gave Fair to Good fits with theoretical prediction, and only in four cases could no fit be obtained. There was no significant difference in the quality of the fits of peaked rounded and smooth forms.

The results for h and D are plotted as fig. 6, showing that peaked and rounded waveforms are found up to about 4000 km, whereas all the smooth atmospherics originate at greater distances. The heights obtained range from 80 to 95 km with an average of $87{\cdot}8 \pm 0{\cdot}6$ km ; the mean values of h for the peaked, rounded and smooth forms,

respectively, are not significantly different. For atmospherics where Sferics fixes were available, the estimates for D did not differ from those obtained by waveform analysis by more than the errors of the two methods. No correlation between the discrepancy in distance estimates and the class of fit with reflection theory was apparent; but an appreciable correlation found between discrepancy and calculated distance indicates a tendency for Sferics fixes to underestimate increasingly the storm distances with increasing distance. It has been deduced that average errors of −200 and −500 km are to be expected in the Sferics fixes at distances of 1500 and 2500 km respectively.

Fig. 6

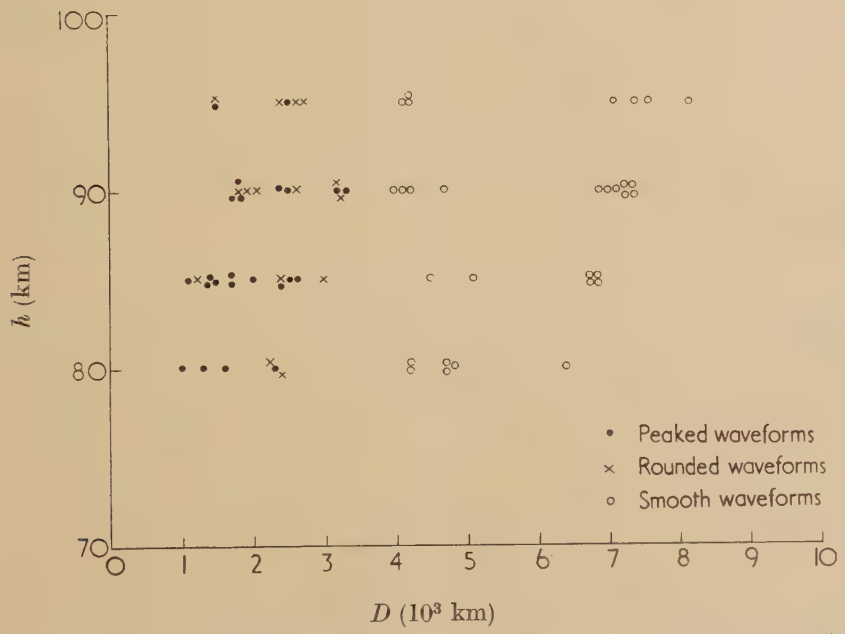

The analysis of the three principal types of long train waveform upon the basis of the simple reflection theory.

The initial portion of a peaked long-train waveform is frequently very complicated with several major and minor peaks (e.g. fig. 2 (D)). In consequence, during the analysis it was often desirable to adopt a peak of comparatively late order (say the fifth) as the reference peak, when measurement of the subsequent pulse intervals usually provided a satisfactory solution for h and D. Extrapolation back to the start of the waveform, on the basis of these values, yielded the surprising result that there was frequently a substantial portion of the atmospheric, of up to half a millisecond duration, occurring before the disturbance corresponding to the ground wave of the reflection theory solution. In many cases, it was also apparent that the number of major peaks preceding the reference peak, was greater than that required by the

reflection theory solution adopted. Even when no discrepancy regarding the number of visible peaks existed, the positions of the first four or five were often significantly removed from those indicated by the solution derived from the major portion of the long train ; the error was generally systematic, with the observed intervals of the initial peaks greater than those predicted. Straightforward application of the reflection hypothesis to the first few oscillations only, assuming the first negative peak to be the first sky wave, often yields an h value of about 40 km (Pierce 1949) and a spurious, very small estimate for D. It was shown in (C.P.) that reflection heights of 40 km, associated with small estimates of range, were incompatible with information derived from Sferics fixes, and it was concluded that they were invalid. Apart from these systematic discrepancies among the earlier peaks, it can be concluded that the time intervals between the major peaks of a long-train waveform are remarkably well described by the simple picture of successive specular reflections from a constant height, and that the majority of waveforms of this type will yield a reliable value for h and D. For Fair or Good fits there is no apparent ambiguity in establishing the order of the reference peak, and the uncertainty in the estimation of D is under 10%.

5.2. *Pulse Amplitudes*

Peak to peak amplitudes were measured for selected pulse orders of the 68 long-train waveforms already analysed for h and D. The maximum pulse amplitude was found to occur at higher reflection orders as the discharge distance increased, the first order being typically the largest at 1000 km, the third or fourth at 4000 km, and the seventh at 7000 km ; at these ranges the average maximum, peak-to-peak field strengths, were approximately 450, 200 and 100 mv/m, respectively. However, an observing technique which utilizes an amplitude-operated trigger tends to select the largest atmospherics, and caution must be exercized in accepting the quoted field strengths as typical of the given distances.

The decrease in the amplitude of the pulses with increasing order, for four ranges of distance, is given in table 1, based upon the mean results of the 68 measured waveforms. The decrease is more rapid for the waveforms of closer origin.

Although the maximum amplitude occurred within the first few orders, it was noted that, in two-thirds of the atmospherics studied, a subsidiary maximum was also present at a later stage in the waveform. The order of the subsidiary maximum increased with distance as depicted in fig. 7, which shows that for distances of 1500, 4500 and 7500 km, the corresponding average orders of the subsidiary maximum are approximately 13, 18 and 21. A typical waveform, from a source 1500 km distant, might have an amplitude of 70 mv/m at pulse order 5, 30 mv/m at order 11 (the first minimum), 35 mv/m at order 13 (the subsidiary maximum), and 20 mv/m at order 20. At 7000 km, characteristic

magnitudes are 6 mv/m at order 15, 10 mv/m at order 20 (the subsidiary maximum) and 3 mv/m at order 40.

Table 1. Pulse Amplitude Variation with Order and Distance

Distance range (km)	Amplitude (mv/m) for pulse order 5	10	15	20	30	40
1000–2000	70	33	26	13	—	—
2000–4000	70	28	20	14	5	3
4000–6000	—	13	9	9	6	4
6000–8000	—	14	8	8	5	3

Fig. 7

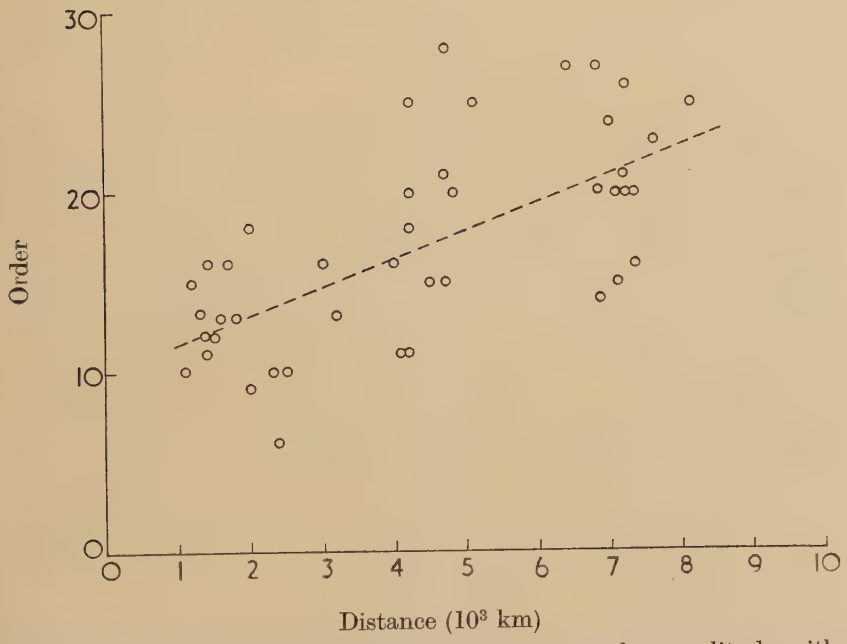

Variation of order at the subsidiary maximum in pulse amplitude with the distance of origin of the waveform.

The pulse magnitudes for eight waveforms recorded during November and December evenings, and originating in the W. Mediterranean area at distances between 1200 and 1800 km, have been examined in greater detail. Their analyses, in reasonable agreement with individual Sferics fixes, gave mean values for the whole group, of $h=85$ km and $D=1400$ km. The variation of amplitude with pulse order shows a minimum in seven cases, at or next to order 10, followed by a subsidiary maximum. In one case the amplitude decay was uninterrupted. In the average curve (fig. 8), the subsidiary maximum is less pronounced although its existence is still recognizable.

Fig. 8

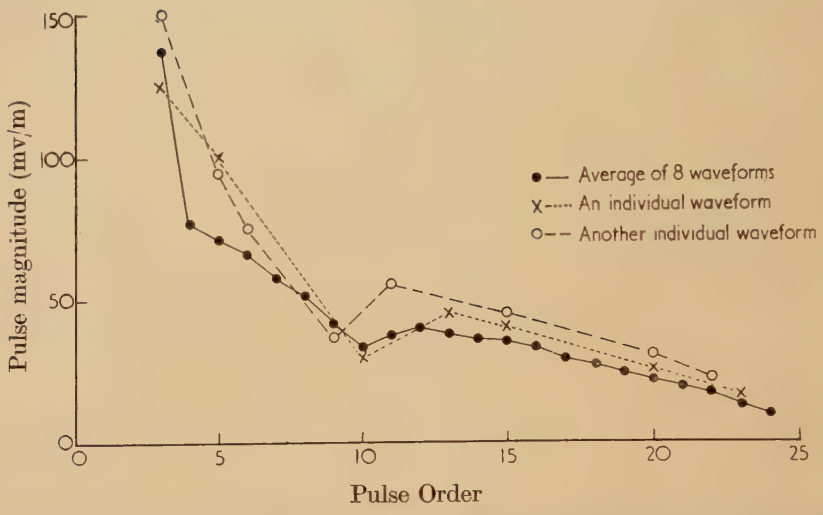

The variation of pulse magnitude with order for a group of 8 atmospherics originating in the same area (D between 1200 and 1800 km). An average curve and two individual examples are given.

§ 6. Origin of Long-Train Waveforms

Whenever peaked or rounded long-train atmospherics were observed, a storm was usually found to be active in the quadrant to the S.E. of the British Isles, and almost all the waveforms of this type with individual fixes originated over S.E. Europe or the Mediterranean area. A few long-train waveforms were recorded from close storms to the S.W., but none were observed to originate from beyond 1500 km in this direction (cf. (C.P.)). When the propagation path lay entirely over regions where full night-time conditions prevailed, such storms to the S.W. and all storms to the S.E. always gave long-train or irregular high-frequency waveforms ; i.e. under these circumstances the long-train atmospheric is the typical form generated by a return-stroke.

The location of the origin of the smooth forms is more difficult because, as analysis indicates, it is beyond the limiting range of the Sferics system (about 3000 km). Thus no significant individual fixes for the smooth forms have been obtained nor is detailed information about storms at such distances available. Examination of the main winter storm centres (Brooks 1925) shows the chief sources to be over the Mediterranean (1000–3000 km), along a band from the Near East and Persia to India (3000–7000 km), in Africa (at distances exceeding 4500 km), this being the most intense activity, and in Central and South America (beyond 6500 km). In view of the existence of transitional waveforms (the Rounded forms) it is natural to consider that the smooth forms originate at greater distances, but in the same direction as the peaked forms. This would suggest sources in Africa for the smooth forms, and the few

D.F. bearings available support this hypothesis. Figure 6, however, shows surprisingly few smooth atmospherics yielding distances between 5000 and 6800 km, which is unexpected considering the extent of the African storm areas. This quiet zone may be largely fortuitous or the enhanced activity at 7000 km may be due to other centres such as S. India or S.E. Asia. It appears unlikely that American storms could produce any of the night-time long-train waveforms recorded ; firstly, the American regions concerned would be in daylight ; secondly, storms located over the intermediate Atlantic areas more than 1500 km from the British Isles, have never been observed to produce long-train waveforms.

§ 7. Discussion of Pulse Amplitude Variation

The amplitude of the vertical field E_n, at the receiving aerial, for a disturbance radiated by a vertical dipole, and suffering n ionospheric reflections, is given (Bremmer 1949) by

$$\frac{P}{D}\sin\theta_n\left(\frac{\alpha_n}{\sin\alpha_n}\right)\sin^2(\theta_n+\alpha_n)C_n\{1+R_g(\theta_n+\alpha_n)\}^2\{R_g(\theta_n+\alpha_n)\}^{n-1}\{R_i(\theta_n)\}^n$$
$$=KF_n\{R_i(\theta_n)\}^n$$

say, where $(\theta_n+\alpha_n)$ and θ_n are angles of incidence at the earth and ionosphere (height h), respectively, D is the great circle surface distance between source and receiver over the earth of radius r, $\alpha_n=D/(2nr)$, $R_i(\theta_n)$ and $R_g(\theta_n+\alpha_n)$ are ionosphere and ground reflection coefficients for the indicated angles of incidence, C_n is the convergence coefficient, P is a constant depending upon the current and size of the original flash, and K a factor, independent of n, $=P/D$.

The mean observed results for E_n given in fig. 8 refer effectively to $D=1400$ km and $h=85$ km. Calculated values for F_n, with the same D and h, show that the variation in F_n with n is primarily due to the factor $\sin\theta_n\sin^2(\theta_n+\alpha_n)$ since C_n and $\alpha_n/\sin\alpha_n$ are both approximately unity, and $R_g(\theta_n+\alpha_n)$ is only slightly less than one for the frequencies (1 to 20 kc/s), and ground electrical constants (conductivity $\sigma=10^{-11}$ to 10^{-15} e.m.u., dielectric constant $\epsilon=3$ to 80) concerned.

The ratio $E_n/F_n=K\{R_i(\theta_n)\}^n$ is plotted in fig. 9 and shows a steady rise with n ; this implies $\{R_i(\theta_n)\}^n$ increasing with n which is most unlikely. An increase may be possible, when the pseudo-Brewster angle corresponds to a fairly high n, but then the reflection coefficients would be too low to give appreciable amplitude in the later orders of the waveform. Calculation confirms that $\{R_i(\theta_n)\}^n$ for an isotropic homogeneous conducting ionospheric layer with $\epsilon=1$, $\sigma=10^{-17}$ to 10^{-12} e.m.u., and frequencies between 1 and 20 kc/sec, cannot increase with n.

7.1. *Horizontal Radiating Channels*

An escape from these difficulties has been sought by considering the possibility that the main radiating channel is horizontal rather than vertical. Ignoring, for the moment, the image current in the earth,

the polar factor ($\sin\theta_n \sin^2(\theta_n+\alpha_n)$ for a vertical transmitting dipole), due to the radiation polar diagrams in the vertical plane of the source and receiving aerials, would be $\sin\theta_n \sin(\theta_n+\alpha_n)\cos(\theta_n+\alpha_n)$ if the horizontal channel lay in the plane of propagation (Haubert 1944). The signal for a similar channel at right angles to the direction of propagation would have its electric vector horizontal. While the response of the receiving aerial is proportional to the vertical electric field at the ground, it is known from long wave propagation experiments (Bracewell *et al.* 1951), and from studies of the polarization of atmospherics (Caton 1952), that considerable interconversion of vertical and horizontal components of field occurs on ionospheric reflection. Indeed this effect may explain many of the difficulties encountered. It seems

Fig. 9

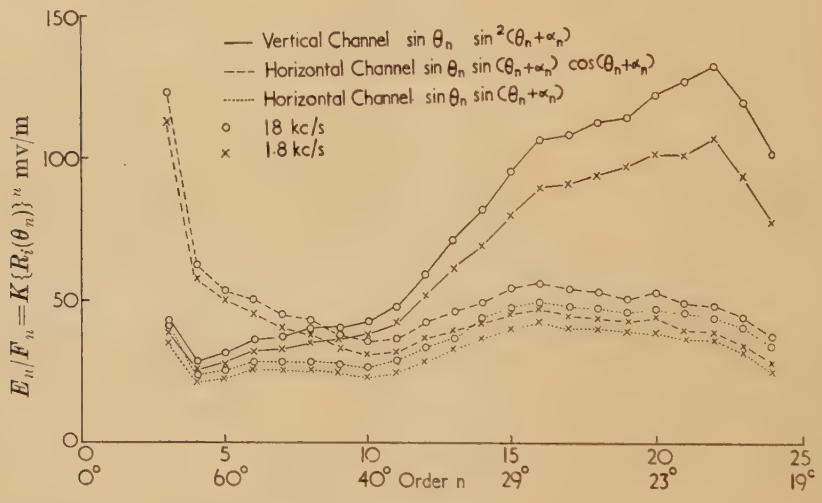

Comparison of observed values for successive pulse amplitudes with those predicted for various lightning channel orientations and polar factors.

legitimate to assume that a horizontal channel at right angles to the plane of propagation can produce an observable signal, the effective polar factor being $\sin\theta_n \sin(\theta_n+\alpha_n)$.

For a horizontal channel, the presence of the earth, assumed perfectly conducting, introduces a further polar factor $\sin\{(2\pi l)/\lambda \cos(\theta_n+\alpha_n)\}$, where l is the height of the channel. If $l \ll \lambda/10$ and $(\theta_n+\alpha_n) \gtrsim 34°$, this factor lies between 0·5 and unity, and thus, for frequencies of 10 kc/s ($\lambda=30$ km) and greater, may, to a first approximation, be ignored for the higher order pulses. In fig. 9 the ratio of observed E_n to F_n (computed for the two horizontal channel polar factors) is plotted, and will be seen to be approximately constant for $n>4$, implying that $R_i(\theta_n) \simeq 1$, i.e. that the ionospheric layer is an exceedingly good conductor. This is far more plausible than the increasing value of $\{R_i(\theta_n)\}^n$ deduced for a vertical

discharge, though the high conductivity implied (almost as great as for the earth) is somewhat unexpected. It should be remembered that the effect of the earth's magnetic field has been completely ignored, and it is well known that its presence can reduce the low frequency propagation attenuation factor enormously.

Table 2. Incidence Angles for Subsidiary Maximum

Average distance (km)	Average order	At ionosphere θ_n	At ground $(\theta_n+\alpha_n)$
1500	12	35·8°	36·4°
4500	17	56·7°	57·9°
7500	22	62·6°	64·1°

It might be expected that the subsidiary amplitude maximum would always occur for particular angles of incidence at the earth and ionosphere. Figure 7, however, shows that the pulse order for the subsidiary maximum, is far from constant at a given range, and even the mean values, if averaging can be justified, give varying angles of incidence (table 2).

7.2. *Vertical and Horizontal Channels*

It is unlikely that the mere deflection of the simple return-stroke channel into the horizontal, on reaching the cloud, for example, would be capable of producing comparable amplitudes from its vertical and horizontal portions. The major source of energy for the radiation pulse, if it is to be sharp, is the charge, deposited during the leader process, upon the lower parts of the channel, where it is easily available to produce a large surge current after establishment of the earth connection. At this stage, the radiation is effectively due to a short vertical channel near the ground. However, many flashes to earth contain a main vertical channel and outspreading branches ending in the air. As the return stroke progresses up the channel and along its branches, the radiation will be generated initially in the vertical channel, but later, appreciable contributions may come from both horizontal and vertical portions, as each branch is reached, and a sudden surge of current flows the whole length of the channel to neutralize the charge on the branch resulting from the leader stage. The branch must be long compared with the vertical channel if its contribution is to predominate, as the horizontal radiating channel has to grow from zero length, whilst the length of the vertical channel is constant at its full value. If the concept of ionization decay (Schonland 1938) is accepted, the return stroke will be accelerating along the branch into regions of more intense ionization, the current in the return stroke channel will increase, and the resulting radiation pulse be sharper. The mobility of the charge on the branch and its own attraction to the advancing return stroke will tend to enhance this effect.

Evidence supporting the concept of the formation of a secondary radiating channel has been given above (§ 5.1) where observations showed that a substantial portion of some atmospherics occurs before the time of the initial disturbance, as given by the best reflection theory solution for the major part of the waveform. The complete atmospheric may be interpreted, as an initial disturbance from the vertical channel giving successive pulses rapidly decreasing in amplitude due to the vertical polar factor ; a stage, after a branch has been reached, when the horizontal channel is producing reflected pulses of small but increasing amplitude (decreasing components from the vertical channel being possible also) ; and a final stage when the reflections from the horizontal channel are dominant.

Although this picture explains the major features of the observed phenomena, many problems remain. When the return-stroke current flows the whole length of a vertical channel and a horizontal branch, the length of the branch must considerably exceed that of the vertical channel, if radiation from the horizontal part is to dominate, but if the image effect is to be negligible the height of the horizontal branch (i.e. the length of the vertical channel) cannot be small ; these two requirements appear to be mutually inconsistent. Again, the precise reason for the subsidiary maximum, and the manner in which the orientation of any horizontal channels affects the received signal, remain obscure.

§ 8. Pulse Shape Variation

The change from a peaked to a smooth waveform, with increasing order for a given distance, and with increasing distance, is consistent with the trend of the variations in $\{R_i(\theta_n)\}^n$. As the result of this factor alone, calculation shows that with ionospheric constants $\epsilon=1$ and $\sigma=10^{-15}$ e.m.u., and atmospherics from 1400 km, for example, the ratio of relative amplitudes at 18 kc/s and 1·8 kc/s, changes from 0·37 for the 6th pulse to 0·17 for the 18th. The corresponding figures are 0·17 and 0·05 for the 18th pulse of waveforms from 1400 and 4200 km respectively.

The intermediate ripples and details of the change in shape of the successive pulses, in a single waveform, have not been explained. Some indication of the causes of these phenomena can be sought in the duration of the original pulse and in the distortion resulting upon reflection. The initial disturbance may last for 30 μsec or more with appreciable Fourier component amplitudes at frequencies less than the peak separation frequency, and although the ionosphere may be a comparatively good conductor, there will inevitably be a lengthening of a pulse at every reflection. It is considered that many of the minor phenomena observed are due to the pulses being of appreciable duration ; the simple reflection picture, successful for the major features of long-train atmospherics, implies a short pulse, and is not therefore entirely valid. Detailed Fresnel

reflection theory would, of course, yield a true interpretation, but in view of the uncertainties concerning many of the parameters involved, its practical application would be unprofitable.

§ 9. Conclusion

Discussion of the long-train waveforms as examples of successive pulses reflected from the ionosphere, has shown the observations to be in good agreement with theory for the temporal relationships. The amplitudes of the reflected pulses suggest the presence of horizontal radiating channels in the lightning discharge ; this concept is supported by certain temporal effects near the beginning of the waveforms. Such a postulation is not without difficulties ; notably, the surprising preponderance of pulses of one sign, considering that the orientation of the horizontal component is random with respect to the direction of propagation, and the difficulty of obtaining sufficient radiation from a horizontal channel.

Acknowledgments

This work forms part of a research programme, supported by the Department of Scientific and Industrial Research, at the Cavendish Laboratory and the Observatories, Cambridge University. We are grateful to the Directors of these two establishments for the provision of suitable facilities, and to Dr. P. G. F. Caton and Mr. R. E. Brundish for assistance with recording.

During the observations and in preparing this paper, Dr. T. W. Wormell has given advice and encouragement, for which the authors desire to express their appreciation.

The Director of the Meteorological Office, and the Sferics staff of the Central Forecasting Office, Dunstable, have been most courteous and cooperative, in supplying Sferics information.

References

Bracewell, R. N., Budden, K. G., Ratcliffe, J. A., Straker, T. W., and Weekes, K., 1951, *Proc. I.E.E.*, **98** (III), No. 53.

Bremmer, H., 1949, *Terrestrial Radio Waves* (Amsterdam : Elsevier Publishing Company).

Brooks, C. E. P., 1925, *Met. Off. Geophys. Mem.*, No. 24.

Budden, K. G., 1951, *Phil. Mag.*, **42,** 1.

Caton, P. G. F., 1952, *Ph. D. Thesis,* Cambridge University.

Caton, P. G. F., and Pierce, E. T., 1952, *Phil. Mag.*, **43,** 393.

Chapman, F. W., 1950, *Proc. of U.R.S.I.*, A. G. Zurich, Comm. IV, Doc. No. 253.

Hales, A. L., 1948, *Proc. Roy. Soc.* A, **193,** 60.

Haubert, A., 1944, *Notes Préliminaires du Lab. Nat. de Radioelectricite,* No. 54.

Pierce, E. T., 1949, *Nature, Lond.*, **164,** 512.

Schonland, B. F. J., 1939, *Proc. Roy. Soc.* A, **164,** 132.

Watson-Watt, R. A., Herd, J. F., and Lutkin, F. E., 1937, *Proc. Roy. Soc.* A, **162,** 267.

Explanation of the Plates

Description of the Waveform Examples (figs. 1, 2, 3 and 4)

Triggering occurs at an arbitrary point of the horizontal sweep which is of 10 msec duration. A vertical deflection of 1 cm corresponds to a field strength of about 100 mv/m. The data given consists of the date and approximate time of recording ; the Sferics fix for the individual waveform or storm-centre in terms of geographical location, range and azimuth ; and a general description of the main features. For clarity, a few of the fainter portions of the records have been traced over with white ink.

Figs. 1 and 2. Peaked long train waveforms, several from the same storm centre indicating the wide variety of detail attributable to source effects. Waveforms of fig. 1 have symmetrical pulses whereas those of fig. 2 have peaks predominantly of one sign associated with slow tails of the opposite sense.

1A. 27/5/51, 23.00. N. Germany, 900 km, 85°. Early order reflection pulses are confused, eventually becoming discrete double impulses separated by almost quiescent intervals.

1B. 28/5/51, 00.50. N. Germany, 900 km, 85°. Distinct early orders, sawtoothed with rippled sloping trace between crests. Pulses become negative after 14th order.

1C. 14/11/50, 22.00. N.E. Italy, 1000 km, 120°. Earliest orders recorded are discrete. Symmetry persists throughout trace.

1D. 14/11/50, 20.00. N.E. Italy, 1200 km, 123°. Precursor triggered waveform with unambiguous early order peaks.

2A. 20/11/50, 20.55. Tyrrhenian Sea, 1400 km, 139°. Early and late orders are discrete negative pulses. Some confusion in mid orders.

2B. 28/5/51, 00.50. N. Germany, 900 km, 85°. Sharp negative peaks throughout waveform separated by near quiescent intervals.

2C. 28/5/51, 00.50. N. Germany, 900 km, 85°. Waveform showing positive peak—double pulse—positive peak transition.

2D. 18/12/50, 20.55. Tyrrhenian Sea, 1400 km, 137°. Confused early orders followed by distinct negative peaks.

Figs. 3 and 4. Fig. 3 shows the rounded waveforms characteristic of more distant sources or recording times earlier in the evening, than for figs. 1 and 2. Examples of the smooth waveforms received from very distant storms are given in fig. 4.

3A. 8/2/51, 21.25. N. E. Greece, 2200 km, 116°. Rounded and distinct pulses of more distant origin.

3B. 20/11/50, 20.00. Corsica, 1300 km, 143°. Rounded waveform from early evening storm. Late order peaks are negative, opposite in sign to the first half cycle of the slow tail.

4A. 28/5/51, 01.20. Sierra Leone, 4000 km, 194°. Smooth pulses of a waveform almost devoid of irregularity from a distant source late at night.

4B. 12/12/50, 18.00. Libya, 3000 km, 160°. Completely smooth form from distant source occurring in early evening. Analysis gives a fair fit with $D=4200$ km, and $h=80$ km.

IB

ID

IA

IC

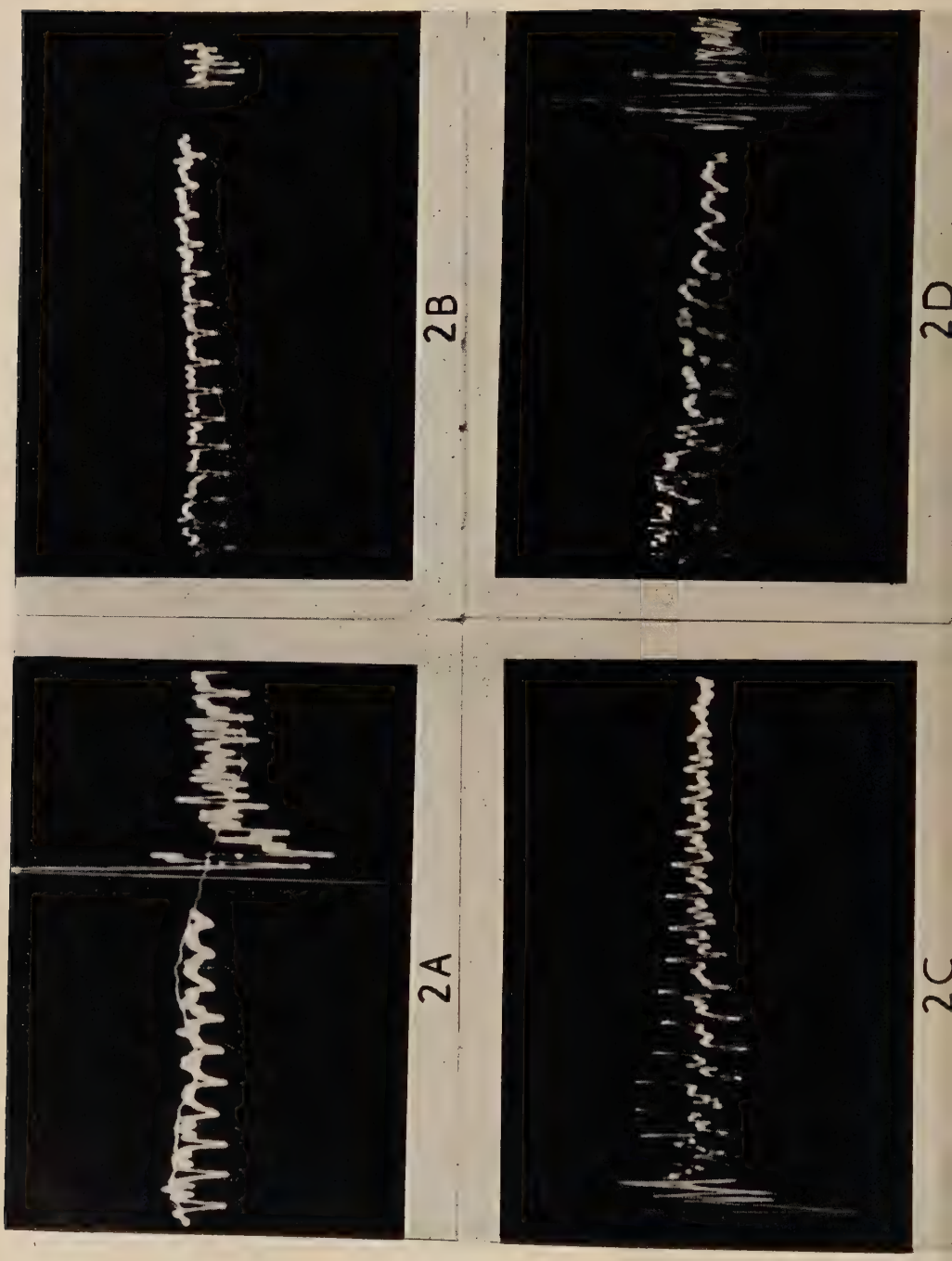
2B
2D
2A
2C

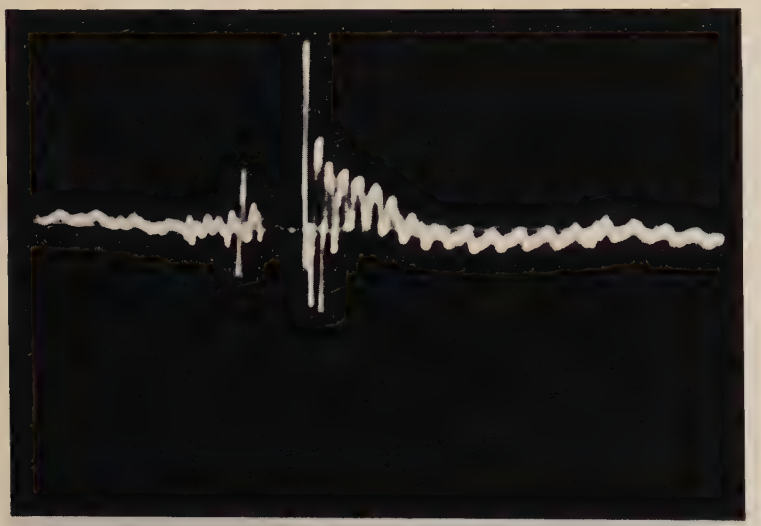

3A

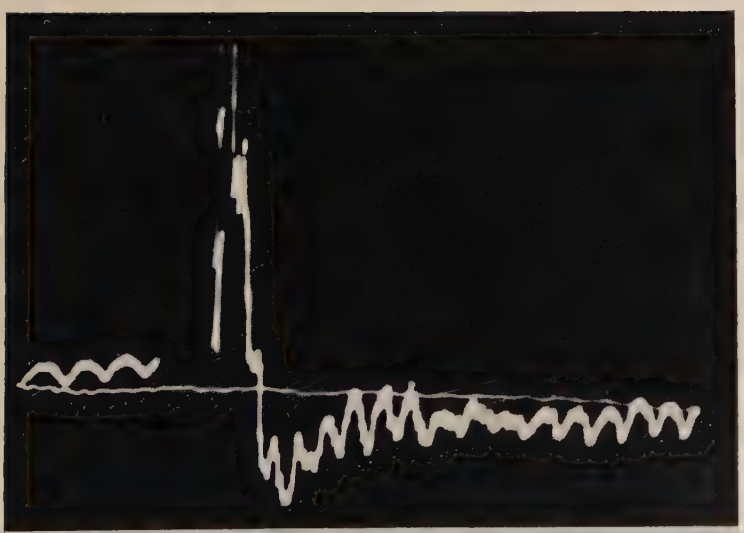

3B

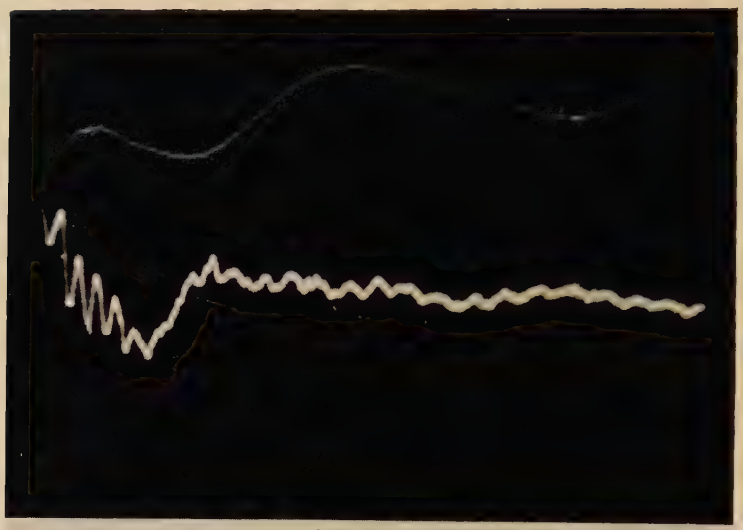

4 A

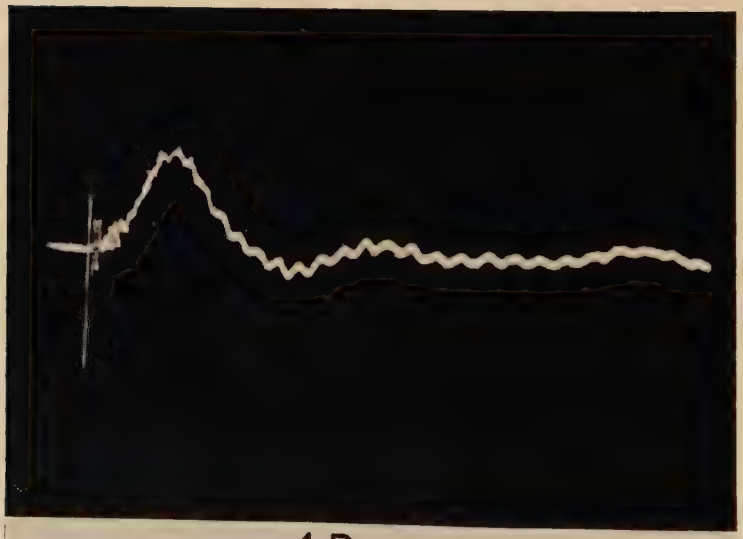

4 B

CII. *Large Angle Scattering of μ-Mesons in Lead*

By I. B. McDiarmid
The Physical Laboratories, The University, Manchester*

[Received April 8, 1954]

Abstract

A multiplate cloud chamber, operated underground, has been used to investigate the scattering of μ-mesons in lead over a wide range of meson energies. The large angle 'tails' of the measured distributions have been compared with those expected from Molière's theory for a 'point' nucleus and Olbert's modification of this theory for a 'solid' nucleus. At energies of a few hundred Mev the method used is not capable of distinguishing between these two theories but at higher energies the measured distributions fall very near to those expected from Molière's theory. No explanation of these departures from the expected distributions for a 'solid' nucleus is offered, but they are in agreement with those found by other workers. It is pointed out that such departures may be due to deficiencies in the theory and do not necessarily indicate a non-Coulomb interaction between fast μ-mesons and nucleons.

§ 1. Introduction

There is strong evidence that apart from Coulomb forces the interaction between stopped μ-mesons and nucleons is extremely weak (see Sard and Crouch 1954). If this is also true for fast μ-mesons, measurement of the scattering distribution at large angles in a finite absorber, which is due mainly to single scattering collisions, should yield information about the processes involved when a particle is scattered by Coulomb forces within the nucleus, i.e. charge distribution, incoherent scattering, etc. If the exact scattering distribution due to Coulomb forces were known, the measurements could be used to investigate the existence of any additional interaction between fast μ-mesons and nucleons. A summary of most of the work reported to date, on the large angle scattering of μ-mesons, is given in a recent paper by Leontic and Wolfendale (1953). In general, more large angles have been observed than can be accounted for by certain scattering theories; this component of the scattering is referred to as 'anomalous', and it has been suggested by several authors that it indicates some additional μ-meson–nucleon interaction.

In the present experiment the large angle 'tails' of the scattering distributions have been examined over a wide range of meson energies. The part of the scattering distribution occurring at smaller angles, and

* Communicated by H. J. J. Braddick.

due mainly to multiple scattering, has been used to estimate the meson energies. The large-angle distributions observed at the different energies have been compared with those expected from Molière's theory for a ' point ' nucleus as given by Bethe (1953) and Olbert's (1952) modification of this theory for a ' solid ' nucleus. This modification amounts to neglecting, in the final distribution, the effect of single scattering collisions through angles greater than $\lambda\!\!\!^{-}/R$ where $2\pi\lambda\!\!\!^{-}$ is the De Broglie wavelength of the particle and R is the nuclear radius. For a given energy Olbert's distribution is nearly Gaussian, while Molière's theory gives at large angles a distribution falling off as the reciprocal of the cube of the scattering angle. These theories have been used only as standards with which to compare the results. Even for elastic Coulomb interactions neither theory might be expected to predict accurately the distributions at high energies and large angles: at best, they probably represent two more or less extreme cases.

Recent experiments (Fitch and Rainwater 1953, Cooper and Henley 1953, Bitter and Feshbach 1953) indicate that the nuclear radius for electromagnetic interactions may be smaller than the value previously accepted. Writing this radius as $R=r_0\times 10^{-13}A^{1/3}$, the above authors find that r_0 lies in the region 1·0 to 1·2 rather than 1·4 as assumed by Olbert. Hence, in some cases, the measurements reported here have also been compared with Olbert's theory for $r_0=1{\cdot}0$. The theory modified in this way still contains the same approximation used to deal with the finite nuclear dimensions and the effect of this may still be large compared to the effect of the smaller nuclear radius.

§ 2. Experimental Arrangement

The experiment was performed underground, at a depth equivalent to 26 metres of water, in order to ensure that the incident flux was practically free from particles with strong nuclear interaction. The cloud chamber, containing six 2 cm lead plates, was of the conventional circular type 43 cm in diameter and with 14 cm illuminated depth. The expansions were triggered by the simple counter telescope shown in fig. 1. The requirement that the triggering particle should pass through the counter tray under the chamber introduced an angular selection which at large scattering angles gave a bias in the scattering distribution. However, for a particle to be selected for the present analysis it must have passed through all six plates and hence some angular selection was present in any case; placing a tray under the chamber increased the bias only slightly while it improved the efficiency of obtaining useful pictures considerably. The effect of this bias on the expected scattering distributions is dealt with in Appendix II.

The tracks were photographed by two cameras, one mounted centrally on the axis of the chamber and the other mounted 15 degrees off the axis. The centrally mounted camera was 210 cm from the chamber and very little of the effects of the gas motion at expansion were observable on the

photograph taken with this camera. Only on the extreme edges of the chamber could any curvature of the track near the plates be detected and this was very slight. Photographs taken with this camera were used to measure the projected angles of scattering. These angles were measured by projecting the image of the track on to a rotatable circular screen on which parallel lines were drawn. The screen was rotated until the lines were parallel to the segment of the track being measured, the angle through which the screen had been rotated was then read off a scale (to 0·1°) ruled on the circumference. This procedure was equal in accuracy to using a microscope fitted with a goniometer eyepiece and produced much less strain on the operator.

Fig. 1

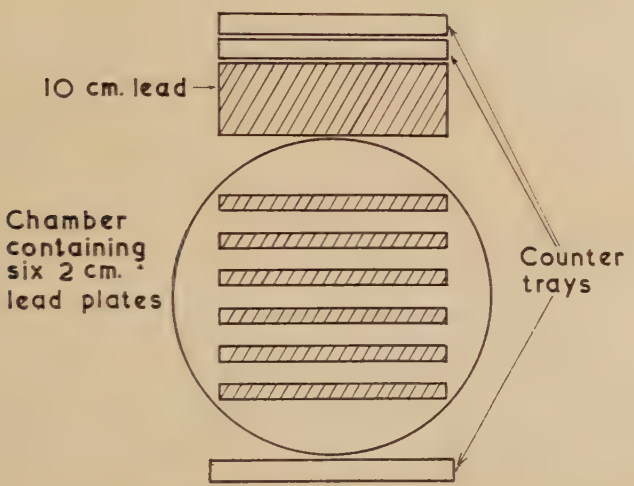

Experimental arrangement.

For a large number of particles selected at random, frequency plots of positive and negative deflections occurring in individual plates showed that systematic errors (due to distortion) in the angle measurements must be less in absolute value than 0·2°. The random errors, which are considerably larger, are discussed below.

§ 3. Momentum Estimation and 'Noise Level' Scattering

The r.m.s. (root mean square) angle of multiple scattering is a function of the quantity $p\beta$ where p is the momentum of the particle, in units of Mev c, and $c\beta$ is the velocity. This fact has been used for some time in photographic emulsion techniques to obtain $p\beta$ for individual particles from a large number of readings of the scattering angles. In a multi-plate cloud chamber where only a small number of readings is available for each particle the method is not very satisfactory, although it still yields useful information (Annis, Bridge and Olbert 1953). For a chamber containing six plates, such as the one used here, the 50% statistical

limits on the $p\beta$ estimate are approximately $\pm 30\%$. However, if from a large number of particles those are selected which have r.m.s. values within a given interval, and if all that is required is the $p\beta$ spectrum of these particles as a group then, under certain assumptions, this can be reasonably well determined even if the individual r.m.s. angles are computed from a small number of readings. In fact, if the assumptions are satisfied, the limits within which the spectrum can be determined depend only on the total number of particles available.

The assumptions made in the determination of $p\beta$ are the following: (*a*) there is no ionization loss in the plates, (*b*) the multiple scattering distribution is normal, (*c*) 'noise level' scattering, which is the result of all random errors affecting the angle measurements, is present and this is normally distributed. The scattering distribution at large angles may depart significantly from normal, and in fact these departures form the subject of this investigation. It was therefore necessary to apply a large-angle cut-off to the angles used for estimating $p\beta$. If one of the six measured angles for any track was greater than 3·5 times the r.m.s. value of the remaining five angles it was excluded. This has ensured that only the essentially multiple part of the scattering distribution has been used in the $p\beta$ estimate and in particular that the assumption of a normal distribution is justified. For reasons of simplicity the calculations have been carried out assuming that all r.m.s. angles are based on six readings and the fact that a small number are computed from only five readings introduces a slight error in the statistical treatment. This approximation has a negligible effect on the final $p\beta$ spectrum.

Let ϕ be the true projected angle through which the particle is deflected in passing through the plate; γ the error in a single determination of this angle; θ the measured projected angle of deflection.

It is assumed that the angles ϕ and γ are normally distributed with variances σ_0^2 and σ_1^2 respectively. Evidently θ is also normally distributed with variance

$$\sigma^2=\sigma_0^2+\sigma_1^2. \quad . \quad . \quad . \quad . \quad . \quad . \quad . \quad . \quad (1)$$

From the theory of multiple scattering

$$\sigma_0^2=\left(\frac{K(t)}{p\beta}\right)^2. \quad . \quad . \quad . \quad . \quad . \quad . \quad . \quad . \quad (2)$$

For lead and $\beta \sim 1$,

$$[K(t)]^2=5{\cdot}09t(5{\cdot}47+1{\cdot}24\log_{10} t)$$

where t is in g/cm^2 and $p\beta$ is in Mev/c. The quantity χ^2 is defined by

$$\tfrac{1}{2}\chi^2=\frac{n\langle\theta\rangle_n^2}{2\sigma^2} \quad . \quad . \quad . \quad . \quad . \quad . \quad . \quad . \quad (3)$$

where $\langle\theta\rangle_n$ is the measured r.m.s. angle obtained from n readings. Then $\frac{1}{2}\chi^2$ is distributed as (Weatherburn 1952),

$$P_1(\tfrac{1}{2}\chi^2)\,d(\tfrac{1}{2}\chi^2)=\frac{1}{\Gamma\left(\frac{n}{2}\right)}(\tfrac{1}{2}\chi^2)^{1/2(n-2)}\exp(-\tfrac{1}{2}\chi^2)\,d(\tfrac{1}{2}\chi^2). \quad . \quad . \quad (4)$$

Equations (1), (2), (3) and (4) give the probability of finding $\langle\theta\rangle_n$ in $d\langle\theta\rangle_n$ at $\langle\theta\rangle_n$ as a function of the two parameters $p\beta$ and σ_1, namely.

$$P_2(\langle\theta\rangle_n)d\langle\theta\rangle_n=\frac{2}{\Gamma\left(\frac{n}{2}\right)}\left(\frac{n}{2}\right)^{n/2}\frac{\langle\theta\rangle_n{}^{n-1}}{\left(\left[\frac{K(t)}{p\beta}\right]^2+\sigma_1{}^2\right)^{n/2}}\exp\left\{\frac{-n\langle\theta\rangle_n{}^2}{2\left(\left[\frac{K(t)}{p\beta}\right]^2+\sigma_1{}^2\right)}\right\}\times d\langle\theta\rangle_n. \quad \ldots\ldots\ldots \quad (5)$$

If σ_1 had been known eqn. (5) could have been used to estimate $p\beta$ from a single value of $\langle\theta\rangle_n$ (provided $\langle\theta\rangle_n$ is considerably greater than σ_1), and this is the problem dealt with by Annis *et al.*

In the present experiment eqn. (5) has been used instead to estimate σ_1. A measurement of $\langle\theta\rangle_n$ for a particle whose energy is so high that there is little real scattering in the plates is essentially a measure of the ' noise level ' scattering. The underground spectrum contains a large fraction of such particles. Hence, if particles are selected at random the frequency distribution of the measured $\langle\theta\rangle_n$ should be given at small angles by eqn. (5) by setting $p\beta\sim\infty$. The most probable value of $\langle\theta\rangle_n$ in this distribution is

$$\langle\theta\rangle_n{}^2\,(\text{Most probable})=\frac{n-1}{n}\sigma_1{}^2. \quad \ldots\ldots \quad (6)$$

Thus a determination of the position of this peak gives a measurement of σ_1. Figure 2 shows a frequency plot of $\langle\theta\rangle_n$ for 200 particles selected at random from which $\sigma_1=0{\cdot}5°$, this being the r.m.s. error (standard deviation) in a single measurement of angle. Also plotted in fig. 2 for comparison is eqn. (5) for the case $p\beta\sim\infty$, $n=6$, $\sigma_1=0{\cdot}5°$, normalized to the maximum of the measured distribution. The measured and calculated distributions do not differ significantly until $\langle\theta\rangle_n$ becomes larger than about 0·8° indicating that there is a sufficiently large fraction of high energy particles in the spectrum to justify the method, i.e. that the position of the peak is not affected by the real scattering of the lower energy particles.

Equation (5) gave the distribution of $\langle\theta\rangle_n$ as a function of $p\beta$ and σ_1, but in order to obtain a $p\beta$ spectrum for a group of particles whose r.m.s. angles lie in a given interval, a function is needed which will give the probability distribution of $p\beta$ as a function of $\langle\theta\rangle_n$ and σ_1. Assuming further that all values of $p\beta$ (or more exactly $1/\sigma$) are equally probable, eqns. (1) to (4) give such a function (see Appendix I), namely

$$P_3(p\beta)\,d(p\beta)=\frac{2}{\Gamma\left(\frac{n+1}{2}\right)}\left(\frac{n}{2}\right)^{(n+1)/2}\left[\frac{\langle\theta\rangle_n{}^2}{\left[\frac{K(t)}{p\beta}\right]^2+\sigma_1{}^2}\right]^{n/2}\frac{\langle\theta\rangle_n K(t)^2}{(K(t)^2+\sigma_1{}^2(p\beta)^2)^{3/2}}\times\exp\left\{\frac{-n\langle\theta\rangle_n{}^2}{2\left(\left[\frac{K(t)}{p\beta}\right]^2+\sigma_1{}^2\right)}\right\}d(p\beta). \quad \ldots\ldots \quad (7)$$

Because of the use of an approximation eqn. (7) is only valid if $\langle\theta\rangle_n$ is greater than about $2\sigma_1$. In the present analysis eqn. (7)

has been only used for values of $\langle\theta\rangle_n$ greater than 1°. It is clear that if $\langle\theta\rangle_n$ is much greater than σ_1 the distribution becomes independent of σ_1. There is, however, a range of values of $\langle\theta\rangle_n$ for which eqn. (7) is valid and the distribution is appreciably affected by σ_1; the high energy tail to the $p\beta$ spectrum of group 2 shown in fig. (3) arises from this cause.

Fig. 2

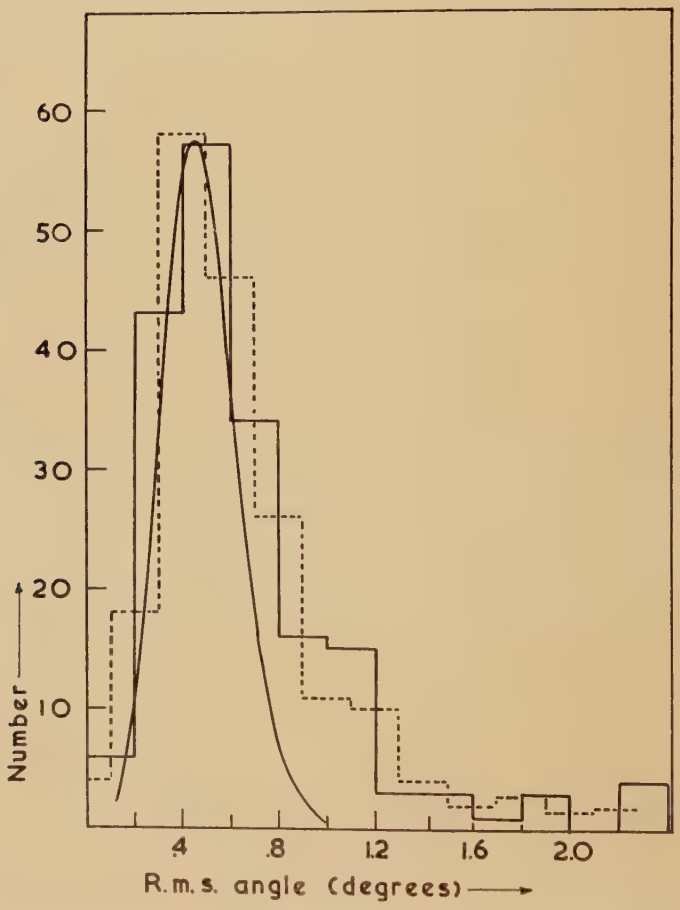

Frequency plot of the r.m.s. angles of 210 tracks selected at random from which the magnitude of the noise level scattering has been determined. The two histograms represent different groupings of the same data. The smooth curve represents eqn. (5) with $p\beta\sim\infty$, $n=6$ and $\sigma_1=0{\cdot}5°$.

Finally, if $N(\langle\theta\rangle_n)\,d\langle\theta\rangle_n$ is the part of a measured distribution of $\langle\theta\rangle_n$ which lies in the range $\langle\theta\rangle_n=a$ to b, the $p\beta$ spectrum of the particles in this range is given by

$$N(p\beta)\,d(p\beta)=\int_{\langle\theta\rangle_n=a}^{b} P_3(p\beta)\,d(p\beta)N(\langle\theta\rangle_n)\,d\langle\theta\rangle_n. \quad . \quad . \quad . \quad (8)$$

It has been assumed throughout that ionization loss in the plates is negligible. If this assumption is incorrect, as it is for some of the particles considered here, then a measurement of $\langle\theta\rangle_n$ gives information about the value $p\beta$ of the particle at the mid point of its trajectory (Bridge, Peyrou, Rossi and Safford 1953). Thus the procedure outlined above gives the $p\beta$ spectrum of the particles between the third and fourth plate when ionization loss is appreciable.

Fig. 3

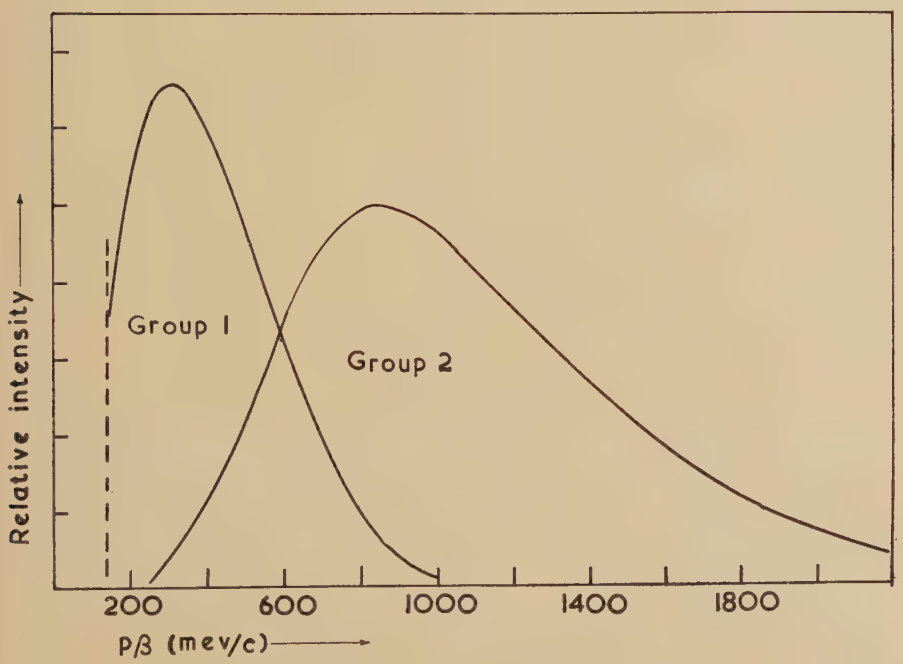

$p\beta$ spectra for groups 1 and 2.

§ 4. Results

Values of $\langle\theta\rangle_n$ have been obtained, using the large angle cut-off mentioned above, for about 6000 particles, which occurred singly in the chamber and traversed the six lead plates. The requirement that the particle should occur singly in the chamber decreased the probability of including secondary π-mesons or protons in the analysis. In fact, from the frequencies of fast π-mesons and protons found by George and Evans (1950, 1951) underground, it is estimated that the number of these particles included in the analysis is completely negligible. The frequency distribution of the measured r.m.s. angles has been divided into three groups covering the following ranges of $\langle\theta\rangle_n$: group 1—greater than or equal to 2·5°, group 2—1·1° to 2·4°, group 3—less than or equal to 1°. For groups 1 and 2 the $p\beta$ spectra have then been determined by a numerical integration of eqn. (8); see fig. 3.

The large-angle scattering analysis has been carried out by calculating

the integral distributions expected for each group from the theories of Molière and Olbert (Appendix II) and comparing these with the distributions observed in the individual plates.

The energies of some of the particles in group 1 are so low that they lose an appreciable fraction while traversing the plates, hence the spectrum shown in fig. 3 for this group refers to the values of $p\beta$ between plates 3

Fig. 4

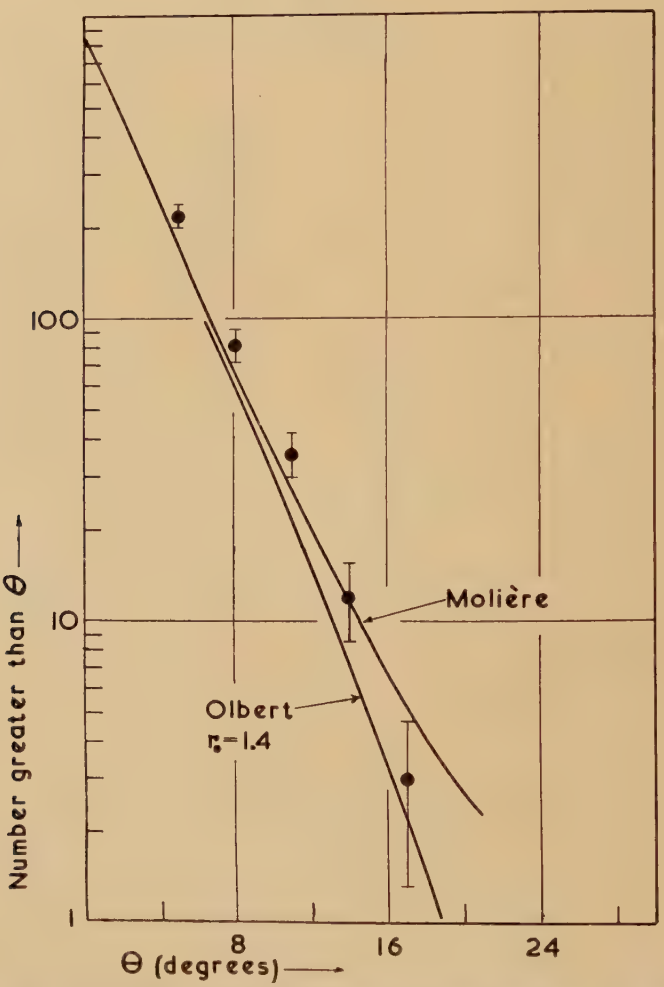

Measured and calculated integral scattering distributions for particles in group 1. The data represents 856 traversals of a 2 cm lead plate.

and 4. For this reason, only the angles in plates 3 and 4 have been used for the large angle scattering analysis. The fact that they have to traverse the remaining plates imposes a lower energy limit on the particles considered, a limit which is shown by the dashed line in fig. 3. In fig. 4 the measured scattering distribution is shown for the particles in group 1

along with the distributions expected from the theories of Molière and Olbert. Unfortunately, for the angles and energies considered, the difference between these two theories is small and little can be said about which distribution is favoured by the measurements. They do not appear to indicate any appreciable anomalous effect such as that suggested by George, Redding and Trent (1953) for particles of approximately the same energy and same scattering angles.

The particles in group 2 are of such high energy that ionization loss in the plates is not important, hence angles occurring in plates 2, 3, 4 and 5 have been used for the large angle scattering analysis. Another consequence of the higher energies in this group is that some of the r.m.s. angles used for the $p\beta$ estimate are affected by the ' noise level ' scattering, and it is this fact that accounts for the high energy tail to the spectrum shown in fig. 3. In fig. 5 the measured and calculated distributions are given for angles greater than 5° and it can be seen that for particles in this group the measurements agree remarkably well with Molière's theory for a ' point ' nucleus but do not agree with Olbert's theory for either of the two values of nuclear radius. Because of the rather large statistical uncertainties in the measurements it is evident that the results would also be consistent with a distribution falling considerably below Molière's, especially at the larger angles.

The $p\beta$ spectrum of the particles in group 3 could not be obtained from eqn. (8) because of the ' noise level ' scattering. Instead this spectrum was found by subtracting the resultant spectrum of the particles in groups 1 and 2 from the underground spectrum assumed to be proportional to $dE/(E+E_0)^{2\cdot7}$ (Barrett *et al.* 1952)* where E is the energy (nearly equal to $p\beta$ here) and $E_0=7$ Bev. A correction was applied to the underground spectrum to take account of those particles which were scattered in the 22 cm of lead between the top and bottom counter trays in such a way that they would not trigger the chamber. Although this correction is important at low energies, it has little effect on the spectrum of the particles above 1 Bev/c in group 3. The $p\beta$ spectrum thus calculated is shown in fig. 6. This spectrum should be reliable at values of $p\beta$ above about 1·2 Bev/c, but there is some uncertainty below this value for the following reasons : (1) it could be affected by errors in the correction applied to the underground spectrum and (2) it is derived from the difference of two nearly equal quantities.

Again, for particles in this group angles occurring in plates 2, 3, 4 and 5 have been used in the large scale scattering analysis. In fig. 7 the measured and calculated distributions are plotted for angles greater than 4°, and again the results are fairly consistent with Molière's theory

* This spectrum assumes that the differential sea level spectrum is proportional to $dE/E^{2\cdot7}$ at energies above 7 Bev. A slightly more accurate underground spectrum has been deduced from the measured sea level spectrum of Holmes, Owen, Rodgers and Wilson (private communication) and this results in a lowering of all the theoretical scattering distributions in fig. 7 by about 20%.

although they would fit better a distribution falling considerably below Molière's at the larger angles. The measurements are not consistent with Olbert's distribution. There is some uncertainty in the calculated distributions shown in fig. 8 (particularly Olbert's) because of the uncertainty of the low energy end of the $p\beta$ spectrum and the fact that low

Fig. 5

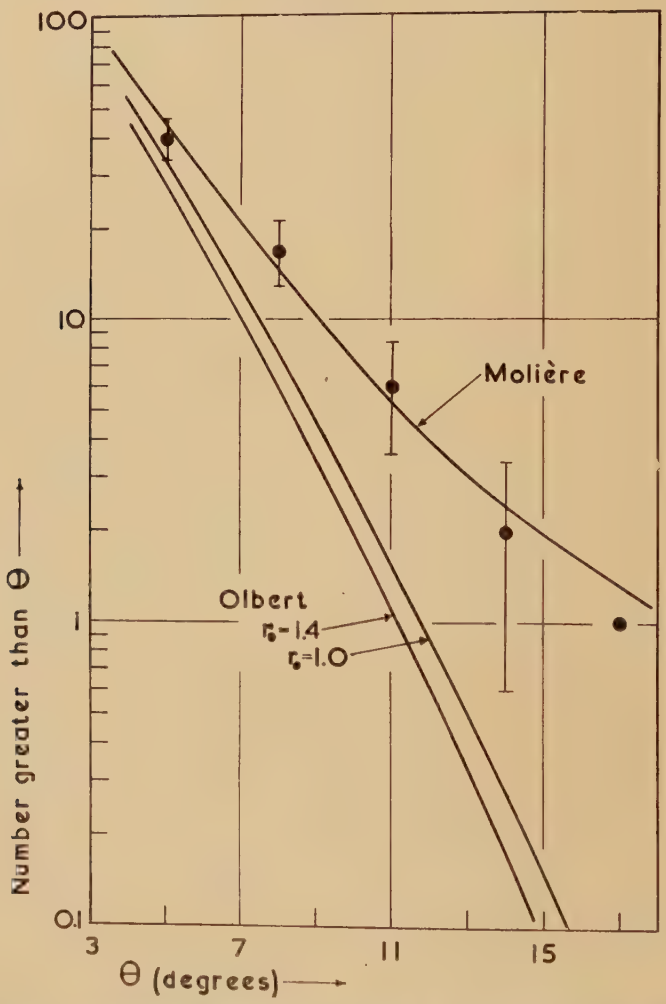

Measured and calculated integral scattering distributions for particles in group 2. The data represent 3016 traversals of a 2 cm lead plate.

energies contribute appreciably to these distributions. If the number of particles below 1·2 BeV/c is uncertain by a factor 2 (it is not likely to be more than this) then Molière's distribution is uncertain by less than $\pm 20\%$ at all angles, and Olbert's by less than $\pm 90\%$ at all angles, so that the results as stated above would not be greatly affected.

Gatto (1953), using the Born approximation, has calculated the incoherent Coulomb scattering cross section and finds a value which at large angles and high energies approaches a maximum value of $1/Z$ times the expected scattering for a ' point ' nucleus. In the case of lead, this incoherent contribution, if added to Olbert's distribution, would only account for a small fraction of the observed angles.

Fig. 6

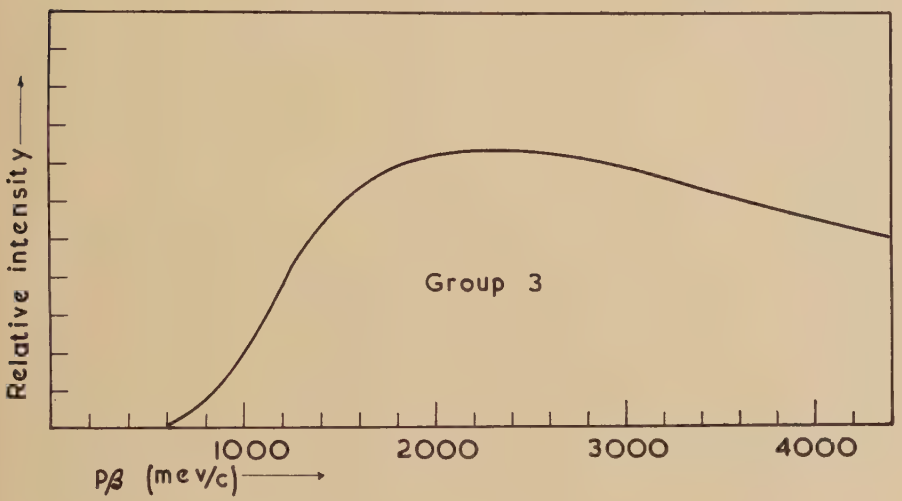

$p\beta$ spectrum for particles in group 3.

§ 5. Conclusions and Discussion

The conclusions drawn from this experiment are the following:— (1) At high energies, from several hundred Mev to several Bev the μ-mesons scattering distribution at large angles in lead falls close to, but at very large angles possibly below, Molière's distribution for a ' point ' nucleus. It is not consistent with Olbert's distribution. (2) At energies of a few hundred Mev the present experiment is not capable of distinguishing between the theories of Molière and Olbert, although it does suggest that there is no appreciable ' anomalous ' effect up to angles of about 17°.

The results for high energies are roughly in agreement with the work of Whittemore and Shutt (1952) and Leontic and Wolfendale (1953) who also measured the scattering distribution in lead at sea level. As was stated earlier the results for energies of a few hundred Mev do not appear to agree with those reported by George, Redding and Trent (1953) who have observed the scattering distribution in lead at a depth underground equivalent to 60 m of water. They report a distribution falling above what they expect even for a ' point ' nucleus and suggest that their results refer mainly to energies in the range 100 to 300 Mev. It would appear

that further measurements are required, particularly at these lower energies.

It does not seem possible at the moment to interpret the measured distributions at large angles since all the calculations, for the energies dealt with here, have been carried out with the Born approximation

Fig. 7

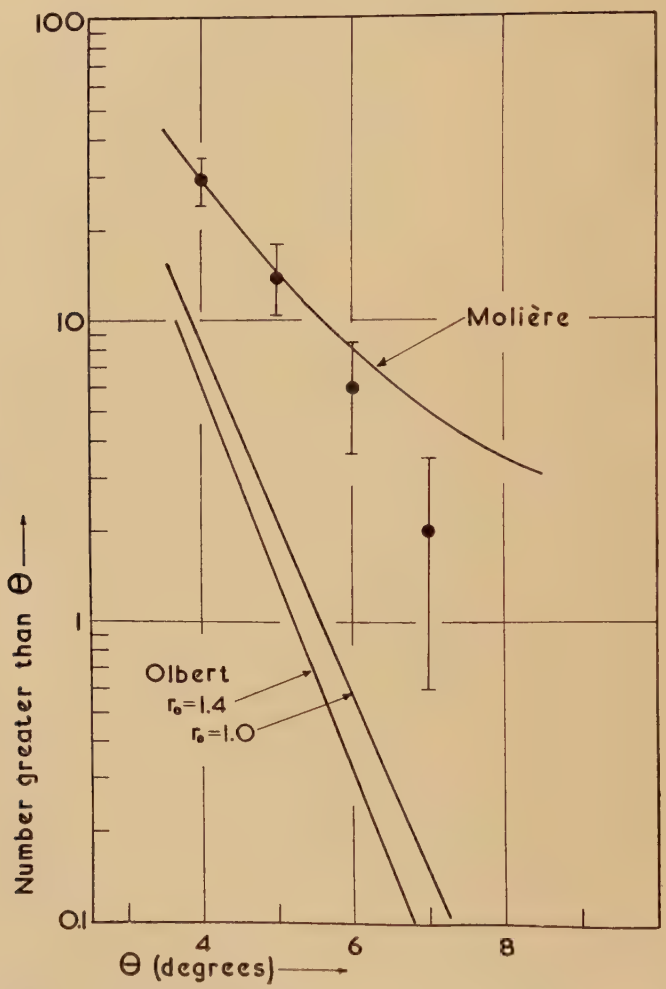

Measured and calculated integral scattering distributions for particles in group 3. The data represent 17 972 traversals of a 2 cm lead plate.

which is known to be unreliable at large angles. For such an interpretation it would seem that first, an exact calculation is required for the elastic Coulomb scattering expected in heavy elements and for various charge distributions and secondly, a more exact calculation for the incoherent Coulomb scattering expected for various nuclear models.

The conclusions drawn by several authors (Whittemore and Shutt 1952, George, Redding and Trent 1953, Kannangara and Shrikantia 1953 and Leontic and Wolfendale 1953) that departures from the expected scattering for a so-called ' solid ' nucleus might indicate some new (i.e. non-Coulomb) interaction between μ-mesons and nucleons seems hardly justified at present.

Recently Rochester and Wolfendale (to be published) have carried out a more detailed analysis of the emulsion data of Kannangara and Shrikantia (1953), and although the disagreement with the expected scattering for a ' solid ' nucleus remains, these authors arrive at conclusions similar to those reported here.

The present experiment is now being repeated with iron instead of lead.

Acknowledgments

During the preparation of this paper I have benefited from numerous discussions with Dr. H. J. J. Braddick, Dr. G. D. Rochester and Dr. A. W. Wolfendale. I am also grateful to Professor M. S. Bartlett for help with the statistical treatment and in particular with Appendix I. The cloud chamber has been operated in conjunction with Mr. B. Leontic to whom I am indebted. I particularly wish to thank Mrs. D. McDiarmid who undertook the long and rather tedious task of measuring the scattering angles. Finally, I am indebted to the Royal Commission for the Exhibition of 1851 for an Overseas Scholarship.

References

Annis, M., Bridge, H. S., and Olbert, S., 1953, *Phys. Rev.*, **89,** 1216.
Barrett, P. H., Bollinger, L. M., Cocconi, G., Eisenberg, Y., and Greisen, K., 1952, *Rev. Mod. Phys.*, **24,** 133.
Bethe, H. A., 1953, *Phys. Rev.*, **89,** 1256.
Bitter, F., and Feshbach, H., 1953, *Phys. Rev.*, **92,** 837.
Bridge, H. S., Peyrou, C., Rossi, B., and Safford, R., 1953, *Phys. Rev.*, **90,** 921.
Cooper, L. N., and Henley, E. M., 1953, *Phys. Rev.*, **92,** 801.
Fitch, Val. L., and Rainwater, J., 1953, *Phys. Rev.*, **92,** 789.
Gatto, R., 1953, *Nuovo Cim.*, **10,** 1559.
George, E. P., and Evans, J., 1950, *Proc. Phys. Soc.* A, **63,** 1248 ; 1951, *Ibid.*, **64,** 193.
George, E. P., Redding, J. L., and Trent, P. T., 1953, *Proc. Phys. Soc.* A, **66,** 533.
Kannangara, M. L. T., and Shrikantia, G. S., 1953, *Phil. Mag.*, **44,** 1091.
Leontic, B., and Wolfendale, A. W., 1953, *Phil. Mag.*, **44,** 1101.
Olbert, S., 1952, *Phys. Rev.*, **87,** 319.
Rose, M. E., 1948, *Phys. Rev.*, **73,** 279.
Sard, R. D., and Crouch, M. F., 1954, *Progress in Cosmic Ray Physics* (Amsterdam : North Holland Publishing Co.), Vol. II, p. 1.
Weatherburn, C. E., 1952, *Mathematical Statistics*, 2nd edn. (Cambridge : University Press), 165.
Whittemore, W. L., and Shutt, R. P., 1952, *Phys. Rev.*, **88,** 1312.

APPENDIX I

Given $\langle\theta_n\rangle$ we wish to calculate the probability $P_4((1/\sigma)/\langle\theta\rangle_n)\,d(1/\sigma)$ that $1/\sigma$ will lie in the interval $1/\sigma$ to $1/\sigma+d(1/\sigma)$ and from this obtain eqn. (7) of the text. It is assumed that all values of $1/\sigma$ are *a priori* equally probable.

From the general inversion rule of probability

$$P_4\left(\frac{1}{\sigma}\Big/\langle\theta\rangle_n\right)d\left(\frac{1}{\sigma}\right)=\frac{P\left(\langle\theta\rangle_n\Big/\frac{1}{\sigma}\right)d\langle\theta\rangle_n\,d\left(\frac{1}{\sigma}\right)}{\int_{(1/\sigma)=0}^{\infty}P\left(\langle\theta\rangle_n\Big/\frac{1}{\sigma}\right)d\langle\theta\rangle_n\,d\left(\frac{1}{\sigma}\right)} \qquad \text{(A 1)}$$

where $P(\langle\theta\rangle_n/(1/\sigma))\,d\langle\theta\rangle_n$ is the probability of finding $\langle\theta\rangle_n$ in $d\langle\theta\rangle_n$ given $1/\sigma$ which from eqns. (3) and (4) is

$$P\left(\langle\theta\rangle_n\Big/\frac{1}{\sigma}\right)d\langle\theta\rangle_n=\frac{1}{\Gamma(n/2)}\left(\frac{n\langle\theta\rangle_n{}^2}{2\sigma^2}\right)^{1/2(n-2)}\left(\frac{n\langle\theta\rangle_n}{\sigma^2}\right)\exp\left\{\frac{-n\langle\theta\rangle_n{}^2}{2\sigma^2}\right\}d\langle\theta\rangle_n.$$

Equation (A 1) for $n=6$ is not particularly sensitive to the exact prior distribution of $1/\sigma$. The assumption of a uniform distribution is justified for small values of $1/\sigma$ (which applies to most of the particles dealt with by this analysis) because here $1/\sigma$ is very nearly proportional to $p\beta$ and this, for the underground spectrum, does have an approximately uniform distribution. At larger values of $1/\sigma$ the assumption of a uniform distribution is not justified, in fact it falls to zero for values of $1/\sigma$ greater than $1/\sigma_1$. However if, as has been done here, $\langle\theta\rangle_n{}^2$ is restricted to values greater than about $4\sigma_1{}^2$ then the function $P(\langle\theta\rangle_n/(1/\sigma))$ in eqn. (A 1) is always practically zero for values of $1/\sigma\sim 1/\sigma_1$ and hence the form of the prior distribution of $1/\sigma$ beyond this is not important. The same argument justifies the integration in the denominator of eqn. (A 1) from 0 to ∞ rather than from 0 to $1/\sigma_1$.

The integration over $1/\sigma$ in the denominator of eqn. (A 1) gives

$$\frac{\Gamma((n+1)/2)\,d\langle\theta\rangle_n}{\langle\theta\rangle_n{}^2\Gamma(n/2)(n/2)^{1/2}}$$

and hence

$$P_4\left(\frac{1}{\sigma}\Big/\langle\theta\rangle_n\right)d\left(\frac{1}{\sigma}\right)=\frac{2}{\Gamma((n+1)/2)}\left(\frac{n}{2}\right)^{(n+1)/2}\left(\frac{\langle\theta\rangle_n}{\sigma}\right)^n\langle\theta\rangle_n \times\exp\left\{\frac{-n\langle\theta\rangle_n{}^2}{2\sigma^2}\right\}d\left(\frac{1}{\sigma}\right).$$

From this and eqns. (1) and (2), eqn. (7) follows.

APPENDIX II

The following indicates how the theoretical distributions shown in figs. 4, 5 and 7, for the projected angles of scattering allowing for geometry have been obtained. Let $f_1(\alpha)\,d\alpha$ be the distribution of the total angle of scattering for either Molière's or Olbert's theory. Bethe (1953) gives $f_1(\alpha)\,d\alpha$ directly for Molière's theory while Olbert gives the distribution

of the projected angle from which $f_1(\alpha)\,d\alpha$ is easily obtained. Further let ϕ and ψ be the projections of α on the plane of observation and on a vertical perpendicular plane respectively. Assume that the angles are small so that $\alpha^2=\phi^2+\psi^2$ and that the particles are incident vertically.

The functions $f_1(\alpha)$ are first averaged over the $p\beta$ spectrum of a particular group to give $f_2(\alpha)\,d\alpha$ the distributions of total angle for this group. Then if there is no limitation imposed on ϕ by the geometry and if a particle incident centrally on the chamber is scattering in a given plate the probability of observing ϕ between ϕ and $\phi+d\phi$ is

$$f_3(\phi, x)\,d\phi=4\int_{\psi=0}^{x}\frac{f_2(\alpha^2=\phi^2+\psi^2)\,d\phi\,d\psi}{2\pi(\phi^2+\psi^2)^{1/2}}$$

where the factor 4 refers to the four quadrants and x is the limiting value of ψ due to the bottom tray, i.e. half the angle, in the plane of ψ subtended at the plate by the counter tray. The function $f_3(\phi, x)$ has to now be averaged over the different plates in which the scattering distributions are measured and also over the different positions of the chamber on which particles are incident. It is sufficient for the first average to consider that the scattering occurs in a plate at the centre of the chamber. Finally the distribution function averaged over all incident positions is

$$f_4(\phi, a)\,d\phi=\frac{1}{a}\int_{x=0}^{a}f_3(\phi, x)\,d\phi\,dx,$$

where a is the maximum value of x for a particle incident on the edge of the chamber.

The function $f_4(\phi, a)$ has to be multiplied by a further correction factor due to the limitation on ϕ also imposed by the bottom counter tray. This is a simple geometrical factor the average value of which is $1-(b\tan\phi)/c$ where b is the distance between the centre of the chamber and the bottom counter tray and c is the length of this tray.

From the differential distributions obtained in this way the integral curves shown in figs. 4, 5 and 7, have been plotted. If account had been taken of the fact that not all of the particles were incident vertically, the calculated curves would have fallen slightly above those shown. The distributions for a ' point ' nucleus at 18° differ by about a factor of 2 from the projected distributions with no limitations on the angles, and the factor decreases with decreasing angle, while the ' solid ' nucleus distributions at the same angle differ by less than this.

CIII. *The Neutrons and Alpha-Particles from the Disintegration of* ^{9}Be *by* 6 MeV *Gamma-Rays*

By J. H. Carver, E. Kondaiah and B. D. McDaniel*
Research School of Physical Sciences, Australian National University, Canberra†

[Received May 12, 1954]

Abstract

By measuring the total photo-neutron yield, the cross section for neutron production from ^{9}Be under irradiation with the ^{19}F(p, α, γ) radiation is found to be $\sigma_t=(12{\cdot}5\pm1{\cdot}2)\times10^{-28}$ cm^2. The energy spectrum of the two alpha-particles, which are emitted in coincidence in the break-up, has also been studied; the cross section for all beryllium photo-processes which lead to the emission of two alpha-particles, both of whose energies exceeds 400 kev, is found to be $\sigma_\alpha=(12{\cdot}8\pm2{\cdot}5)\times10^{-28}$ cm^2. The near equality of σ_t and σ_α shows that the disintegration rarely proceeds through the ^{8}Be ground state, while a detailed examination of the coincident alpha-particle spectrum suggests that (γ, n) and (γ, α) reactions are present. The (γ, n) transitions are mainly through the 2·9 MeV excited state of ^{8}Be and the (γ, α) transitions mainly through the ^{5}He ground state, the branching ratio being roughly 1·2 : 1.

§ 1. Introduction

The neutron yield from the photodisintegration of ^{9}Be has been extensively investigated at gamma-ray energies below ~3 MeV (for a summary see Hamermesh and Kimball 1953). It is usually assumed that the disintegration proceeds in the following way:

$$\left.\begin{aligned} {}^{9}\mathrm{Be}+h\nu &\rightarrow {}^{8}\mathrm{Be}+\mathrm{n}-1{\cdot}66\ \mathrm{MeV},\\ {}^{8}\mathrm{Be} &\rightarrow {}^{4}\mathrm{He}+{}^{4}\mathrm{He}+0{\cdot}096\ \mathrm{MeV}. \end{aligned}\right\} \quad \ldots\ (1)$$

Guth and Mullin (1949) have calculated the cross section for this reaction assuming that the ^{9}Be nucleus may be represented by a ^{8}Be core plus a 'valency' neutron. By adjusting the parameters specifying the strength of the interaction between the neutron and the ^{8}Be core they are able to fit the low energy cross section data.

At a sufficient gamma-ray energy other modes of disintegration are possible. For example:

$$\left.\begin{aligned} {}^{9}\mathrm{Be}+h\nu &\rightarrow {}^{4}\mathrm{He}+{}^{5}\mathrm{He}-2{\cdot}57\ \mathrm{MeV},\\ {}^{5}\mathrm{He} &\rightarrow {}^{4}\mathrm{He}+\mathrm{n}+1{\cdot}0\ \mathrm{MeV}. \end{aligned}\right\} \quad \ldots\ (2)$$

Moreover reactions similar to (1) and (2), but proceeding instead through excited states of ^{8}Be and ^{5}He, may also occur. Very little consideration seems to have been given to these other possible modes of disintegration.

The present investigations have been made at a gamma-ray energy of

---

* On leave from Cornell University, Ithaca, New York.
† Communicated by Professor E. W. Titterton.

6 MEV. The total neutron yield has been measured using a Szilard–Chalmers method ; this gives the total cross section for all the processes under consideration, but does not distinguish between them. In addition a dual proportional counter has been used to count the two alpha-particles in coincidence ; from their energy distribution it should be possible to distinguish between the several possible modes of disintegration.

§ 2. THE GAMMA-RAY SOURCE

Protons accelerated by the 1·2 MV. Canberra H.T. set were used to bombard thin evaporated CaF_2 targets to produce gamma-rays by the well-known $^{19}F(p, \alpha, \gamma)$ reaction. The 874 and 935 kev levels in fluorine were excited yielding gamma-rays of 6·1 MEV and 7·0(6·9+7·1) MEV in the ratio of about 3 : 1 (Chao, Tollestrup, Fowler and Lauritsen 1950).

There were several complications involved in the use of this gamma-ray source.*

(*a*) For the neutron yield measurement : There was some neutron contamination of the source presumably due to alpha-particles, from the primary $^{19}F(p, \alpha, \gamma)$ reaction, reacting with further fluorine nuclei in the target to produce neutrons through the reaction $^{19}F(\alpha, n)$. To minimize this a target about 20 kev thick for protons was chosen ; the neutron background from this was less than 10% of the photo-neutron yield.

(*b*) For the alpha-particle measurements : The impure gamma-ray spectrum somewhat complicates the analysis. Unfortunately the counting rates were too low to permit the use of the almost pure 6·1 MEV radiation which can be obtained, at a much lower intensity, at the 340 kev resonance. For these measurements a target 80 kev thick for protons was employed in order to get sufficient intensity.

§ 3. THE NEUTRON YIELD MEASUREMENTS

The cross section for neutron emission was determined by a comparison of the neutron yields from beryllium and heavy water samples when irradiated under identical conditions.

The chief requirements for a neutron detector in such measurements are high sensitivity and a flat energy response. They can be well satisfied by the Szilard–Chalmers technique. In the present instance the detector was 130 litres of potassium permanganate solution (of concentration 30 g/litre) contained in a perspex tank ; the solution occupied a nearly cubical volume. After exposure to neutrons the solution was filtered to extract, as manganese dioxide, the radioactive ^{56}Mn produced by neutron capture and the activity of the filtrate was measured by means of a standard beta-sensitive Geiger counter. Before commencing any series of runs several ' clean-up ' extractions following exposure to a 3·5 mc Ra–Be source were made.

* Further complications would be involved in any attempt to use much more energetic gamma-rays (such as those of 17·6 MEV from ^{7}Li(p, γ)) owing to the production of photo-neutrons and charged particles in the detection apparatus and in other neighbouring material.

The beryllium and heavy water samples were enclosed in identical 10·4 cm^3 perspex containers and attached to the end of the target tube from the accelerator. The amounts of beryllium and heavy water were accurately determined by weighing. During the irradiations (which were for $1\frac{1}{2}$ hour periods) the samples were placed at the centre of the potassium permanganate tank and the radiation was continuously monitored by a Geiger counter. Similar irradiations were made with an empty perspex container in order to correct for the neutron background. After a number of preliminary runs, four irradiations of each type (beryllium, blank and then heavy water) were performed and the relative neutron yields were obtained from the measured ^{56}Mn activities. The results were corrected for background effects, for fluctuations in the gamma-ray yield during the irradiations and for the decay of the ^{56}Mn (half life 2·6 hours).

From these measurements and the data of Barnes, Carver, Stafford and Wilkinson (1952) on the $D(\gamma, n)$ cross section, the total cross section for photo-neutron emission from beryllium was found to be

$$\sigma_t = (12{\cdot}5 \pm 1{\cdot}2) \times 10^{-28} \text{ cm}^2.$$

§ 4. The Alpha-Particle Measurements

The dual proportional counter shown in fig. 1 was used to detect the two alpha-particles which occur in coincidence from either reactions (1) or (2). It was arranged that simultaneous voltage pulses were induced when a disintegration occurred in the beryllium foil (situated midway between the two chambers) such that an alpha-particle emerged into each chamber ; the pulses were proportional to the energies lost by the alpha-particles in the chamber.

Because of the reaction kinetics different pulse height distributions are expected for the reactions mentioned in § 1. The dotted lines near the origin of fig. 2 show the distribution expected for reaction (1) proceeding through the ground state of ^8Be ; the line indicating the lower alpha-particle energy corresponds to the 6·1 Mev gamma-ray while the other line corresponds to the 7·0 Mev gamma-ray. The two dotted lines in the upper part of fig. 1 show the distribution expected for excitation of the 2·9 Mev ^8Be level in the intermediate stage of the reaction, neglecting the broadening due to the width of the level. The effect of the broadening is shown by the solid contour lines* which corresponds to a level width of 1 Mev. The selected width is somewhat arbitrary since the measurements range between 1 and 2 Mev (Burcham and Freeman 1950).

---

* Both the angular correlation of the direction of emission of the two alpha-particles relative to the direction of the original recoil, and the correlation of the recoil with the initial gamma-ray will affect the density of the distribution. But for the present rough estimate it is sufficient to neglect such correlations and assume isotropy in all cases. Under these conditions, the density distribution of the two alpha-particle energies is uniform along the direction of the dotted lines.

Fig. 1

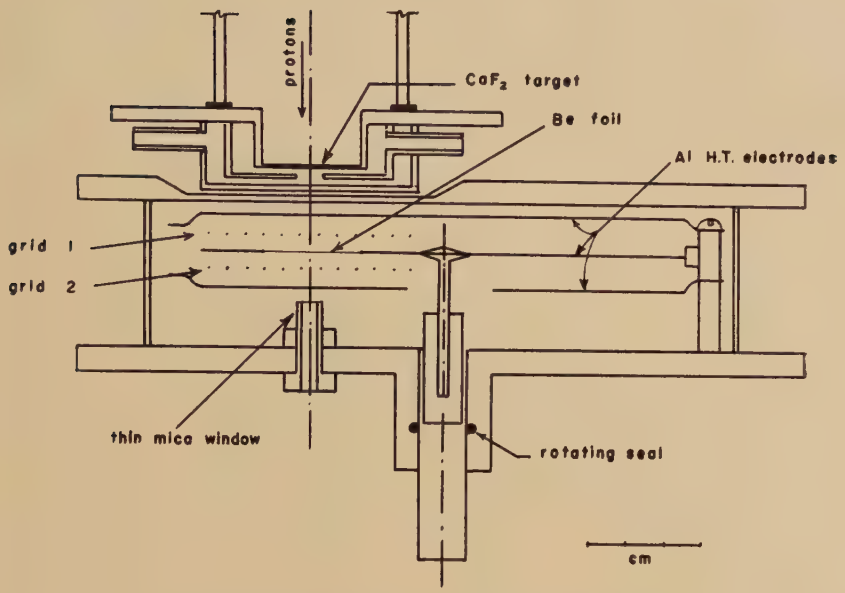

Dual proportional counter and target assembly.

Fig. 2

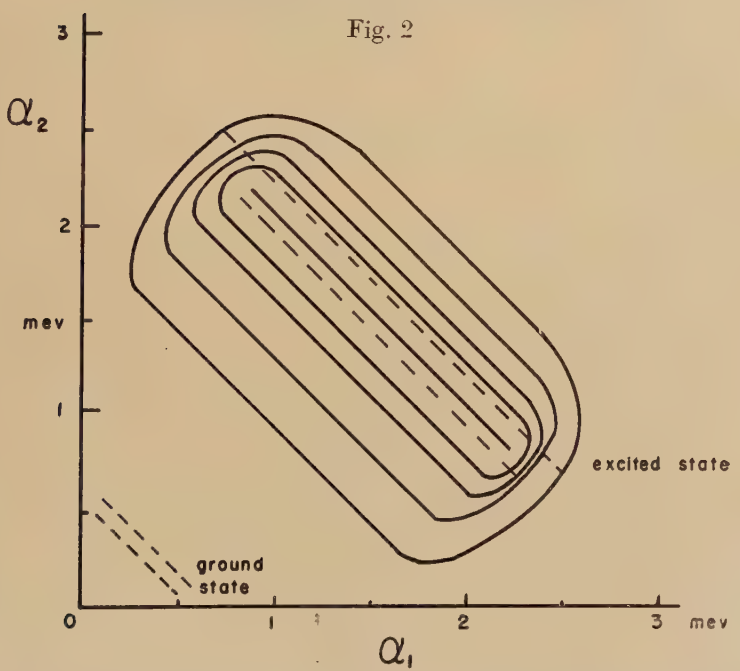

Reactions passing through ^{8}Be and ^{8*}Be. Calculated values of the energy loss (α_1) of an alpha-particle in one chamber plotted against loss of energy (α_2) of alpha-particle in second chamber using 6·1 and 7·0 Mev gamma-rays. Dotted lines assume zero width for the intermediate state. Equally spaced solid contour lines give the probability distribution of energies assuming a width of 1 Mev for the 2·9 Mev excited state.

The dotted lines of fig. 3 show the distributions expected for reaction (2) passing through the ground state of ^{5}He. The pattern is broadened by the natural width of this state (taken to be 0·5 MeV, Burge, Burrow, Gibson and Rotblat 1951) as is shown by the solid contour lines. A reaction proceeding through an excited state of ^{5}He would give similar patterns at lower energy in the diagram.

Fig. 3

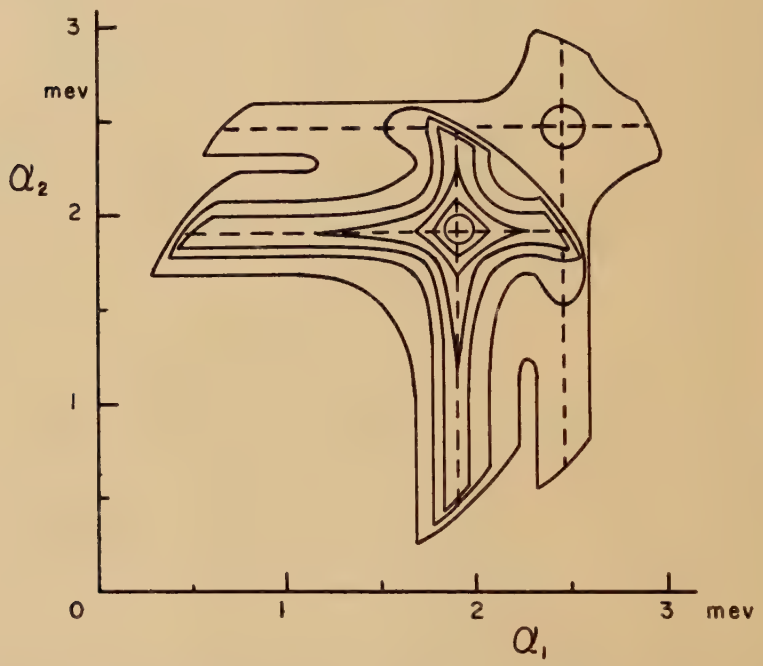

Reaction passing through ^{5}He ground state. Calculated values of α_1 vs. α_2 for 6·1 and 7·0 MeV gamma-rays. Dotted lines assume zero width for the intermediate state. Equally spaced solid contour lines give the probability distribution of energies assuming a width of 0·5 MeV for the ^{5}He ground state.

The proportional counter (fig. 1) was made as compact and thin as possible so as to obtain the maximum intensity by providing a large solid angle for the irradiation of the beryllium foil ;* the counter was filled with

* The energy resolution is limited by the thickness of the foil for alpha-particles. A foil was made by evaporating beryllium onto each side of a film composed of a 2 to 1 mixture of collodion and glyptal. The thickness was 0·83 mm air equivalent of which 0·54 mm was beryllium. The energy loss of a 2·5 MeV alpha-particle in this foil was about 150 kev. To determine the background, if any, from the collodion a similar collodion foil was made with just enough aluminium evaporated onto its surface to make it electrically conducting. A third aluminium foil (2 mm air equivalent) was also placed on the high voltage electrode. Any of these three foils (all one inch in diameter) could be put in position by means of a rotating seal, without disturbing the gas mixture or electronic equipment.

two atmospheres of argon (90%) and carbon dioxide (10%) and operated at a gas amplification of ~8. The use of light chamber walls and wide-band electronic circuits reduced the accidental counting rate due to electron pile-up to less than 2% when the chamber was operated in the maximum beam intensity of $\sim 2 \times 10^9$ quanta/sec total. Tests with a ThC+C′ alpha-particle source showed that the variation in pulse height with the position and direction of the alpha-particle track was less than $\pm 6\%$.

Fig. 4

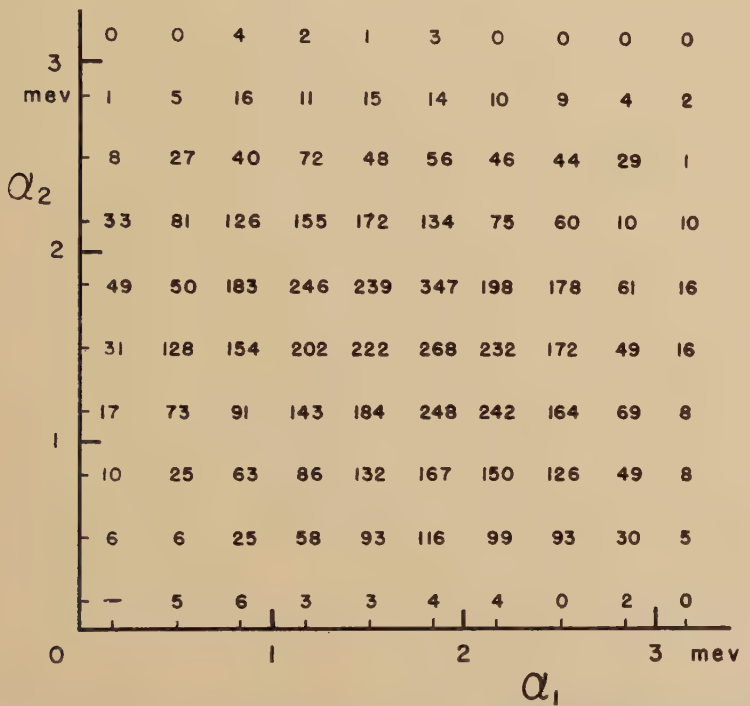

Observed distribution of intensity of α_1 vs. α_2. Numbers shown are the total number of coincidences observed having alpha-particle energies falling in the chosen intervals of α_1 and α_2.

The voltage pulses from the two multiplying grids of the counter were injected into separate amplifiers each having an overall rise time of about 0·1 μsec, the clipping time constant being 0·8 μsec. After passing through discriminators and pulse shapers (producing 0·5 μsec rectangular pulses) the pulses were fed into a coincidence circuit. When a coincidence occurred each pulse was stretched to give a rectangular pulse of 20 μsec duration and of amplitude proportional to the input pulse. These signals were applied to the x and y plates, and a gating signal to the intensifier electrode, of a cathode-ray tube. Thus a two dimensional display of the pulse heights in the two channels was obtained which could be recorded photographically.

The results of the measurement with the thin beryllium foil are shown in fig. 4. This is a tabulation, in a two-dimensional array, of the distribution of observed coincidences. A contour presentation of the results is shown in fig. 5. In each of these figures the background, predominately near the origin, has been subtracted.*

Fig. 5

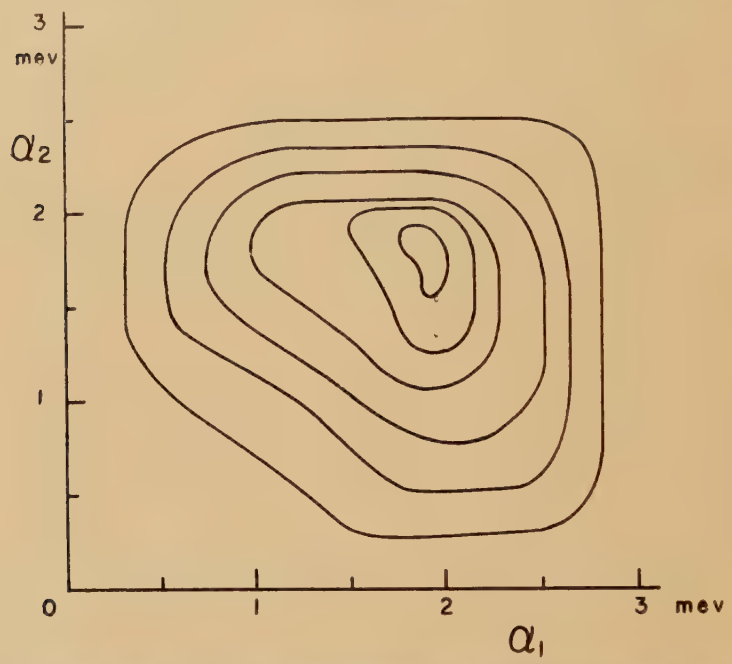

A contour presentation of the experimental data for α_1 vs. α_2 given in fig. 4. The contours are equally spaced.

During the irradiations the absolute gamma-ray flux was determined by means of a standard thick-walled Geiger counter identical in construction with the one described and calibrated by Barnes, Carver, Stafford and Wilkinson (1952). The beryllium content of the foil was obtained from alpha-particle range measurements and by ashing and weighing. After correcting for gamma-ray absorption in the chamber face and for the variation of detection efficiency with the angle between the two alpha-particles (assuming isotropy in the centre of mass system for all processes, which gives a counting loss of 10%) one obtains for the cross section for the observed reaction

$$\sigma_\alpha = (12{\cdot}8 \pm 2{\cdot}5) \times 10^{-28} \text{ cm}^2.$$

* There seems to be a slight asymmetry between the first and second chamber which probably arises from a faulty calibration of their relative sensitivities. This may result from the uncertainty in the position of the beryllium foil which determines the depth of both chambers and hence the apparent sensitivity as determined by the test source of alpha-particles.

This is the cross section for the disintegration of ^{9}Be by 6 MeV gamma-rays, which results in the production of two alpha-particles with an energy greater than about 400 kev each. Less energetic alpha-particles cannot be observed uuder the conditions of minimum bias and background of this experiment.

§ 5. Discussion

The most obvious conclusion to be drawn from these measurements is that few, certainly less than 20%, of the ^{9}Be photodisintegrations at a gamma-ray energy of 6 MeV proceed according to reaction (1) involving the ground state of ^{8}Be. This follows from the close agreement (within the admittedly large errors) found between the cross section σ_t for all disintegrations which lead to neutron emission, and the cross section σ_α for disintegrations leading to the emission of two alpha-particles each of energy exceeding 400 kev (that is, σ_t includes disintegrations proceeding through the ^{8}Be ground state, while σ_α does not).

Further information about the disintegration mechanism can be obtained from a detailed comparison of the observed distributions, figs. 4 and 5, with the predicted distributions, figs. 2 and 3. The ' squareness ' of the observed pattern and the intense area located near 1·8 MeV is very similar to that of fig. 3 and suggests that a large fraction of the reactions proceed through the ^{5}He ground state. The observed pattern, however, is broadened towards the origin. While some of the broadening may be due to instrumental factors, such as the finite resolution of the proportional counter, amplifier noise and the thickness of the beryllium foil, nevertheless it is appreciably more than would be estimated for the ^{5}He process after allowing for such resolution effects. It seems likely, therefore, that the extra broadening is due to a branching through the ^{8*}Be excited state (cf. fig. 2). Using the observed and calculated distributions it is concluded that the relative probabilities for disintegrations proceeding through ^{8*}Be and ^{5}He are 1·2 : 1. It should be emphasized that this ratio is uncertain because of the statistical errors, the assumed isotropic angular distributions and the various resolution effects. There is no evidence for any appreciable branching through an excited state of ^{5}He or states of ^{8}Be higher than 2·9 MeV.

The measured value of the total photo-neutron cross section,

$$\sigma_t = (12{\cdot}5 \pm 1{\cdot}2) \times 10^{-28} \text{ cm}^2,$$

is in good agreement with the value 14×10^{-28} cm^2 calculated by Guth and Mullin (1949) for the disintegration of beryllium by gamma-rays of 6 MeV. However, in view of the fact that Guth and Mullin assume that the reaction proceeds through the ground state of ^{8}Be, this agreement is fortuitous. Since the completion of the present measurements the photo-neutron yield measurements of Nathans and Halpern (1953), using electron bremsstrahlung, have been published. Their result at 6 MeV is in substantial agreement with the value of σ_t found in this experiment.

Acknowledgments

We wish to thank the several members of this laboratory who helped, in one way or another, during the course of the work. One of us, B. D. McDaniel, carried out the work while visiting Canberra under a Fulbright award of the U.S. Educational Foundation.

References

Barnes, C. A., Carver, J. H., Stafford, G. H., and Wilkinson, D. H., 1952, *Phys. Rev.*, **86,** 359.

Burcham, W. E., and Freeman, J. M., 1950, *Phil. Mag.*, **41,** 921.

Burge, E. J., Burrow, H. B., Gibson, W. M., and Rotblat, J., 1951, *Proc. Roy. Soc.* A, **210,** 534.

Chao, C. Y., Tollestrup, A. V., Fowler, W. A., and Lauritsen, C. C., 1905, *Phys. Rev.*, **79,** 108.

Guth, E., and Mullin, C. J., 1949, *Phys. Rev.*, **76,** 234.

Hamermfsh, B., and Kimball, C., 1953, *Phys. Rev.*, **90,** 1063.

Nathans, R.. and Halpern, J., 1953, *Phys. Rev.*, **92,** 940.

CIV. *The Photo-Production of an Isomeric State in* ^{207}Pb

By J. M. Reid and K. G. McNeill
Department of Natural Philosophy, The University of Glasgow*

[Received May 17, 1954]

Summary

The 0·8 second activity produced in Pb by irradiation in the x-ray beam of a 23 Mev synchrotron was shown to arise from a disintegration of ^{208}Pb by comparing the effects produced in a target of 'natural' Pb and a similar target of Pb enriched in the 208 isotope. The γ-rays emitted by the short-lived activity were investigated with a scintillation spectrometer. The resulting spectrum, and the half-life of the activity agree with the known spectrum and half-life associated with the $i_{13/2}$ isomeric state in ^{207}Pb. The reaction was thus determined to be ^{208}Pb(γ, n)^{207}*Pb.

An estimate of the threshold for the production of the isomer was made by comparing, at different settings of the maximum x-ray energy from the machine, the intensity of the isomeric activity and the activity produced in Ag. The value thus obtained was 9·0$\pm$0·1 Mev.

The threshold calculated from the ground state mass differences, the energy of the isomeric level and the centrifugal barrier corresponding to the orbital angular momentum of the emitted neutron is shown to be significantly greater than 9·0 Mev. It is suggested that the isomeric state is reached, not directly, but through a level of spin 11/2 lying slightly above the isomeric level.

§ 1. Introduction

In a previous note (Reid and McNeill 1953) we reported the production of a short-lived radioactivity of half-life 0·8 sec by the irradiation of natural lead in the x-ray spectrum from a synchrotron of maximum energy 23 Mev. The value of the half-life strongly suggested that the isomer ^{207}Pb was the end product of the reaction taking place. The order of magnitude of the cross section was found by direct comparison to be one-tenth that of the well-known reaction ^{63}Cu(γ, n)^{62}Cu. Since the overall spin change in the reaction was of the order of 6 units, it was conjectured from the value of the cross section that a (γ, n), rather than a (γ, γ) process was taking place.

^{208}Pb is a 'doubly magic' nucleus, and hence on the basis of the shell model some predictions can be made about the energy levels of this isotope, and about those of its neighbours. It, therefore, seemed worth

* Communicated by the Authors.

while to establish the above reaction with more certainty and, if possible, to discover if the transition to the isomeric state takes place directly, or if it proceeds via a cascade from a higher level in ^{207}Pb.

§ 2. Establishment of the Parent Isotope

Natural lead is a mixture of 52% ^{208}Pb, 21% ^{207}Pb and 26% ^{206}Pb. There is also present a trace of ^{204}Pb. As in the beam of a synchrotron there is always present in addition to x-ray quanta a considerable neutron flux due to (γ, n) reactions taking place in the synchrotron target and elsewhere, it is possible by irradiation in this beam to produce ^{207}Pb, starting from any of the three predominant isotopes in the natural lead. Professor F. Soddy generously lent to us a specimen of lead which he had separated from a thorium mineral in the course of his classical work on isotopes (Soddy 1916). The specimen is a mixture of natural lead and ^{208}Pb, and has an atomic weight of 207·7. This figure for the atomic weight implies an isotopic mixture in the ratios 80% ^{208}Pb, 10% ^{207}Pb and 10% ^{206}Pb. Comparison of the activity produced in this specimen with a corresponding activity produced in an identical specimen of natural lead enabled us to determine the parent isotope in the reaction leading to the 0·8 sec activity.

In our previous note we have described the cycle of operations used to detect the existence and measure the strength of the short-lived activity. The synchrotron beam was allowed to irradiate a lead target for 1 second, and was then switched off. Radiations from this target were detected by a NaI(Tl) crystal placed permanently below the target. Amplified pulses from the crystal occurring during the first period of 1 second after beam switch-off were passed to one scaling unit, while those occurring during the second period of 1 second were passed to a second scaling unit. After this the cycle of irradiation and detection was repeated. With this arrangement the difference in the readings of two scalers provides a measure of the activity produced in the lead target. During all runs Cu foils were irradiated for periods of 15 minutes each, and their resultant activity measured with a standard Geiger counter arrangement. This monitoring enabled corrections to be made for beam fluctuations.

The experiment, therefore, consisted of performing a large number of 15-minute runs, in half of which a target of lead enriched with ^{208}Pb was used, and in the other half of which the target was of natural lead.

The ratio of the activities induced in these two targets is shown in table 1, together with the ratios of the principal isotopes in the two lead specimens. The results leave little doubt that the dominant reaction producing the 0·8 sec activity starts from ^{208}Pb.

§ 3. Establishment of the End Product of the Reaction

As previously reported (Reid and McNeill 1953) the half-life induced in the lead specimen by radiation with bremsstrahlung x-rays of maximum

energy 23 MeV was found to be $0{\cdot}8 \pm 0{\cdot}1$ sec. An isomeric state of ^{207}Pb with this half-life formed by the decay of ^{207}Bi is known. Its decay scheme has been investigated (Neumann and Perlman 1951, Grace and Prescott 1951) and has been found to consist predominantly of two cascade gamma rays of 1 MeV and 0·5 MeV from the isomeric level to the ground state (fig. 1).

Table 1

	Normalized difference in scaler readings	Experimental ratio
208 enriched lead	12890 ± 836	$1{\cdot}71 \pm 0{\cdot}17$
natural lead	7540 ± 525	

Expected ratio for		
^{206}Pb(n, γ)^{207}Pb	^{207}Pb(γ, γ)^{207*}Pb	^{208}Pb(γ, n)^{207}Pb
0·4	0·4	1·6

In the present experiment the pulses from the gating circuit which previously went to the scalers were fed from each channel to pulse height analysers. The gate widths and radiation time in this experiment were increased to 2·4 sec. In fig. 2 we have plotted the difference between the spectra corresponding to the two counting channels. This difference between the spectra shows clearly the effects produced by the 0·8 sec activity, effects of longer-lived activities produced by the x-ray beam disappearing in the subtraction. The peaks occur at pulse heights corresponding to γ-rays of 0·50 and 1·01 MeV. The ratio of the heights of the peaks in the two spectra which were subtracted were consistent with a half-life of 0·8 sec. As these results agree within the errors of measurement with the known half-life and the spectrum of γ-rays associated with the isomeric level, the product of the disintegration is shown to be ^{207*}Pb.

§ 4. Threshold Measurements

Pryce (1952) has assigned spin values to many of the levels of ^{207}Pb including that of the isomeric state with which we are here concerned. As the ground state of ^{208}Pb has spin zero, it appears that the overall spin change in the (γ, n) reaction we observe is 13/2. It is important to know how the total spin change is to be divided between the three possible stages of the reaction, viz. : capture of the gamma-ray, emission

Fig. 1

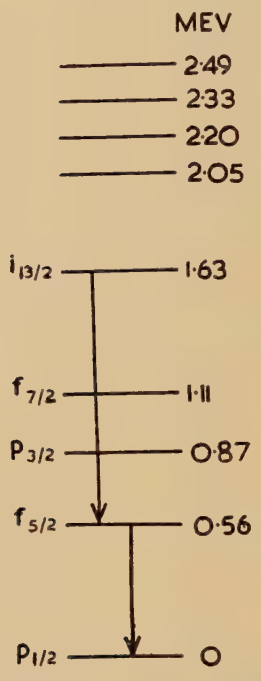

Energy level scheme for ^{207}Pb (after Pryce 1952).

Fig. 2

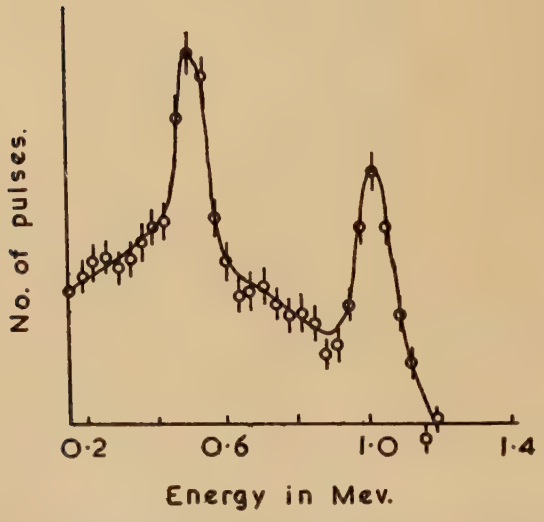

Energy spectrum of the γ-rays associated with the 0·8 sec activity in lead. The energy scale is based on measurements of the photopeaks of ^{60}Co (1·17 Mev and 1·33 Mev) and ^{137}Cs (0·67 Mev).

of the neutron and possible emission of cascade gamma-rays by the ^{207}Pb. Information about the threshold energy of the (γ, n) reaction is, as shown below, very relevant in this connection.

To investigate behaviour near the threshold we employed the technique of comparing the ratios of the rates of production of ^{207}*Pb at given maximum energies of the synchrotron to the rates of production of known radioactivities by the same x-ray beam. These ratios we call the activation ratios, written ^{207}*Pb/A, where A is the comparison daughter radio isotope. Activation ratios were measured as a function of the maximum energy of the x-ray spectrum. This maximum energy was varied by varying the time in the synchrotron acceleration cycle at which the r.f. was switched off.

The comparison isotopes which were used were ^{62}Cu, ^{106}Ag and ^{108}Ag. As before, the production of ^{207}*Pb was measured by the difference of the two scaler readings. The copper and silver activities were measured by placing the irradiated specimens under a Geiger counter, and counting under standard conditions. In all cases the lead and the comparison material were irradiated simultaneously to eliminate effects of variation of beam intensity. With copper as the comparison element, the irradiation time was 15 minutes, a time comparable with the half-life of 10 minutes. In the case of ^{108}Ag, an irradiation comparable with the half-life of 2·3 minutes was not convenient. Instead the radiation time was again made 15 minutes, a time suited to the longer-lived isotope ^{106}Ag. It was, therefore, important to ensure that the beam remained at the same intensity during the silver irradiation, so that the ^{108}Ag activity, which would mainly depend on conditions during the last two minutes of the radiation, could fairly be compared with the lead activity, for the latter would be proportional to the average beam during the whole 15 minutes. A constant check on the beam intensity was, therefore, maintained by means of an ionization chamber feeding a d.c. amplifier.

The results are shown in fig. 3. It will be seen from curve (a) that the activation ratio ^{207}*Pb/^{62}Cu increases steeply with decreasing x-ray energy. If it be assumed that the activation curves for the reactions considered have a similar shape, a point which will be discussed later, this result implies that the ^{208}Pb(γ, n)^{207}*Pb threshold is less than the threshold of the ^{63}Cu(γ, n)^{62}Cu reaction, which is known to be 10·1 Mev (Montalbetti, Katz and Goldemberg 1953). It was found impossible to obtain statistically significant results at energies less than 2 Mev above the Cu threshold because of the weakness of the induced activities.

The curves (b) and (c) for the Ag isotopes show that the activation ratio ^{207}*Pb/^{106}Ag increased with decreasing x-ray energy, while the ratio involving the 2-minute activity increased at a much smaller rate with decreasing x-ray energy. The statistical errors again tended to be large at low energies, owing to the weakness of the induced activities. For comparison, the curve of the activation ratio ^{108}Ag/^{106}Ag is included

in fig. 3. It will be seen that this ratio increases with decreasing synchrotron energy, and that, moreover, the rate of increase is slightly less than in the ^{207}*Pb/^{106}Ag case. On the assumption that the excitation functions of all the isotopes considered have similar shapes, we interpret these results as meaning that the ^{207}*Pb threshold lies just below the ^{109}Ag(γ, n)^{108}Ag threshold.

Fig. 3

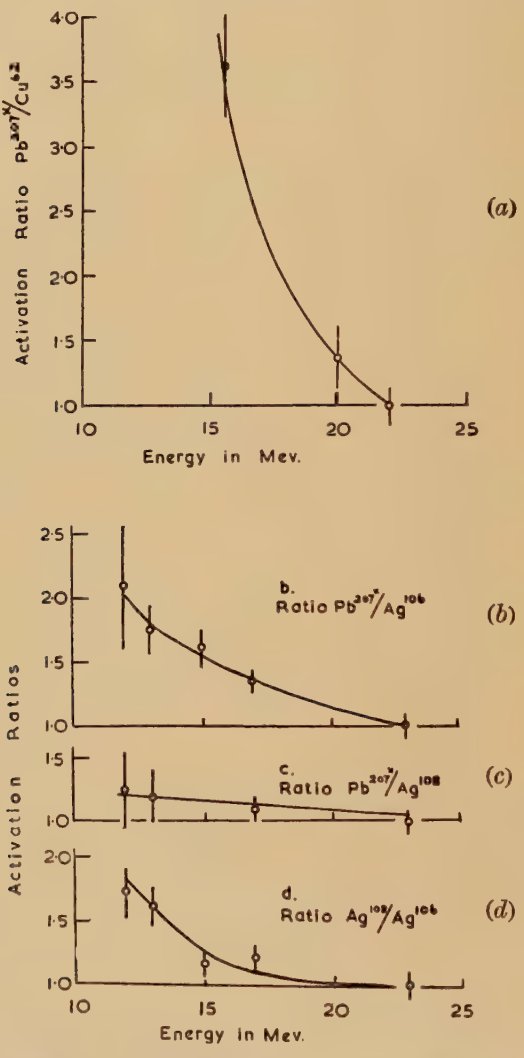

Curves showing the variation of activation ratios with maximum x-ray energy. Curve (*a*) ^{207}*Pb/^{62}Cu, (*b*) ^{207}*Pb/^{106}Ag, (*c*) ^{207}*Pb/^{108}Ag, (*d*) ^{108}Ag/^{106}Ag.

The ^{109}Ag(γ, n)^{108}Ag threshold is 9·07 Mev (Birnbaum 1954), and the ^{107}Ag(γ, n)^{106}Ag threshold is 9·5 Mev (Montalbetti *et al.* 1953). With

these figures we therefore place the threshold energy for the production of ^{207}*Pb by a (γ, n) process as 9·0 MEV $\pm$0·1 MEV.

§ 5. Discussion of Measured Threshold

The method on which the threshold measurement is based depends on the activation curves of the reactions being compared having similar shapes. Two factors support the validity of this assumption. Firstly there is the general consideration that all (γ, n) activation curves for the heavier nuclei measured with any accuracy do have a notable similarity in shape. Secondly, in the particular elements here being discussed, namely Ag and Pb, a detailed measurement of the neutron yields indicates that nothing anomalous takes place near the threshold (Montalbetti *et al.* 1953). These measurements, it should be noted, relate to the natural mixture of isotopes and, of course, to all modes of disintegration leading to the release of a neutron. If, however, this assumption about activation curves be made, the effective threshold for the excitation of ^{207}*Pb from the ground state of ^{208}Pb is 9·0$\pm$0·1 MEV.

It is reasonably certain from general photodisintegration studies that close to the threshold the first step in the process is a M1 or E2 γ-ray transition in ^{208}Pb. This will lead to an excited state in ^{208}Pb of spin 1 or 2 and even parity. Having regard to the even parity of the isomeric state the l value of the emitted neutron, assuming a direct transition to the isomeric state, will be 6 in the case of the magnetic transition and 4 in the case of the electric transition. Now the transition probabilities, T_l, of reactions involving neutrons of l values of this magnitude can be calculated and are shown in fig. 4 for l values up to 5. Due to the centrifugal barrier the emitted neutron must in practice be released with a certain minimum energy. In the case of l=4 this minimum energy is of the order of 0·8 MEV. If we now add this to the energy of the $i_{13/2}$ level above the ground state of ^{207}Pb, viz. 1·63 MEV, and take into account the energy difference between the ground states of ^{207}Pb and ^{208}Pb (7·3 MEV) we would predict an effective threshold of 9·7 MEV for E_2 capture and at least 11 MEV for M_1 capture. The uncertainty in this figure will be the combination of the uncertainty of the height of the centrifugal barrier and the uncertainty of the ground state differences. The latter difference, which has been estimated both by neutron capture radiation in ^{207}Pb and by mass spectrometry, has been taken to be 7·3$\pm$0·1 MEV. The barrier effect has been estimated for l=4 from fig. 4 and taken to be 0·8$\pm$0·1. It would appear, therefore, that the threshold for direct transition to the level following an E_2 transition is significantly higher than that measured.

It is, of course, possible that a γ-ray transition between levels in ^{207}Pb takes place following neutron emission. Even if it be assumed that a hitherto unobserved level is involved, the following considerations, in conjunction with the observed threshold energy, limit the possibilities severely.

There will be competition between transitions to the $i_{13/2}$ level and those to the lower lying levels, the spins and parities of which are known if one accepts the shell model allocations. For any postulated level above the $i_{13/2}$ level an estimate can then be made of the seriousness of this competition. It must also be borne in mind that the transition to the $i_{13/2}$ level cannot be of too high a multipole order or it would lead to a life-time which would have shown up in the original life-time measurements.

Fig. 4

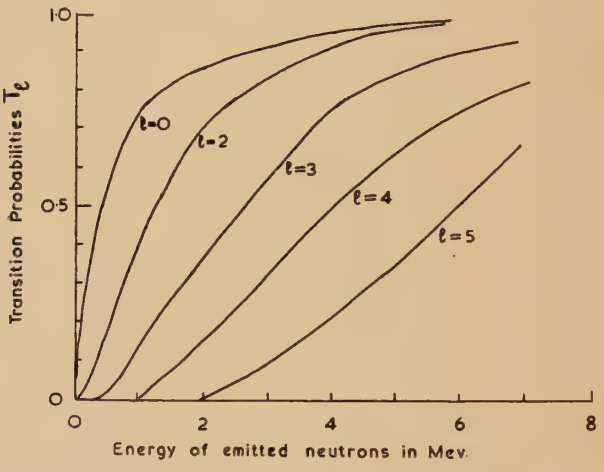

Transition probabilities, T_l, for the emission of a neutron of given l value from ^{208}Pb.

An examination of the possibilities in view of these limitations suggests that the most likely $(\gamma-n, \gamma)$ modes are (*a*) M_1 capture, neutron ($l=4$) emission to a level of spin 11/2 and even parity followed by an M_1 transition to the 13/2 level ; or (*b*) an E_2 capture, neutron ($l=3$) emission to a level of spin 11/2 and odd parity followed by an E_1 transition to the 13/2 level. These two in conjunction with (*c*) the direct transition to the isomeric state following E_2 capture and neutron ($l=4$) emission form the three most likely modes of disintegration. Of these (*c*) as stated above would lead to a threshold of 9·7 Mev while (*a*) would lead to a threshold higher than this by the energy difference between the postulated 11/2 level and the 13/2 level. Both, therefore, seem to be rather inconsistent with our measurement. The remaining possibility (*b*) would lead to a threshold greater than 9·2 Mev by the difference in energy between the postulated level of spin 11/2 and the $i_{13/2}$ level. While, therefore, it is still higher than our measured value it appears to lead, all things considered, to the lowest effective threshold.

It may be mentioned in this connection that in the experiments of Neumann and Perlman (1951) in which the formation of ^{207*}Pb by

electron capture in ^{207}Bi was being investigated a soft γ-ray of energy 0·137 or 0·064 Mev was found. This transition has not been fitted into the decay scheme proposed by Pryce and might possibly correspond to the level of spin 11/2 suggested above.

Acknowledgments

We wish to express our thanks to Mr. J. D. Prentice for valuable assistance with the measurement of the γ-ray spectra, and to Prof. P. I. Dee and Dr. K. M. Guggenheimer for helpful discussions.

Note added in proof.—A further discussion of the decay of ^{207}Bi has recently been given by Prescott (J. R. Prescott, 1954, *Proc. Phys. Soc.* A, **67,** 540). The appearance of the low energy line in the measurements of Neumann and Perlman is now attributed to Auger effect and not, as we accepted, to a low energy γ-ray line. Prescott also presents experimental evidence that suggests that the 1.11 Mev line in the ^{207}Pb level scheme does not exist, and that there is at least one other level in the neighbourhood of the isomeric level.

References

Birnbaum, M., 1954, *Phys. Rev.*, **93,** 146.
Grace, M. A., and Prescott, J. R., 1951, *Phys. Rev.*, **84,** 1059.
Montalbetti, R., Katz, L., and Goldemberg, J., 1953, *Phys. Rev.*, **91,** 659.
Neumann, H. M., and Perlman, I., 1951, *Phys. Rev.*, **81,** 958.
Pryce, M. H. L., 1952, *Proc. Phys. Soc.* A, **65,** 773.
Reid, J. M., and McNeill, K. G., 1953, *Proc. Phys. Soc.* A, **66,** 1179.
Soddy, F., 1916, *Ann. Rep. Chem. Soc.*, **13,** 247, 272.

CV. *Coulomb Excitation of Isomeric States in Silver*

By Torben Huus and Arnold Lundén*
Institute for Theoretical Physics, University of Copenhagen†

[Received May 19, 1954]

Summary

The time-delay in the decay of Coulomb excited nuclei can be used to improve background conditions so that weaker excitations can be detected. As an example the excitation of the 40 second isomeric activity in silver has been investigated. The measured yield curve shows that the excitation takes place mainly via a higher-lying rotational state. A brief discussion of the rotational spectrum and the decay scheme is given.

In the Coulomb excitation process, the states most strongly excited are those having large nuclear matrix elements for electric multipole transitions and correspondingly short lifetimes for radiative decay. Thus, the nuclear rotational states (Bohr and Mottelson 1953), which have strongly enhanced E2 matrix elements, are especially easy to excite (Huus and Zupančič 1953, Temmer and Heydenburg 1954).

Nuclear excitations which require a change in the binding states of individual particles have much smaller matrix elements. While it may be difficult to observe such weak transitions during the bombardment, due to the background effects resulting from atomic processes induced in the target (Zupančič and Huus 1954), the conditions for observation are greatly improved if the excited states have a sufficiently long lifetime to make possible a measurement of the activity after the beam has been shut off.

The technique for such measurements is especially simple for activities with lifetimes in the region of seconds or minutes. The excitation of such long lived states in general requires a transition of multipole order higher than two; however, the cross sections for Coulomb excitation decrease far less rapidly with increasing multipole order than do the low energy radiative transition probabilities. Moreover, the isomeric states may also be produced as a decay product of more strongly excited states of higher energy.

As an example we have chosen to study the excitation of the E3 isomeric states of the two stable silver isotopes, which are very similar to each other. The states are characterized by the following properties (Hollander,

* On leave from Chalmers Tekniska Högskola, Gothenburg, Sweden.
† Communicated by Professor Niels Bohr.

Perlman and Seaborg 1953), for ^{107}Ag and ^{109}Ag, respectively : Half-lives : 44·3 sec and 39·2 sec ; excitation energies : 94 kev and 87 kev ; both have total conversion coefficient $\simeq 15$ and ratio $K/L \simeq 1$.

The experiment was performed by detecting the conversion electrons emitted from a thick target of natural silver after the bombardment with about one micro-amp protons of energies up to 2 MEV. The electrons were detected with an anthracene crystal spectrometer, so that a large solid angle (25% of 4π) could be used. The crystal was covered with a brass plate when the target was put in position for the bombardment, in order to protect the crystal from strong irradiation with scattered protons. After the beam was shut off and the brass plate removed, an activity in the target could be followed for a few minutes.

The counter was first set to count all electrons of energies between 45 kev and 100 kev, and with this setting the half-life of the produced activity was measured. The average for a dozen runs was 40 sec, with a standard deviation of 1 sec.

Then a beam integrator was made, which consisted of a 1 micro-farad capacitor shunted with a leakage resistor of 60 MΩ to give a half-discharge time of 40 sec. The voltage to which this capacitor was charged by the beam was used as a measure of the relative number of radioactive silver nuclei present in the target at the end of the bombardment. The spectrum shown in fig. 1 was obtained by counting the corresponding number of electrons emitted with various energies during the first two minutes after the irradiation. In order to calibrate the spectrometer, pulse spectra were also measured, when the crystal was bombarded with 65 kev and 90 kev electrons emitted from a tungsten target under proton bombardment and selected by means of a magnetic spectrometer. The sum with even weight of the two curves obtained in this way should approximately imitate the common spectrum of K and L plus M electrons emitted from a thin Ag target. The sum is shown as a solid curve in fig. 1, normalized to give the same area as the measured spectrum. The energy lost by the electrons on their way out of the thick silver target accounts for the small shift of the experimental points towards lower energies. The points were measured for the case where the angle between the proton beam and the target surface was 25°. With a beam perpendicular to the surface the distortion of the spectrum was much greater.

The characteristic half-life and β-energy made it easy to distinguish the isomeric activity from others also produced in the target, mainly by capture processes in ^{12}C and ^{16}O nuclei from vacuum oil deposits on the target surface. These activities were also found in an experiment with a dummy target of Cu, which, however, emitted no measurable amount of low energy electrons.

After we had identified in this way the low energy β-particles as due to the isomeric states in silver, an excitation curve was measured for the part of the spectrum which lies between the two marks on the abscissa axis in fig. 1. Under the assumption that this part constitutes about 75% of the

total spectrum at all bombarding energies, one obtains the thick target yields shown in fig. 2.

First one can compare the measured yield with the theoretical yield for the direct excitation process. From the known values for the half-life and total conversion coefficients of the E3 radiation, one can calculate the reduced transition probability (Bohr and Mottelson 1953), which in turn determines the absolute cross section for E3 Coulomb excitation.* For 2 MeV protons one gets a cross section of the order of 10^{-32} cm^2. The

Fig. 1

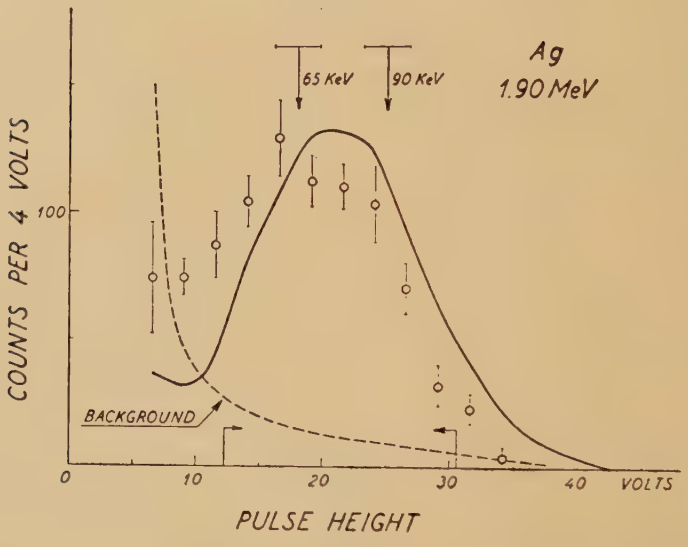

Spectrum of conversion electrons emitted from a thick target of natural silver after bombardment with about 1 micro-amp of 1·9 MeV protons. The measured points are corrected for the background noise. The arrows on the abscissa axis indicate the part of the spectrum used in the measurements of the yield function. The solid curve represents the spectrum corresponding to an even number of 65 kev and 90 kev monoenergetic electrons.

calculated thick target yield curve is shown in fig. 2. Evidently, it is unable to account for the measured activity both with regards to magnitude and energy dependence. The relatively large experimental yield must therefore mainly be due to E2 excitations of higher lying states, which to some extent decay through cascade transitions to the isomeric states.

By bombardment of natural silver targets with 1·75 MeV protons we had found previously a prompt gamma ray at 320 kev, whereas Temmer and

* Cf. J. H. Bjerregaard and T. Huus, 1954, *Phys. Rev.*, **94,** 204. The function $f_3\{\xi\}$ has now been evaluated by Alder and Winther (private communication). For the present purpose, no great error is made by substituting $f_3\{0\}=0{\cdot}038$ for $f_3\{\xi\}$, since $\xi\simeq 0{\cdot}15$ for the direct excitation.

Heydenburg, with 3 MeV α-particles, have observed gamma rays at 318 kev and 432 kev.* Using separated isotopes, these authors have also shown that the two isotopes ^{107}Ag and ^{109}Ag have excitation energies which are closely equal. Because of the small conversion coefficients, our search for the K-electrons gave a negative result in the case of the 430 kev lines whereas the measured spectra clearly exhibited the peaks due to the lower pair of lines. The corresponding excitation energies were 306 kev and 321 kev. In the present work we may disregard the differences in the behaviour of the two isotopes.

Fig. 2

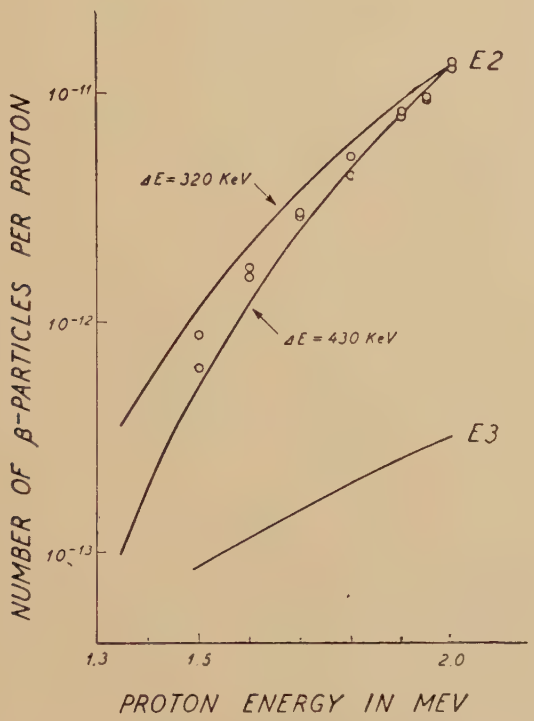

Total thick target yields measured as a function of the bombarding energy. The E3 curve gives the theoretical absolute yield of the direct octopole excitation of the isometric states. The E2 curves give the theoretical energy dependences for the quadrupole excitations of rotational states at 320 kev and 430 kev. The latter curves are normalized at 2 MeV.

These high energy excitations have the large matrix elements characteristic for rotational transitions of E2 type. The silver isotopes are known to have a ground state spin of 1/2 (Hollander, Perlman and

* We are indebted to these authors for a private communication of their results on the Coulomb excitation of silver. We too found a line at 430 kev, but that is believed to be due mainly to the reaction ^{10}B(p, $\alpha\gamma$)^{7}Be in a surface contamination of borax.

Seaborg 1953), and are thus expected to have the anomalous rotational spectrum (Bohr and Mottelson 1953)

$$E_I=(\hbar^2/2\mathscr{I})[I(I+1)+a(-1)^{I+1/2}(I+1/2)], \quad . \quad . \quad . \quad . \quad (1)$$

where $\mathscr{I}$ is the moment of inertia and where a is a decoupling parameter depending on the binding state of the last odd proton, for which the component of angular momentum Ω along the nuclear axis is 1/2. This parameter can be written as

$$a=-\Sigma_j(-1)^{j+1/2}(j+1/2)\,|c_j|^2, \quad . \quad . \quad . \quad . \quad . \quad (2)$$

where $|c_j|^2$ is the probability for the particle to have total angular momentum j. While the normal rotational spectrum for an odd A nucleus is given by the spin sequence

$$I=I_0,\ I_0+1,\ I_0+2,\ \ldots \text{ (all same parity as the ground state)}, \quad . \quad (3)$$

where I_0 is the ground state spin, it may happen that the second term in formula (1) for large values of a leads to level inversions. However, the evidence discussed below indicates that the silver isotopes have the normal sequence 1/2, 3/2, 5/2.

With this spin assignment for the observed levels, one calculates

$$\hbar^2/2\mathscr{I}=64 \text{ kev} \quad \text{and} \quad a\simeq 2/3. \quad . \quad . \quad . \quad . \quad . \quad (4)$$

The former value may be compared with the excitation energy of the first excited (2^+) state of neighbouring even–even nuclei, which for the same moment of inertia would be $E_2=6(\hbar^2/2\mathscr{I})\simeq 380$ kev. It is of interest that the first excited state in $^{108}_{46}$Pd has an energy of 420 kev (Scharff-Goldhaber 1953), thus suggesting a rather similar deformation to that of the silver isotopes.

For a pure $p_{1/2}$ state for the last odd proton in silver the quantity a would be unity, and, consequently, the $3/2^-$ and $5/2^-$ states would coincide. However, a small admixture of the $p_{3/2}$ state would suffice to account for the observed value of a. Such admixtures of neighbouring states are expected (Bohr and Mottelson 1953) as a consequence of the non-central character of the nuclear binding field.

At a proton bombarding energy of 1·75 Mev the excitation cross section for the 320 kev state was measured to be of the order of 0·1 millibarn, from which value one can derive an intrinsic nuclear quadrupole moment Q_0 of about 2×10^{-24} cm^2. This moment is of the same order of magnitude as that obtained for the neighbouring Indium isotope from spectroscopic measurements.

In order to test which level feeds the isomeric states we have calculated the thick target E2 yield curves for the 320 kev and 430 kev states. They are shown in fig. 2, normalized to coincide with the experimental yield of the isomeric activity at 2 Mev. The measured energy dependence of this activity seems to be somewhere in between these limits. However, the shift of the electron spectrum (cf. fig. 1, as discussed earlier) is more important at the higher bombarding energies, where the electrons come from a relatively thicker layer and therefore more of them escape the

counting. Consequently, the measurements are best accounted for by assuming the excitation to take place via the levels at 430 kev.

Since the isomeric state has spin 7/2 and even parity (Goldhaber and Hill 1952), it can be reached from the $5/2^-$ rotational state by an E1 transition, but from the $3/2^-$ rotational state only by an M2 transition. This makes it very probable that the excitation takes place via the $5/2^-$ state, which should thus be the higher of the two rotational states. The resulting level scheme for the silver isotopes is shown in fig. 3.

Since the cross section for the 430 kev level can be calculated from the Q_0 value, one can by comparison with the yield of the isomeric activity estimate the fraction of the 430 kev excitations which decay via the isomeric state. This fraction is found to be about 0·5%. Under the assumption that the $5/2^-$ to $3/2^-$ cascade decay does not essentially

Fig. 3

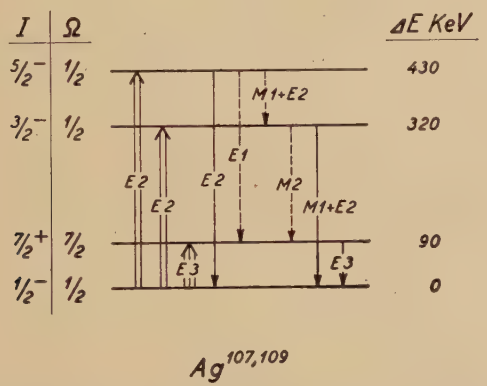

Suggested level scheme for the two silver isotopes, fitting the available experimental data. Observed transitions are drawn in full. The two nuclei have slightly different excitation energies; the values given in the figure are therefore only approximate.

influence the total decay probability of the 430 kev state, one can also estimate the reduced transition probability for the E1 decay, which is found to be about 2×10^6 times smaller than single particle estimates (Blatt and Weisskopf 1952).

Such a strong reduction of the transition probability is actually expected from the fact that, although $\Delta I=1$, the quantum number Ω changes by three units, since the isomeric state has $\Omega=7/2$. If Ω were an exact constant of motion, such a transition would have to be of multipole order three. However, the expected small admixtures in the wave function of other values suffice to make the transition dominantly of dipole type, but with a much reduced intensity (Bohr and Mottelson 1953, Alaga, Alder, Bohr and Mottelson, in preparation).

We have also tried the present experiment with 1·9 MeV α-particles and

deuterons. No effect was detected with α-particles, as is also to be expected, if the excitation of the isomeric activity takes place via the higher lying levels, which are more difficult to excite with α-particles at such a low bombarding energy. In the case of deuterons, extremely strong activities due to the process ^{12}C (dn) ^{13}N (β^+) ^{13}C prevented measurements of the isomeric activities.

In conclusion we wish to thank Professor Niels Bohr for his kind interest, and A. Bohr and B. R. Mottelson for discussions on the subject. We are grateful to J. H. Bjerregaard and B. S. Madsen for experimental aid. One of us (A. L.) is further indebted to " Landsforeningen ' Det frie Nord ' og Generalløjtnant Erik With's Nordiske Fond " for financial support during his stay in Copenhagen.

References

Alaga, G., Alder, K., Bohr, A., and Mottelson, B. R. (in preparation).
Blatt, J. M., and Weisskopf, V. F., 1952, *Theoretical Nuclear Physics* (New York : J. Wiley and Sons).
Bohr, A., and Mottelson, B. R., 1953, *Dan. Mat. Fys. Medd.*, **27,** no. 16.
Goldhaber, M., and Hill, R. D., 1952, *Rev. Mod. Phys.*, **24,** 179.
Hollander, J. M., Perlman, I., and Seaborg, G. T., 1953, *Rev. Mod. Phys.*, **25,** 469.
Huus, T., and Zupančič, Č., 1953, *Dan. Mat. Fys. Medd.*, **28,** no. 1.
Scharff-Goldhaber, G., 1953, *Phys. Rev.*, **90,** 587.
Temmer, G. M., and Heydenburg, N. P., 1954, *Phys. Rev.* (in press).
Zupančič, Č., and Huus, T., 1954, *Phys. Rev.*, **94,** 205.

CVI. *The Emission Polar Diagram of the Radio-Frequency Radiation from Sunspots*

By K. E. Machin and P. A. O'Brien
Cavendish Laboratory, Cambridge*

[Received May 13, 1954]

Summary

A statistical analysis of daily measurements of the intensity of radio emission from the sun over a number of years has led to a determination of the variation in sunspot emission caused by the solar rotation. The total widths to half intensity of the emission polar diagrams derived in this way for an average sunspot are 15°, 20° and 36° for frequencies of 81·5, 175 and 500 Mc/s respectively.

The analysis also suggests that there is a decrease in the life-time of the sources of radio emission as the frequency decreases; the life-time at 175 Mc/s is comparable with that of a visible spot.

§ 1. Introduction

Early observations on metre wavelengths (Appleton and Hey 1946, McCready, Pawsey and Payne-Scott 1947, Allen 1947, Hey, Parsons and Phillips 1948) showed that the received intensity of the radiation associated with sunspots exhibited a marked maximum near the time of central meridian passage of the visible spot. On centimetric wavelengths, however, it was found (Covington 1948) that the intensity was strongly correlated with the sunspot number, a result which suggested that the emission occurred over a wide angle. The latter result has recently been confirmed by Takakura (1953) for a frequency of 3260 Mc/s; his analysis for frequencies of 1200, 600 and 200 Mc/s indicated that the emission polar diagram was narrower than on 3260 Mc/s, but the results were not conclusive owing to the large standard errors in the analysis.

The present communication describes the results of a quantitative statistical analysis of observations taken over long periods on frequencies of 81·5, 175 and 500 Mc/s.

§ 2. The Statistical Method

Consider the intensity of the radiation which would be received at the earth as a single sunspot crosses the solar disc. The variation with time of the intensity will be given by $AP(t)$ where A represents the maximum intensity of the radiation and $P(t)$ represents the emission polar diagram of the source which is swept across the earth by the rotation of the sun. We shall call the increased intensity $AP(t)$ a ' pulse '.

* Communicated by M. Ryle, F.R.S.

In practice the ' pulses ' occur at random times and with random amplitudes, and sometimes ' pulses ' from neighbouring sources overlap. Let $I(t)$ be the time variation of the intensity due to all the ' pulses ' occurring over a long time. We may now show how $P(t)$ may be deduced from a knowledge of $I(t)$.

We assume that (i) $P(t)$ is a symmetrical function of time, t, (ii) the successive sources cross the central meridian of the sun at random times, and (iii) A is a constant for any one source.

$I(t)$ is then made up of a series of ' pulses ' of the same shape $P(t)$, with randomly distributed amplitudes, and randomly distributed in time.

If the auto-correlation function, $\rho_I(\tau)$, of a function such as $I(t)$ is defined by

$$\rho\ (\tau)=\frac{\overline{I(t)I(t+\tau)}-\{\overline{I(t)}\}^2}{\overline{\{I(t)\}^2}-\{\overline{I(t)}\}^2},$$

then the auto-correlation function, $\rho_P(\tau)$, of the quantity $P(t)$ will be given by

$$\rho_P(\tau)=\rho_I(\tau).$$

The procedure, then, is to determine the auto-correlation function, or auto-correlogram, $\rho_I(\tau)$, of $I(t)$ and then to deduce $P(t)$ from $\rho_P(\tau)$. This can be obtained from the power spectrum, $W(f)$, of the function $P(t)$ by the Wiener–Khintchine relation

$$W(f)=\int_{-\infty}^{+\infty}\rho_P(\tau)\cos 2\pi f\tau\, d\tau,$$

and the relation between $P(t)$ and the power spectrum

$$\{W(f)\}^{1/2}=\int_{-\infty}^{+\infty}P(t)\cos 2\pi ft\, dt.$$

§ 3. The Results Obtained

The method was applied to measurements of the intensity of solar radiation extending over a period of four years for the frequencies 81·5 and 175 Mc/s, and over nine months for 500 Mc/s. Daily values of intensity, averaged over the observing period of six hours, were used to construct the time-series $I(t)$.

The auto-correlograms obtained are shown in figs. 1, 2 and 3 in the form of bands within which the true correlograms will almost certainly fall. The limits of the bands are shown at twice the standard error on either side of the calculated value of $\rho_I(\tau)$. Smooth curves (shown dotted) have been fitted and from them the emission polar diagrams for an ' average sunspot ' were derived by the method outlined above ; these polar diagrams are shown in fig. 4. It can be seen that the radiation is emitted over a restricted angle whose total width to half intensity is : 15° for 81·5 Mc/s, 20° for 175 Mc/s and 36° for 500 Mc/s.

Fig. 1

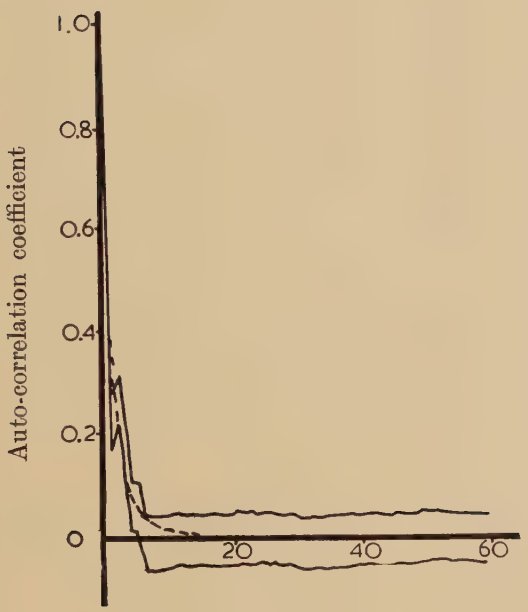

The auto-correlogram of the time-series $I(t)$ for a frequency of 81·5 Mc/s.

Fig. 2

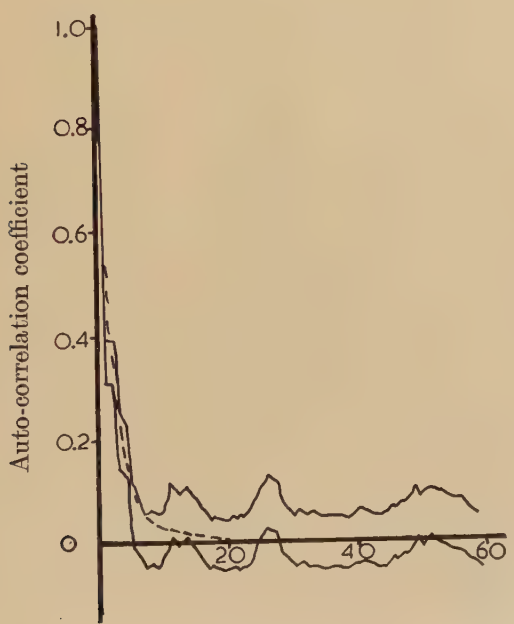

The auto-correlogram of the time-series $I(t)$ for a frequency of 175 Mc/s.

Fig. 3

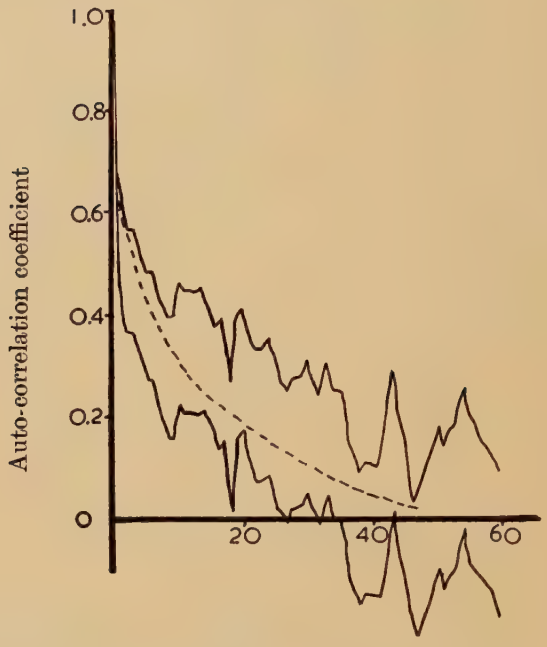

Time in days

The auto-correlogram of the time-series $I(t)$ for a frequency of 500 Mc/s.

Fig. 4

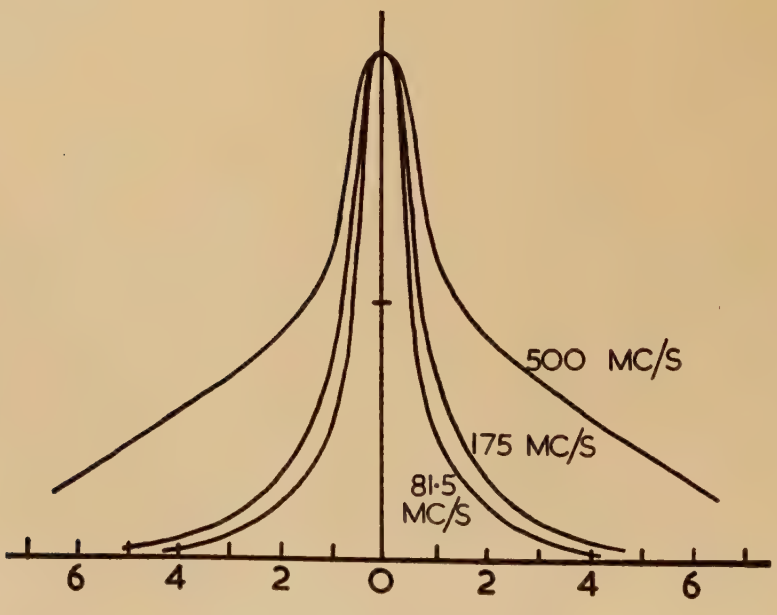

Days from central meridian passage

The emission polar diagrams of the radio-frequency radiation from sunspots for frequencies of 81·5, 175 and 500 Mc/s.

§ 4. Possible Sources of Error

(*a*) When determining the intensity/time curve $I(t)$ it is only possible to make use of observations of intensity over a period of about six hours every day. This restriction can give rise to errors in two ways.

The first kind arises at the lower frequencies, where the polar diagram is so narrow that it is swept across the earth in one or two days. Results obtained over only about six hours each day cannot therefore give an accurate representation of $I(t)$; the derived polar diagram is therefore liable to some distortion, although the widths are likely to be accurate to within 30%.

The second error arises from the possibility that large changes of intensity associated with ' outbursts '—the sudden enhancements associated with solar flares—may have been interpreted as effects due to the solar rotation. In deriving the curve $I(t)$ every effort was made to exclude such disturbances, but it would be difficult to detect an outburst which started before the period of observation and lasted longer than six hours; the inclusion of such phenomena would give rise to a reduction in the apparent width of the polar diagram.

An analysis was therefore made of the life-time of outbursts, from which it became clear that very few disturbances of long duration were likely to occur. The resulting errors introduced in the widths of the polar diagrams are unlikely to exceed 15%.

Both of these effects could be eliminated if continuous observations of the intensity were available; a solution may be provided by observations on the same frequency by stations at different longitudes, or alternatively by summer observations at a station situated within the Arctic Circle.

(*b*) Errors may also be introduced if the intensity A of the emitted radiation is not constant but varies within a time comparable with the width of the emission polar diagram. This effect causes the calculated polar diagram to be narrower than the true one.

It is difficult to separate such time variations of A from the polar diagram function $P(t)$ merely by inspection. A further analysis was therefore carried out in which the time series $I(t)$ was cross-correlated with a time series constructed from the areas of visible sunspots at central meridian passage. The cross-correlograms are not affected by time variations of A and the analysis should produce cross-correlograms which are similar to those of figs. 1–3.

However, errors may arise if the maxima of the emission polar diagrams of different spots are not normal to the solar surface but are inclined at different angles to the normal. This effect would produce an artificial widening in the polar diagrams deduced from cross-correlograms.

The results of the cross-correlation analysis showed that the widths of the cross-correlograms were comparable with the widths of the auto-correlograms in figs. 1–3.

Since the two different correlation analyses lead to upper and lower limits of the widths of the polar diagrams, it follows that the derived widths are not seriously in error.

§ 5. The 'Life-Time' of the Sources of Radio Emission

In addition to providing information on the emission polar diagram, the auto-correlogram of $I(t)$ gives information on the average life-time of the source of radio emission associated with a sunspot. For 81·5 Mc/s it is seen from fig. 1 that there is no significant tendency for the auto-correlation coefficient to increase at times corresponding to one or two solar rotations, but at 175 Mc/s there is definite evidence for a 27-day recurrence (fig. 2). At 500 Mc/s the observations were maintained for a shorter period, and the large standard error in fig. 3 masks any recurrence tendency.

For comparison a similar analysis has been carried out on visible sunspots, using a time-series consisting of daily values of the total area of sunspots lying within $\pm 7°$ of the longitude of the centre of the disk, i.e. of spots which crossed the meridian on each day. The auto-correlogram of this series is given in fig. 5.

Fig. 5

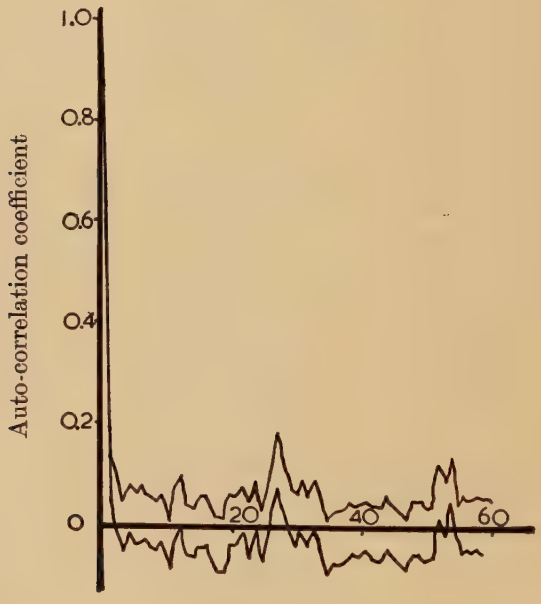

The auto-correlogram of a time-series consisting of daily values of the total area of sunspots lying within $\pm 7°$ of the longitude of the centre of the disk.

A comparison of the curves shows that the source of 175 Mc/s radiation persists for a time comparable with that of the visible spot, whilst at 81·5 Mc/s the life-time is considerably less.

Piddington and Davies (1953) have shown that on frequencies between 600 and 9400 Mc/s there is a tendency, which is more marked at the higher frequencies, for the emission to persist for several solar rotations, even after the associated spot has disappeared.

The results therefore suggest that there is a progressive decrease in the life-time of the sources of radio emission as the frequency decreases ; the life-time at 175 Mc/s is comparable with that of the visible spot.

Acknowledgments

This work was carried out as part of a programme of research at the Cavendish Laboratory supported by the Department of Scientific and Industrial Research. The computations were carried out on EDSAC through the kindness of the Director and staff of the University Mathematical Laboratory.

References

Allen, C. W., 1947, *M.N.R.A.S.*, **107,** 386.
Appleton, E. V., and Hey, J. S., 1946, *Phil. Mag.*, **37,** 73.
Covington, A. E., 1948, *Proc. I.R.E.*, **36,** 454.
Hey, J. S., Parsons, S. J., and Phillips, J. W., 1948, *M.N.R.A.S.*, **108,** 354.
McCready, L. L., Pawsey, J. L., and Payne-Scott, R., 1947, *Proc. Roy. Soc.* A, **190,** 357.
Piddington, J. H., and Davies, R. D., 1953, *Nature, Lond.*, **171,** 692.
Takakura, T., 1953, *Nature, Lond.*, **171,** 445.

CVII. *The Anomalous Scattering of μ-Mesons*

By G. D. Rochester and A. W. Wolfendale
The Physical Laboratories, The University, Manchester*

[Received May 15, 1954]

Abstract

A re-examination of the data on the scattering of fast μ-mesons in the photographic emulsion has been made for a number of nuclear models. It is shown that the most reasonable models still predict less scattering than is observed. However, because of the absence of an exact model of the nucleus and exact scattering calculations for μ-mesons, it is not possible to conclude that the anomaly indicates the existence of a *non-electric*, short-range interaction between the μ-meson and the nucleon.

§ 1. Introduction

The purpose of this note is to re-present the analysis of the μ-meson scattering experiment of Kannangara and Shrikantia (1953) (to be called paper A), as a result of a more accurate evaluation of the underground spectrum, and to assess the new results in the light of the comments of Rainwater, Fitch and Koslov (private communication) and recent work on the charge distribution in nuclei. These authors have brought to our notice the fact that the nuclear model postulated by Williams (1939), and used in paper A, leads to a gross over-estimate of the size of the nucleus. The error introduced into the analysis arises in two ways: (1) from the reduction in the value of r_0 in the usual expression for the nuclear radius, i.e., $R_0=r_0A^{1/3}$ (from $1{\cdot}5\times10^{-13}$ cm to $(1{\cdot}15-1{\cdot}2)\times10^{-13}$ cm (Fitch and Rainwater 1953, Cooper and Henley 1953, Bitter and Feshbach 1953)), and (2) from the parameter $\langle r^2\rangle$ which enters into scattering theory. Williams assumed a nucleus with a uniform charge distribution (' Uniform nuclear model ', called U.N.M.) of radius R_0 and approximated the electrostatic potential to a simple continuous function valid both inside and outside the nucleus. Rainwater has pointed out that this approximation does not, in fact, lead to a uniform charge density ρ_0 but one varying according to the function,

$$\rho(r)=\frac{4}{3}\rho_0\frac{R_0}{r}\exp\left(-\frac{2r}{R_0}\right). \quad . \quad . \quad . \quad . \quad . \quad . \quad (1)$$

This function results in the quantity $\langle r^2\rangle$ being 2·5 times larger than the correct value for a U.N.M. with the reduced value of r_0.

Both errors cause an underestimate of the theoretical number of deflections and therefore the use of the more accurate nuclear model should lead to better agreement between the theoretical and the experimental

* Communicated by the Authors.

results. However, we have now been able to obtain a more accurate estimate of the number of low-energy μ-mesons than was possible when paper A was written, and this correction largely compensates for the effect of the more accurate nuclear model. The various factors are considered in detail in §§ 2 and 3.

§ 2. The Underground Spectrum

The form of the underground differential spectrum of cosmic-ray μ-mesons assumed in paper A was the one given by George (1952), namely,

$$N(E)dE = \frac{392\,dE}{(E+14)^3} \quad . \quad . \quad . \quad . \quad . \quad . \quad . \quad (2)$$

where E is the total energy in Bev. This form assumes a constant exponent 3·0 in the differential production spectrum and an energy loss of 14 Bev from production to a depth of 60 m.w.e. The differential spectrum at sea-level has been measured by Caro *et al.* (1950) and by Holmes, Owen, Rodgers and Wilson (private communication) ; both groups find that for energies appreciably above 20 Bev the spectrum has an exponent 3·0 so that at high energies underground, where this exponent is valid, the spectrum will be correctly represented by eqn. (2). For mesons at 60 m.w.e. underground, with energies less than about 500 Mev, however, which class includes all the large-angle deflections under discussion, the energies at sea-level are less than 20 Bev and the spectrum is not represented accurately by (2). The accurate spectrum of Holmes *et al.* shows that for energies above about 8 Bev (at sea-level), the exponent varies rapidly with increasing energy, the value at 13 Bev being $2{\cdot}0 \pm 0{\cdot}1$, increasing to 3·0 above 20 Bev. From this spectrum the percentage of mesons with kinetic energies less than 1 Bev at 60 m.w.e. is $(9{\cdot}0 \pm 0{\cdot}5)\%$ compared with 13% calculated from (2). The value of 9% is probably still an overestimate because of the loss of low-energy mesons by scattering before they enter the emulsion. Thus the number of low-energy mesons used in paper A was overestimated by at least 30%. Expressing this number in terms of the track lengths in the emulsion in definite energy bands, the figures given in table 1 are obtained.

Table 1. Track Length per 100 Mev as a Function of Kinetic Energy

Kinetic Energy (Mev)	200	400	600	800	1000
Track length per 100 Mev (cm)	118	116	113	110	107

These values when combined with the appropriate integral cross section give the numbers of deflections to be expected. Thus, if the scattering is of the Rutherford type (i.e. point nucleus) the expected number of large-angle deflections greater than 7° per cm length of track, due to nuclei of charge $Z_i e$, with n_i nuclei of type 'i' per cm^3 is given by eqn. (3), namely,

$$N\,(>7^\circ) = 1{\cdot}74 \times 10^{-23}\,(Z_i^2\, n_i/p^2\beta^2)\ \mathrm{cm}^{-1}, \quad . \quad . \quad . \quad . \quad (3)$$

where p is in MeV/c. The actual number of deflections is found by summing expressions of the type (3) over the elements of the emulsion and multiplying the results by the track lengths.

§ 3. Comparison with Different Nuclear Models

In this section a comparison is made of the observed deflections with those calculated for different nuclear models. Since the Born approximations are used throughout, the justification for this procedure will now be considered by taking as an example the Coulomb scattering of a particle of velocity βc, charge e, through an angle θ by a point charge Ze. With the second Born approximation the differential cross section for this type of scattering is

$$\sigma=\sigma_R\left\{1-\beta^2\sin^2\frac{\theta}{2}+\pi Z\alpha\beta\sin\frac{\theta}{2}\left(1-\sin\frac{\theta}{2}\right)\right\}, \quad . \quad . \quad . \quad (4)$$

where σ_R is the Rutherford cross section. For the elements present in the emulsion and the relatively small scattering angles observed, the second and third terms of (4) are negligible and the cross section reduces to σ_R. The *exact* phase shift calculations for low-energy electrons have been made by Mott and Massey (1949) and for high-energy electrons by Yennie *et al.* (1953). These calculations show that there is an appreciable increase in cross section over σ_R and the value from the Born approximation, at large angles (i.e., $>30°$). However, when the results of Mott and Massey are taken over to μ-mesons, after making the appropriate change in the rest-energy, and assuming that the theory is otherwise valid for these particles, the values of σ/σ_R for the observed deflections differ from unity by 30% at most. Moreover, the differences are alternately positive and negative, for negative and positive particles respectively, so that for the underground cosmic-ray spectrum, which contains approximately equal numbers of particles of both signs, the divergence from the Rutherford cross section should be small.

The effect of the finite size of the nucleus is to reduce the number of large-angle deflections. The new cross section, σ_S, can be written,

$$\sigma_S=K\sigma_R, \quad . \quad . \quad . \quad . \quad . \quad . \quad . \quad . \quad . \quad . \quad (5)$$

where K is a function of the nuclear charge distribution, and the momentum transfer from the scattered particle to the nucleus.

The factor K can be obtained for different nuclear models, for example, for a sphere of constant charge density (U.N.M.), or for a tapering charge density of some specific form—exponential, gaussian, etc. For the U.N.M. K has been given by Rose (1948), namely,

$$K=\left[\frac{3}{(qR_0)^2}\left(\frac{\sin qR_0}{qR_0}-\cos qR_0\right)\right]^2, \quad . \quad . \quad . \quad . \quad (6)$$

where $\hbar q$ is the momentum transfer. This expression predicts diffraction maxima and minima which are *not* observed in high-energy electron scattering. However, for the μ-mesons considered here the values of qR_0

concerned are well below the first diffraction minimum and the Born approximation should be valid. This conclusion is in line with the results of the recent calculations of Yennie *et al.* (1953), already referred to, who have shown that for electrons and the U.N.M. (and also the exponential charge distribution), the divergence from the Born approximation is small for small scattering angles.

The expected number of events for the U.N.M. with $R_0=1{\cdot}15\times10^{-13}A^{1/3}$ cm has been calculated from the expressions (3), (5), and (6), and the data given in table 1. The results are given in table 2, and are presented in the form of the number of deflections (with $\theta>7°$) $v\,p\theta$, where p is the momentum in Bev/c and θ the scattering angle in degrees. As an example of the significance of these figures it may be noted that assuming a Poisson Distribution the chance of observing 7 or more deflections when 3·5 are expected is about 6%. The distribution with

Table 2. Observed and Calculated Deflections as a Function of $p\theta$

$p\theta$ (Bev/c deg.)	1	2	4
Observed numbed $>p\theta$	7	5	2
Expected number $>p\theta$ for point nucleus	6·3	4·8	2·5
Expected number $>p\theta$ for U.N.M. with $R_0=1{\cdot}15\times10^{-13}A^{1/3}$ cm	3·5	2·1	0·31

Table 3. Observed and Calculated Deflections as a Function of $p\beta$

Range of $p\beta$ (Mev/c)	(100–200)	>200
Observer number	3	4
Expected number for point nucleus	2·7	3·6
Expected number for U.N.M. with $R_0=1{\cdot}15\times10^{-13}A^{1/3}$ cm	2·2	1·3

$p\beta$ is given in table 3. The expected number of events at low momenta may have been somewhat overestimated because of the uncertainty in the number of low-energy mesons traversing the emulsions. It is to be noted that, within the poor statistical weight, there is still better agreement with the point nucleus model. Similar results are obtained from the scattering distributions evaluated by Gatto (1953). Gatto shows also that the predicted *incoherent* scattering is quite insufficient to account for the experimental results.

Some information on the nuclear charge distribution comes from the recent work on high-energy electron scattering by Hofstadter *et al.* (1953). Hofstadter finds that a charge distribution of the form

$$\rho(r)=\rho_0 \exp(-r/a), \quad \ldots\ldots\ldots \quad (7)$$

fits the experimental results, the best value of a for lead, for example, being $2{\cdot}36\times10^{-13}$ cm.

The exponential charge distribution gives

$$K=\frac{1}{(1+q^2a^2)^4} \quad \ldots\ldots\ldots \quad (8)$$

and in the case of lead with the value of a given above, K lies below the value for a U.N.M. with $r_0=1{\cdot}15\times10^{-13}$ cm for the significant range of scattering angles. Thus our analysis includes a nucleus of this type. However, Schiff (1953) has shown that Hofstadter's results are consistent with a range of values of a, from 1·6 to $2{\cdot}9\times10^{-13}$ cm, due to the fact that the theoretical distribution is normalized to the experimental curve at a particular point and only gradients are compared. Feshbach (1951) has shown that low-energy scattering is model-independent, the operative parameter being the fourth moment of the charge distribution. The exponential charge distribution with $a=2{\cdot}36\times10^{-13}$ cm gives a fourth moment in disagreement with the results for low-energy electrons. The lower limit to the range of values of a, namely $1{\cdot}6\times10^{-13}$ cm, gives a fourth moment of the correct magnitude. Such a sharply peaked charge distribution would of course give better agreement with our experimental results but it is thought to be unlikely in view of other experiments yielding information on nuclear structure. Brenner *et al.* (1954) have shown that it is unnecessary to postulate rapidly tapering charge distributions in order to explain high-energy electron scattering. These authors find that the form

$$\rho=\rho_0\Big/\left\{1+\exp 2\left(\frac{r^2}{0{\cdot}55R_0^2}-1\right)\right\} \quad \ldots\ldots \quad (9)$$

with $R_0=1{\cdot}2\times10^{-13}A^{1/3}$ cm gives a smooth decrease consistent in form with Hofstadter's results. The K-factor is similar to that for a U.N.M. over the range important in our experiment.

It appears likely then that if the results for electrons can be taken over to μ-mesons the figures given for the U.N.M., i.e., row 4 of table 2, represent the numbers of events expected from most reasonable nuclear models.

§ 4. Conclusion

It is clear from the results presented in § 3 that within the rather poor statistics, an anomaly is still evident in the large-angle scattering of fast μ-mesons in the photographic emulsion for all of the most reasonable nuclear models. The anomaly is shown in a more striking manner in cloud-chamber experiments, a summary of which has been given by Leontic and Wolfendale (1953). Work now in progress in these laboratories

by Lloyd and Wolfendale (see Owen, Sciuti and Wolfendale, Report of Cagliari Conference 1953), and by McDiarmid (1954), confirms the existence of the anomaly at energies above 1 Bev. Because of the lack of an exact model of the nucleus, however, and the absence of detailed calculations of the deflections to be expected for fast μ-mesons on theoretical grounds, it is not possible to state, at this stage, whether the anomaly indicates the existence of a *non-electric*, short-range interaction between μ-mesons and nucleons.

Acknowledgments

We are most grateful to Professor Rainwater of Columbia University for pointing out to us the inadequacy of the model used in the original papers and for informing us of the (then unpublished) new work on the charge distribution in nuclei and the results of the scattering of fast electrons. We also wish to express our indebtedness to Dr. G. N. Fowler of the Theoretical Physics Department, and Miss S. Brenner of the Department of Mathematical Physics, Birmingham, for numerous discussions. Mr. A. L. Rodgers kindly made some calculations for us on the underground spectrum. Dr. R. Gatto of Rome, Dr. M. T. L. Kannangara of Colombo, and Dr. C. M. York of the California Institute of Technology have also made helpful comments.

References

Bitter, F., and Feshbach, H., 1953, *Phys. Rev.*, **92,** 837.
Brenner, S., Brown, G. E., and Elton, L. R. B., 1954, *Phil. Mag.* **45,** 524.
Caro, D. E., Parry, J. K., and Rathgeber, H. D., 1950, *Nature, Lond.*, **165,** 689.
Cooper, L. N., and Henley, E. W., 1953, *Phys. Rev.*, **91,** 480.
Feshbach, H., 1951, *Phys. Rev.*, **84,** 1206.
Fitch, V. L., and Rainwater, J., 1953, *Phys. Rev.*, **92,** 789.
Gatto, R., 1953, *Il Nuovo Cim.*, **10,** 1559.
George, E. P., 1952, *Progress in Cosmic Ray Physics*, Vol. I., p. 429 (Amsterdam : North Holland Publishing Company).
Hofstadter, R., Fetcher, H. R., and McIntyre, J. A., 1953, *Phys. Rev.*, **92,** 978.
Leontic, B., and Wolfendale, A. W., 1953, *Phil. Mag.*, **44,** 1101.
Kannangara, M. L. T., and Shrikantia, G. S., 1953, *Phil. Mag.*, **44,** 1091.
McDiarmid, I., 1954, *Phil. Mag.* (in the press).
Mott, N. F., and Massey, H. S. W., 1949, *The Theory of Atomic Collisions*, p. 81 (Oxford : Clarendon Press).
Owen, B. G., Sciuti, S., and Wolfendale, A. W., 1954, *Report of the Cagliari Conference, Nuovo Cim.* (in the press).
Rose, M. E., 1948, *Phys. Rev.*, **73,** 279.
Schiff, L. I., 1953, *Phys. Rev.*, **92,** 988.
Williams, E. J., 1939, *Proc. Roy. Soc.* A, **169,** 531.
Yennie, D. R., Wilson, R. N., and Ravenhall, D. G., 1953, *Phys. Rev.*, **92,** 1325.

CVIII. CORRESPONDENCE

The Diffusion of Carbon in Alpha Iron

By W. R. Thomas and G. M. Leak
British Iron and Steel Association

[Revised MS. received June 14, 1954]

To interpret the results of the authors' investigations of the effect of interstitial solutes on the strain ageing properties of mild steel it has been necessary to determine the diffusion coefficients of these solutes in alpha iron in the range 0–100°c where most of the experimental work is being done. The results for the diffusion of nitrogen have been reported earlier (Thomas and Leak 1954) and only the results for the diffusion of carbon are dealt with here.

All measurements were made by observing the change in internal friction or damping capacity caused by carbon in solution in alpha iron. References to the original method and theoretical treatment were given in the earlier note.

Temp. °c.	Frequency of oscillation sec^{-1}	Diffusion coefficient $\times 10^{16}$ cm^2 sec^{-1}
24	0·154	0·22
34·5	0·62	0·89
43·25	1·37	1·96
53	3·83	5·5
58	5	7·15
65·5	9·58	13·5
74	16·75	23·9

The same high purity iron was used again, in the form of wire 0·080 in. and 0·040 in. in diameter. After annealing in flowing wet hydrogen for 5 days at 700°c, carbon was introduced by annealing in a sealed system for 7 days at 700°c. The specimens were packed in carburized pure iron chips containing no nitrogen. Air was removed from the system and replaced by nitrogen-free oxygen to give a pressure of rather less than 1 atmosphere at 700°c. This treatment gave homogeneous specimens containing less than 0·001 wt. % nitrogen, with about 0·020% carbon. The wire was quenched into water from 715°c to retain the carbon in solution.

The diffusion coefficients were calculated from the frequency of the mechanical oscillation. The method of calculation has been discussed before. The results are given in the table.

The results are plotted in the figure as $-\log D$ vs. $1000/T$. The high temperature conventional diffusion data of Stanley (1949) are included to give greater precision to the estimation of Q and D_0. The activation energy for the diffusion process is given directly by the slope of the line as $Q=20\,400$ cal. The intercept at $1000/T=0$ gives D_0 as $3{\cdot}16\times10^{-2}$ cm^2 sec^{-1}. Stanley's data appears to give the only available high temperature

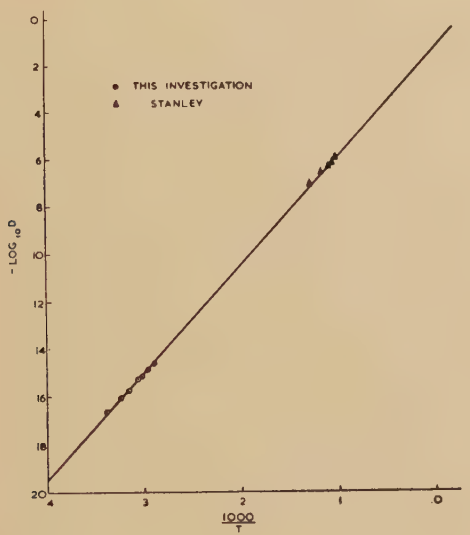

measurements for carbon in alpha iron, although by themselves they give $D_0=7{\cdot}9\times10^{-3}$ cm^2 sec^{-1} and $Q=18\,100$ cal. The present results agree substantially with those of Wert (1950) who gave $D_0=2\times10^{-2}$ cm^2 sec^{-1} and $Q=20\,100$ cal.

References

Stanley, G. K., 1949, *Trans. A.I.M.M.E.*, **185,** 752.
Thomas, W. R., and Leak, G. M., 1954, *Phil. Mag.*, **45,** 656.
Wert, C. A., 1950, *Phys. Rev.*, **79,** 601.

The Absolute Photo-Neutron Yield from Copper for the Lithium Gamma-Rays

By J. H. Carver and E. Kondaiah
Research School of Physical Sciences, Australian National University, Canberra*

[Received June 29, 1954]

In many photo-disintegration studies of the heavier elements the photo-neutron yield from copper has been taken as standard. McDaniel, Walker and Stearns (1950) used a ' long ' BF_3 neutron counter to measure the absolute photo-neutron yield from copper under the action of the 14·8 and 17·6 Mev gamma-rays from the ^{7}Li (p, γ) reaction ; they quote a cross section of $(55 \pm 12) \times 10^{-27}$ cm^2, the calibration being made by means of a standard Ra–Be neutron source. Other absolute measurements of the cross section for the lithium gamma-rays have been obtained by activation techniques. Thus Wäffler and Hirzel (1948) found the cross section for the ^{63}Cu (γ, n) ^{62}Cu reaction to be $(120 \pm 30) \times 10^{-27}$ cm^2 and the ratio of the ^{65}Cu (γ, n) ^{64}Cu to ^{63}Cu (γ, n) ^{62}Cu cross sections to be 1·5 : 1. Glättli, Seippel and Stoll (1952) found the cross section for the ^{63}Cu (γ, n) ^{62}Cu reaction to be $(48 \pm 8) \times 10^{-27}$ cm^2. Further estimates of the cross section, for the lithium gamma-ray mixture, can be made from the cross section versus gamma-ray energy curves obtained using electron bremsstrahlung. The Saskatoon group bases its cross sections on activation measurements of the copper cross section (Johns, Katz, Douglas and Haslam 1950, Montalbetti, Katz and Goldemberg 1953). Their value, for natural copper and the lithium gamma-ray mixture, is 95×10^{-27} cm^2 and is in good agreement with results obtained in a similar way by Diven and Almy (1950), Byerly and Stephens (1951) and Krohn and Shrader (1952).

In view of the large discrepancy between the photo-neutron yield measurement of McDaniel, Walker and Stearns (1950) and the various activation measurements (excepting that of Glättli, Seippel and Stoll 1952), it was decided to repeat the neutron yield measurement using different techniques for the neutron and gamma-ray intensity determinations.

In the present experiment the Szilard–Chalmers method has been used to measure the photo-neutron yield from natural copper when exposed to the radiation from the ^{7}Li (p, γ) reaction. The neutron detector was 130 litres of an aqueous potassium permanganate solution (concentration 30 g/litre) contained in a perspex tank ; the solution occupied a nearly

---

* Communicated by Professor E. W. Titterton.

cubical volume and the neutron source was placed at its centre. Protons of 440 kev, accelerated by the 1·2 Mev Canberra H.T. Set, were used to bombard thin, evaporated, lithium targets producing gamma-rays of 14·8 and 17·6 Mev in the ratio of 1·7 : 1 (Stearns and McDaniel 1951). The copper sample, enclosed in a thin perspex box, was attached to the end of the target tube from the accelerator and placed at the centre of the Szilard–Chalmers tank. During the irradiations (which were for one hour periods) the radiation was continuously monitored by a thick-walled Geiger counter identical in construction with the one described and calibrated by Barnes, Carver, Stafford and Wilkinson (1952). In order to correct for the neutron background* similar irradiations were made with an empty perspex box in place of the copper sample. After irradiation the solution was filtered to extract, as manganese dioxide, the radioactive ^{56}Mn produced by neutron capture, and the activity of the filtrate was measured by means of a standard beta-sensitive Geiger counter. After a number of preliminary runs, five irradiations with the copper and five background irradiations were performed and the relative neutron yields per quantum were obtained from the measured ^{56}Mn activities and the gamma-ray flux measurements. The results were corrected for counter backgrounds, for fluctuations in the gamma-ray yield during the irradiations, for the decay of the ^{56}Mn (half-life 2·6 hours) and for absorption of the gamma-rays in the copper.

Two methods were used to calibrate the neutron detector. In the first method the neutrons from the D (γ, n) reaction at a gamma-ray energy of 6·14 Mev were used. The gamma-rays were obtained by bombarding a thin CaF_2 target with 350 kev protons, yielding almost pure 6·14 Mev radiation (Chao, Tollestrup, Fowler and Lauritsen 1950). These gamma-rays were used to bombard a sample of heavy water contained in a perspex box of identical size with that which contained the copper sample. The geometrical arrangements were the same as those used for the copper irradiations and the same experimental procedure was employed; three calibration runs were made.† The data of Barnes, Carver, Stafford and Wilkinson (1952) on the D (γ, n) cross section were used in this calibration.

---

* One of the chief causes of background is photo-neutron reactions in the material of the target tube and in the detector. To minimize this the target tube was made of perspex (which has a low photo-neutron yield) and the thinnest possible copper backing for the target was used. The other major contribution to the background comes from (α, n) reactions due to the reaction of alpha-particles produced in the ^{7}Li (p, γ) ^{8}Be reaction with further lithium nuclei in the target; this was minimized by using a thin target. Even so, the background count was about half of that obtained with the copper.

† So as to correct for the neutron background similar irradiations were made with an empty perspex box. The neutron background in this case is small (less than 10% of the true count) and presumably arises from the reaction of alpha particles produced in the primary ^{19}F (p, α, γ) reaction with further fluorine nuclei in the target. A thin CaF_2 target ($\sim$20 kev) was used to minimize the background.

In the second method a standard Ra–Be neutron source* was used. The source was placed at the centre of the tank and the induced ^{56}Mn activity following the irradiation was measured ; a number of calibrating runs of this kind was made, interspersed between the other types of irradiations. The two calibrations differed by less than 10%. The D (γ, n) neutrons have a mean energy of 1·96 MeV and the Ra–Be neutrons have a complex spectrum with an average energy of about 5 MeV so that the agreement between the two calibrations shows that the tank has a flat energy response as is to be expected.

As a result of these measurements the cross section for photo-neutron production in copper by the 14·8 and 17·6 MeV gamma-rays from the ^{7}Li (p, γ) reaction was found to be

$$\sigma=(85\pm15)\times10^{-27}\ \text{cm}^2.$$

This result is considerably higher than that obtained by McDaniel, Walker and Stearns (1950) being in better agreement with the determination made by the Saskatoon group.

References

Barnes, C. A., Carver, J. H., Stafford, G. H., and Wilkinson, D. H., 1952, *Phys. Rev.*, **86**, 359.

Byerly, B. R., and Stephens, W. E., 1951, *Phys. Rev.*, **83**, 54.

Chao, C. Y., Tollestrup, A. V., Fowler, W. A., and Lauritsen, C. C., 1950, *Phys. Rev.*, **79**, 108.

Diven, B. C., and Almy, G. M., 1950, *Phys. Rev.*, **80**, 407.

Glättli, H., Seippel, O., and Stoll, P., 1952, *Helv. Phys. Acta*, **25**, 491.

Johns, H. E., Katz, L., Douglas, R. A., and Haslam, R. H. N., 1950, *Phys. Rev.*, **80**, 1062.

Krohn, V. E., and Shrader, E. F., 1952, *Phys. Rev.*, **87**, 685.

McDaniel, B. D., Walker, R. L., and Stearns, M. B., 1950, *Phys. Rev.*, **80**, 807.

Montalbetti, R., Katz, L., and Goldemberg, J., 1953, *Phys. Rev.*, **91**, 659.

Stearns, M. B., and McDaniel, B. D., 1951, *Phys. Rev.*, **82**, 450.

Wäffler, H., and Hirzel, O., 1948, *Helv. Phys. Acta*, **21**, 200.

* The source was made and calibrated at the Radiochemical Centre, Amersham, England.

Nuclear Spin of 241 Pu.

By B. Bleaney, P. M. Llewellyn, M. H. L. Pryce
Clarendon Laboratory, Oxford

and

G. R. Hall
Atomic Energy Research Establishment, Harwell

[Received July 22, 1954]

The paramagnetic resonance spectrum has been analysed of a single crystal of $(UO_2)Rb(NO_3)_3$ containing about 40 micrograms of the plutonium isotope 241. Using a wavelength of 3·3 cm and temperatures of 10° to 20°K, six equally spaced lines were observed due to the 241 isotope, showing that the nuclear spin is 5/2. The separation between successive lines was 245 ± 1 gauss, while the separation between the two hyperfine lines due to the isotope 239 (observed in the same crystal) was 347 ± 1 gauss. Since the nuclear spin of the latter isotope is 1/2, the ratio of the nuclear magnetic moments is $\mu(241)/\mu(239) = 3{\cdot}53 \pm 0{\cdot}02$.

The resonance results may be summarized in the spin Hamiltonian (with a fictitious spin $S = \frac{1}{2}$)

$$\mathscr{H} = g_{\parallel} \beta H_z S_z + A S_z I_z + P\{I_z^2 - \tfrac{1}{3} I(I+1)\} + \Delta_x S_x + \Delta_y S_y$$

where the last two terms represent the effect of departures of the crystalline electric field from the full symmetry associated with the crystal structure. The allowed transitions are then given by the formula

$$h\nu = \{(g_{\parallel} \beta H_z + Am)^2 + \Delta^2\}^{1/2}$$

where $\Delta^2 = \Delta_x^2 + \Delta_y^2$. This is similar to the formula of Bleaney and Scovil (1952) except that we now assume that Δ has a two-dimensional Gaussian distribution of values centred on zero, corresponding to random ' strains ' in the crystal. Intensity considerations show that this distribution gives an asymmetrical line shape, falling more steeply on the high field side to zero at the point corresponding to $\Delta = 0$ if no other source of line broadening is present. Though no detailed study of the line shape has been made experimentally, the line shape corresponds roughly to that expected on this basis (with a ' width ' at half intensity of about 18 gauss) and a correction for the asymmetry has been applied in obtaining the value of $g_{\parallel} = 5{\cdot}32 \pm 0{\cdot}02$. The following values of the parameters are obtained, which are more accurate than those previously reported (Bleaney, Llewellyn, Pryce and Hall 1954):

Isotope 239 : $I = 1/2$, $\quad A = 0{\cdot}0862 \pm 0{\cdot}0005$ cm^{-1};

Isotope 241 : $I = 5/2$, $\quad A = 0{\cdot}0609 \pm 0{\cdot}0004$ cm^{-1}.

The value given previously for isotope 239 ($A=0{\cdot}11$ cm^{-1}) contained a numerical error. With the same range for the possible value of $\overline{1/r^3}$ in the 5f state as assumed previously, the nuclear magnetic moments are found to be

$$\mu(239)=0{\cdot}4\pm0{\cdot}2 \text{ n.m.}; \quad \mu(241)=1{\cdot}4\pm0{\cdot}6 \text{ n.m.}$$

No information is obtained about the quadrupole interaction parameter P.

References

Bleaney, B., Llewellyn, P. M., Pryce, M. H. L., and Hall, G. R., 1954, *Phil. Mag.*, **45**, 773.

Bleaney, B., and Scovil, H. E. D., 1952, *Phil. Mag.*, **43**, 999.

Paramagnetic Resonance in Neptunyl Rubidium Nitrate

By B. Bleaney, P. M. Llewellyn, M. H. L. Pryce
Clarendon Laboratory, Oxford

and

G. R. Hall
Atomic Energy Research Establishment, Harwell

[Received July 23, 1954]

Paramagnetic resonance at 3·2 cm wavelength and at temperatures from 10° to 20°K has been observed in a single crystal of $(UO_2)Rb(NO_3)_3$ containing 400 micrograms of neptunium 237 as $(NpO_2)Rb(NO_3)_3$. Two types of transition are observable, depending on whether the microwave magnetic field is parallel or perpendicular to the d.c. magnetic field. In the parallel case, with the crystal axis also parallel to the d.c. field, the spectrum consists of five nearly equally spaced lines, with mean spacing 1422 gauss and relative intensities roughly 0·6 : 1 : 1 : 1 : 0·6. With the crystal axis again parallel to the d.c. field, but with perpendicular microwave field, there are six lines of equal intensity and nearly equal spacing (mean spacing 1044 gauss).

These observations are compatable with the known spin, $I=5/2$, of ^{237}Np (Tomkins 1948). The spin Hamiltonian of the system is, neglecting the direct effect of the magnetic field on the nucleus,

$$\mathscr{H}=g_{\parallel}\beta H_z S_z+g_{\perp}\beta(H_x S_x+H_y S_y)+AS_z I_z+B(S_x I_x+S_y I_y)$$
$$+P\{I_z{}^2-\tfrac{1}{3}I(I+1)\},$$

with

$$g_{\parallel}=3{\cdot}40\pm0{\cdot}05,$$
$$g_{\perp}\sim1(\pm0{\cdot}5),$$
$$A=0{\cdot}166\pm0{\cdot}002 \text{ cm}^{-1},$$
$$|B|=0{\cdot}02\pm0{\cdot}02 \text{ cm}^{-1},$$
$$P=-0{\cdot}030\pm0{\cdot}002 \text{ cm}^{-1}.$$

The relative sign of A and P is directly determined, and the absolute signs quoted are those suggested by present theoretical ideas concerning the electronic structure of the NpO_2^{++} complex and the nuclear moments of ^{237}Np. Neither $g_\perp$ nor B can be measured accurately with the present apparatus and special experiments are being planned to determine them more precisely.

An estimate of the nuclear moment, using the same provisional parameters for the NpO_2^{++} as have already been used (previous letter) for PuO_2^{++}, gives $\mu = 6 \pm 2{\cdot}5$ nuclear magnetons. No estimate of the nuclear quadrupole moment can yet be given.

Reference

Tomkins, F. S., 1948, *Phys. Rev.*, **73**, 1214.

CIX. *Notices of New Books and Periodicals received*

Geometrical Mechanics and de Broglie Waves. By J. L. Synge. (Cambridge Monographs on Mechanics and Applied Mathematics. Cambridge : University Press, 1954.) [Pp. vi+167.] Price 25*s*.

Professor Synge's brilliant tract has that touch of strong originality and unpractical elegance which characterizes the best productions of the Gaelic mind and gives them such a delightful unexpectedness. Here is a book on relativistic quantization in which no new method of renormalization is proposed, no wild attempt is made on the two-body problem, no scheme is even offered for labelling the pictures in the family album of the fundamental particles. What is the use of it, then ? the American reader will ask. None at all, I am afraid, except to provide a beautiful vista in Minkowskian space of the well-known relationship between dynamics and geometrical optics and to bring out with striking clarity the effect of quantization on it by means of a simplified formulation of the quantum conditions.

I wish this book would be read by every student of theoretical physics, at any rate by those who do not narrow their horizon to prosaic pursuits but are also anxious to get a feeling of the deep harmonies of nature. Professor Synge, unrivalled authority on Hamilton's profound thought, takes up the master's ideas and gives them a new formulation in 4-dimensional space which enhances still more their original beauty. Perhaps I ought to warn the inexperienced reader not to be carried away by Professor Synge's persuasiveness in believing that the remarkable geometrical patterns of quantized waves obtained by him could create " some doubt of the assertion sometimes made that quantum theory removes physics from the domain of direct intuitive conception derived from kinematic pictures ". But it would be pedantic to cavil at some stray irrelevant remark like this, which only adds to a fascinating tale the adequate flavour of Shavian flippancy. L. R.

The Sciences of Energy. By J. G. Crowther. (London : Muller.) [Pp. 271.] Price 12*s*. 6*d*.

This book is an attempt to present for the general reader the essence of 18 books, and 21 journals and papers, on astronomy, nuclear physics and chemistry, nearly all published since 1950. It is difficult to see how such a summary could make a coherent book, especially for the general reader, although one can only applaud anyone who tries the feat. Mr. Crowther, apparently undaunted, begins well with the cosmology of Lemaître (' Catholic creation '), of the Gamow school (' American explosion '), of Bondi and Gold (' English magic '), and of the Russian school (' Soviet realism '). After this, in the parts on atomic energy and chemistry, the book seemed to me to fall off, in spite of the appeal of its up-to-dateness. Its short, journalistic, one-sentence paragraphs began to be irritating, and made me uncomfortably aware of the lack of any real unifying theme. However, I ought to add that, as a result of reading this book, I have bought two of the books in the bibliographies. J. F. N.

Reports on Progress in Physics, Vol. 17. Published by The Physical Society.

The Papers Committee of the Physical Society has been as successful as usual in getting together a series of really authoritative reports. Of these only a selection can be mentioned here. Professor M. H. L. Pryce writes with great clarity on nuclear shell structure, a subject which in the last few years has begun to make sense and to be really useful in stimulating experiments.

Dr. Edward Teller of the University of California has contributed a short article on the origin of cosmic rays. W. Moffit from Harvard University writes on atomic valence states and chemical binding, a subject to which he has made important contributions. Finally the Cambridge school of radio-physics is represented by an article by B. H. Briggs and M. Spencer on horizontal movements in the ionosphere. One feels that the appearance of this volume is an annual event of real importance, to which every physicist looks forward.

N. F. M.

Text-Book of Physics. Edited by R. Kronig. (Pergamon Press.) [Pp. 850.] Price £3 10*s*.

This book—a translation from the Dutch—is a co-operative effort by nine authors. They are each responsible for a section, the sub-divisions of the work being :—Mechanics (110 pp.) ; Vibrations and Waves (50) ; Electrodynamics (1950) ; Physical Optics (90) ; Atomic Structure (50) ; Atomic Theory of Heat (70) ; Atomic Electricity (45) ; Thermodynamics (70) ; Electrical Instruments (30) ; Optical Instruments (70) ; and Medical Physics (40).

A great difficulty in a work of this kind is the preservation of some uniformity of treatment and of standard. On the whole, this has been successfully done, although each reader will doubtless pick out his own anomalies. For example, to a reader capable of benefiting by the main body of the work, the introductory section explaining what is meant by differentiation would seem to be somewhat superfluous.

The standard is roughly that of a pass degree at an English University, but in many places the book goes a good way beyond this point. To cover so much ground has called for a rather condensed style which in turn means that it is not an easy book to read ; the ordinary pass degree student is usually fed on a much less solid diet.

But the most striking feature of the book as a whole is its complete divorce from laboratory practice. It is not, in fact, as its title claims, a textbook of Physics, but much more nearly an introduction to Theoretical Physics. There is no treatment of experimental methods, and singularly little reference to experimental results. Surface tension is a corollary from Van der Waals' equation ; viscosity is a correction to Bernoulli's equation ; specific heat is a differential coefficient ; and thermal expansion is not mentioned. There are paragraphs on the Fermi–Dirac distribution, and on Brillouin zones—but no mention of acoustics. It may be that the traditional English text spends too long describing n different methods of measuring surface tension, and m elegant modifications of the Wheatstone bridge. But this surely is the other extreme.

Of the individual sections, perhaps the best are those on mechanics and thermodynamics ; the grouping of subject matter in the three 'Atomic' sections is interesting, and some of it would not normally be included in a similar English text. But one might think that radio-activity and nuclear physics deserved more than eight pages out of the total eight hundred in the book ! The section on electrical instruments is not up to the standard of the rest, while that on medical physics is necessarily superficial, quite out of place in a book of this kind.

The book is well printed, copiously indexed, stoutly bound, and shows little evidence of being a translation. But, for reasons indicated above, and even apart from the price, there is little prospect of it becoming a 'recommended text-book' in English Universities. It should, however, be purchased and carefully studied by all those responsible for University teaching in Physics, and to such it will prove to be a most interesting and stimulating volume.

N. T.

On the Origin of the Solar System. By H. Alfven. (Oxford: Clarendon Press, 1954.) Price 30*s*.

In this book Professor Alfven presents his theory of the origin of the solar system. This theory has reached its present state from its earlier formulation by Alfven twelve years ago, as a result of the author's further detailed work, partly in response to ter Haar's criticism.

A careful and clear discussion is given of the processes taking place in an ionized gas stopped by electromagnetic forces in a gravitational field. This occupies chapters II and III following the brief introduction and even briefer chapter I. Unfortunately the author has not included any account of the actual stopping process, according to which ionized gas is prevented from falling in beyond a certain limit by the sun's magnetic field and is concentrated towards the equatorial plane. As the whole theory rests on this somewhat debatable process which is described only in Alfven's earlier work in a rather inaccessible publication, the omission must be greatly regretted and seriously detracts from the value of the book.

The full discussion of the origin of various detailed features of the solar system in the middle chapters makes fascinating reading and must carry considerable weight. In the last chapters the conditions required for the applicability of the theory are discussed and a summary of the most important processes is given.

The book is greatly to be welcomed as an addition to the growing literature on the problem. As a clear and detailed account of an original and highly significant approach it is very valuable, though the omission referred to above is unfortunate. H. B.

Physical Properties of Solid Materials. By C. Zwikker. (London: Pergamon Press.) [Pp. 300+viii.] Price 60*s*. net.

This is a somewhat unusual book, in that it covers an exceptionally wide field in quite a short space, and not in a particularly elementary or popular way. It includes elasticity, molecular constitution of solids, plasticity, dislocations, diffusion, transformations in solids, semi-conductors and photographic emulsions, friction and electron theory of solids. With so wide a field it is inevitably rather scrappy, and the reviewer cannot help wondering for whom it is intended. Probably it would make good introductory reading for a scientist in some other branch, a chemist, a nuclear physicist or an engineer, who needed to know something of the physics of the solid state and wanted to find out in general what was being done, and what he should follow up further. The author has a wide experience of industrial physics, and the reviewer feels that the chief merit of the book is some information that it gives on properties of materials of practical rather than theoretical interest, such as for instance the porosity of powders, which are not easily found in most of the standard text-books.

N.F.M.

[*The Editors do not hold themselves responsible for the views expressed by their correspondents.*]